JSCSEN 77(12)1687–1825(2012)

ISSN 1820-7421 (Online)

Journal of the Serbian Chemical Society

Electronic Version

Society 115th Anniversary 1897 - 2012

VOLUME 77

No 12

BELGRADE 2012

Available on line at

www.shd.org.rs/JSCS/

The full search of JSCS is available through
Available online at shd.org.rs/JSCS/
DOAJ DIRECTORY OF OPEN ACCESS JOURNALS
www.doaj.org
2012 Copyright (CC) SCS

Штампање ове свеске је суфинансирао
Технолошко–металуршки факултет Универзитета у Београду

Publication of this issue is financially co-suported by the
Faculty of Technology and Metallurgy, University of Belgrade

Journal of the Serbian Chemical Society
JSCS-info@shd.org.rs • www.shd.org.rs/JSCS

J. Serb. Chem. Soc. Vol. 77, No. 12 (2012)

CONTENTS

Published by the Serbian Chemical Society
Karnegijeva 4/III, 11000 Belgrade, Serbia
Printed by the Faculty of Technology and Metallurgy
Karnegijeva 4, P.O. Box 35-03, 11120 Belgrade, Serbia

2012 Copyright (CC) SCS

EDITORIAL

This issue of *the Journal of the Serbian Chemical Society* contains selected papers from the *First International Conference on the Processing, Characterisation and Application of Nanostructured Materials and Nanotechnology (Nano-Belgrade 2012)*, held in Belgrade, Serbia, 26–28 September, 2012. The Conference was organized by the Nanotechnology and Functional Materials Centre, Faculty of Technology and Metallurgy, University of Belgrade (NANOTECH FTM) within the FP7 project "Reinforcing of the Nanotechnology and Functional Materials Centre" (No. 245916).

The Conference was attended by approximately 100 participants representing authors from 10 countries, who presented 80 papers within four topics and three symposia (including a poster session) dedicated to identify current research directions as well as limitations in the areas of nanotechnology and nanomaterials, to present a broad scope of multidisciplinary approaches to the field, and to provide a stimulating environment for interactions among the participants with a special focus on the promotion of young scientists. We were fortunate at this meeting to have had excellent representation from renowned scientists from all over the world (a report on the Conference is available at: http://nanobelgrade.tmf.bg.ac.rs).

The selected papers for this special issue cover a variety of contemporary research topics. They were considered sufficiently illustrative to give a representative, albeit incomplete, record of the Conference.

The Guest Editors wish to thank heartily all the invited speakers, participants, NANOTECH FTM staff and members of the Scientific and Program Committees for their efforts that ensured the successful organisation of the conference and performed their duties as Session Chairpersons and reviewers. We also express our profound gratitude to the international and domestic reviewers whose expert comments aided the Editors in their selection of the original and contemporary papers. The Guest Editors wish to take this opportunity to express their sincerely thanks to the Editor and Technical Editors of the Journal of the Serbian Chemical Society for their support in the process of compiling this special issue.

Guest Editors
Djordje Janaćković
Petar Uskoković

2012 Copyright (CC) SCS

Journal of the Serbian Chemical Society
JSCS-info@shd.org.rs • www.shd.org.rs/JSCS
J. Serb. Chem. Soc. 77 (12) 1689–1699 (2012)
JSCS–4381
UDC 544.558:61:576:61.088:614.48.014.4:539.12
Original scientific paper

Application of non-equilibrium plasmas in medicine

ZORAN LJ. PETROVIĆ[1]*, NEVENA PUAČ[1], GORDANA MALOVIĆ[1], SAŠA LAZOVIĆ[1], DEJAN MALETIĆ[1], MAJA MILETIĆ[2], SLAVKO MOJSILOVIĆ[3], PAVLE MILENKOVIĆ[2] and DIANA BUGARSKI[3]

[1]*Institute of Physics, University of Belgrade, Pregrevica 118, 11080 Zemun, Serbia,* [2]*Faculty of Dental Medicine, University of Belgrade, Dr Subotića 8, Serbia and* [3]*Institute for Medical Research, University of Belgrade, Dr Subotića - starijeg 4, Serbia*

(Received 20 October, revised 10 December 2012)

Abstract: The potential of plasma applications medicine, the connections to nanotechnologies and the results obtained by our group are reviewed. A special issue in plasma medicine is the development of the plasma sources that would achieve non-equilibrium at atmospheric pressure in an atmospheric gas mixture with no or only marginal heating of the gas, and with desired properties and mechanisms that may be controlled. Our studies have shown that control of radicals or chemically active products of the discharge, such as ROS (reactive oxygen species) and/or NO, may be used to control the growth of the seeds. Simultaneously, a specially designed plasma needle and other sources were shown to be efficient to sterilize not only colonies of bacteria but also planktonic samples (microorganisms protected by water) or bio films. Finally, it was shown that a plasma might induce differentiation of stem cells. Non-equilibrium plasmas may be used in detection of different specific markers in medicine. For example proton transfer mass spectroscopy may be employed in the detection of volatile organic compounds without their dissociation and thus as a technique for instantaneous measurement of the presence of markers for numerous diseases.

Keywords: low temperature plasmas; plasma technologies; sterilization; functionalization; stem cells.

INTRODUCTION

This paper provides a survey of current plasma medical research/applications in the context of nanotechnologies, in particular, some of the research that was realized in our laboratory.

Low temperature, non-thermal or more precisely non-equilibrium plasmas have shown extraordinary range of applications and range of targets that may be

* Corresponding author. E-mail: zoran@ipb.ac.rs
doi: 10.2298/JSC121020142P

Available online at shd.org.rs/JSCS/

2012 Copyright (CC) SCS

treated. Some of the applications, such as plasma etching for integrated circuit production plasma sources of light, gas lasers and deposition of thin films, have already shaped the existing civilization,[1–5] some on the other hand promise to make a similar impact in the future. Medical applications are at the forefront of future technologies associated with low temperature plasmas and the most active front of present day research.[6–9]

Non-thermal plasmas are being widely used in nano-technological and biomedical applications due to several distinctive properties.[1,2,10,11] The key feature is that it is possible to achieve dramatic changes of surface chemistry at low temperatures. Most of the generator power is absorbed by the electrons in the discharge, which then become hot, typically of the order of 10000 K or more, while, at the same time, ions and neutral molecules maintain room temperature, or close to it. The gas composition, the electron energy distribution function and the cross sections for the dominant interactions between electrons and the background gas particles dictate the production of huge amounts of chemically active species. If the gas composition is chosen properly and if the applied fields are designed efficiently and appropriately, the effects required by a certain application may be achieved while simultaneously fulfilling the criterion of maintaining a low temperature of the background gas.[12]

For the nano-technological applications, the main advantage is the anisotropic ion bombardment of surfaces (Fig. 1). Namely, sheaths are formed near surfaces due to the difference in particle masses. These high field regions conveniently accelerate ions, often with no collisions, to allow (nearly) normal incidence impacts at the surfaces, converting the potential energy in the sheath into kinetic energy at the surface.[14] A normal incidence angle is a crucial factor for contact holes to be obtained and interconnects with high aspect ratios. It is thought that the technology of combined photolithography and plasma etching is the most widely employed nanotechnology (belonging to the top down group) ever since the barrier in miniaturization of 200 nm was broken. The present day resolution of 32 nm in manufacture and aspect ratios of up to 20 (and much smaller dimensions achieved in laboratories) truly challenge even the bottom up technologies.

Furthermore, ion impacts on the sample surface are isolated because the time between impacts onto an area of ≈1 nm^2 is about 10^{-3} s. This should be compared to the time of 10^{-12} s required for the energy of a single impact to dissipate to the background heat. In unison, a single ion impact dissipates several hundreds of eV locally, which is sufficient to make a significant albeit localized modification of the surface. A typical flux of 10^{17} ions cm^{-2} s^{-1}, on average, dissipates power densities of the order of 1 W cm^{-2}. Thus, significant local and superficial changes of the surface structure are obtained while the overall temperature is not

2012 Copyright (CC) SCS

increased significantly. The point here is that the peak power is sufficiently high to break chemical bonds easily and to perform functionalization of the surface.

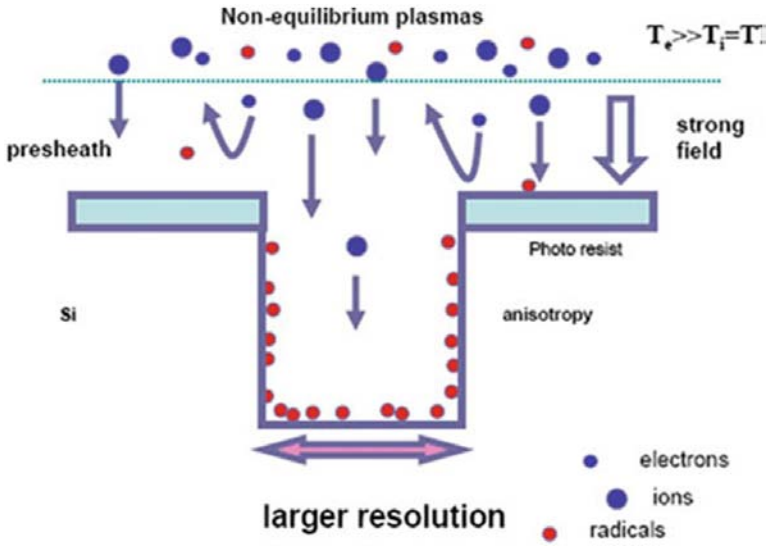

Fig. 1. Schematics of anisotropic plasma etching in non-equilibrium plasmas. The bulk of the plasma produces low energy ions and somewhat higher energy electrons that produce new ions and chemically active radicals. The sheath slows down the electrons and accelerates the ions, thus giving them energies of the order of several 100 eV. Hence, when they hit the surface they do so at a right angle and they facilitate anisotropic etching without sidewall undercutting. Electrons hit the surface with an almost isotropic distribution. The combined effect of the ions and radicals is much greater than the sum of the individual effects of the two species.[13]

It is also well known that the individual effects of ions and neutral chemically active species can be dramatically increased[13] when they both impact surfaces. This kind of synergy of the plasma agents is another crucial property in nano-technological applications.

Neutral, chemically active radicals are created in large numbers by electron-impact dissociation in molecular gas plasmas. It could easily be assumed that the surface flux of reactive particles (density) scales with pressure but gas phase collisions and slower diffusion as well as three body processes, which may change the chemistry entirely, have to be taken into consideration. The higher fluxes of active particles are one of the main arguments for atmospheric pressure non-thermal plasma sources over the low-pressure sources. This was one of the driving forces towards replacing low-pressure plasmas with atmospheric pressure/gas composition plasmas, together with the increased simplicity and decreased cost of atmospheric pressure systems. Thus, the needs of modern nano-technologies gave impetus for the development of more efficient and varied at-

2012 Copyright (CC) SCS

mospheric pressure sources of low temperature plasmas. With the opportunity for such a development, a new front easily opened - that of medical applications.

Another advantage of atmospheric pressure, non-equilibrium plasmas is, of course, the fact that most biomedical systems cannot be subjected to vacuum. Moreover, for most biomedical applications, the temperature of the background gas should not exceed 42 °C, when cell death due to the overheating is induced. Hence, the ultimate conditions for biomedical applications would be not to overheat the sample but rather to induce subtle and selective cell and tissue responses to the plasma-generated chemicals and other species. Similar to nano-technological applications, but probably even more important is the understanding of the synergetic effects of the plasma agents, namely ions, electrons, electric fields and currents, light, neutrals, radicals and metastables. It can be concluded that common goals together with a common need for a localized synergistic effect of several agents drive the applications in both nanotechnologies and plasma medicine. Sometimes plasma medical effects that may be observed over a larger area are in essence due to very localized and specific effects that are fully in tune with nanotechnologies, their criteria and needs.

A BRIEF HISTORY OF PLASMA MEDICINE AND ITS CURRENT STATUS

The history of atmospheric pressure plasma applications in medicine can be divided into several periods. The first generation of plasma devices dating back to 1900 were those when heat was mainly used for tissue removal (plasma cutter). This period was followed by the second generation (since 1970) where thermal plasma energy was used for the surface treatment of tissues (argon plasma coagulator). In addition, there were numerous associated applications such as those using dielectric barrier discharges (DBD) for water purification, electrostatic precipitators to cleanse the air in hospitals and plasma activated hydrogen peroxide as sterilizer. At the same time, low-pressure plasmas were efficiently used in the early 1990s to sterilize equipment.[15] The third generation commenced in the late 1990s when plasmas were used, mainly at atmospheric pressures, for surface treatment with charged particles, reactive UV photons and electric fields.

The first commercial plasma devices date back to the beginning of the 20th century and those were aimed at surgery.[16] At present, there are numerous surgical devices but one has to be aware of the distinction between whether a plasma is just a conducting medium between an electrode and the treated tissue while the effect is due to thermal heating that is the result of the passage of the current or whether the surgical effects are due to plasma-created particles and their interaction with the fields and surface. One of the most successful devices associated with surgical interventions are plasma related devices for stopping bleeding, both by thermal effects and/or by plasma influence on the surface.

2012 Copyright (CC) SCS

These devices include the endoscopic usage of APC (argon plasma coagulation) developed in 1995.[17]

Another front of medical applications that proved to be very successful expanded from low pressures[15] to atmospheric pressures in the late 90s. Very efficient sterilization of bacteria *Escherichia coli* was demonstrated by Laroussi in 1999 using a helium DBD.[18] This line of studies was pursued either directly in Petri dishes[19] or in planktonic samples (in liquid)[20] or even in biofilms.[21] More importantly, sterilization by a plasma was shown to be one of the benefits in the treatment of wounds.[22]

In addition to sterilization, plasmas were shown to benefit proliferation of new cells and the removal of scar tissue.[23] Thus, numerous wounds were treated including burns and chronic wounds, such as diabetic foot.[23] One of the recent applications of microwave plasma applications in dermatology for the treatment of chronic wounds is the application of the plasma torch MicroPlaSter®.[22]

In vitro treatment of cancer cells was demonstrated in 2007 using a floating electrode dielectric barrier discharge (FE-DBD) plasma.[24]. With this device, it was possible to induce programmed death of cells, so-called apoptosis. The Plasma acts directly on the cell without poisoning the solution in which they are located, even when the cells are covered with a medium.

The ion source of a proton transfer mass spectrometer (PTR-MS) operates using a non-thermal plasma. PTR-MS, compared to other analyzing devices, is more sensitive and can detect volatile organic compounds (VOC) down to parts per trillion in real time sampling. Breath sampling and analysis can provide data on VOC for the early stage detection of various diseases, such as breast and lung cancer, diabetes *etc*. Breath is a very complex mixture of various organic compounds.[25] For lung cancer, VOC-31 (m/z = 31), tentatively protonated formaldehyde, and VOC-43 (m/z = 43), tentatively a fragment of protonated 2-propanol, were found at significantly higher concentrations in the breath of cancer patients than in the breath of the control group.[26] One of the biomarkers for diabetes is acetone[27] and its higher concentration in breath, as well as the dynamics of its removal can be an indicator for the disease.

EXPERIMENTAL SETUP AND PROCEDURE

The main reason for the application of plasmas in medicine is that they can replace old conventional procedures in surgery and wound sterilization. Another important feature is the simplicity and low production cost of these plasma devices. Various plasma sources are used in plasma medicine, such as plasma jets, plasma needle, APC and FE-DBD (Fig. 2). Most of the plasma devices have low working gas temperatures because of the great non-equilibrium between the energies of the electrons and heavy particles. This feature is crucial for treatment without damaging the sample. In order to ignite and maintain a discharge at atmospheric

2012 Copyright (CC) SCS

pressure, a noble gas is often used (usually helium or argon). The main role of the noble gas is to lower the breakdown voltage and with its flow, the treated area is also cooled. The complex chemistry and reactions in a plasma produce a unique mixture of particles, for instance atomic species, radicals, UV photons and electrons, important for the efficiency of the treatment of a biological sample. In order to produce higher concentration of the reactive species, a mixture of the noble and a molecular gas, usually oxygen, can be used.

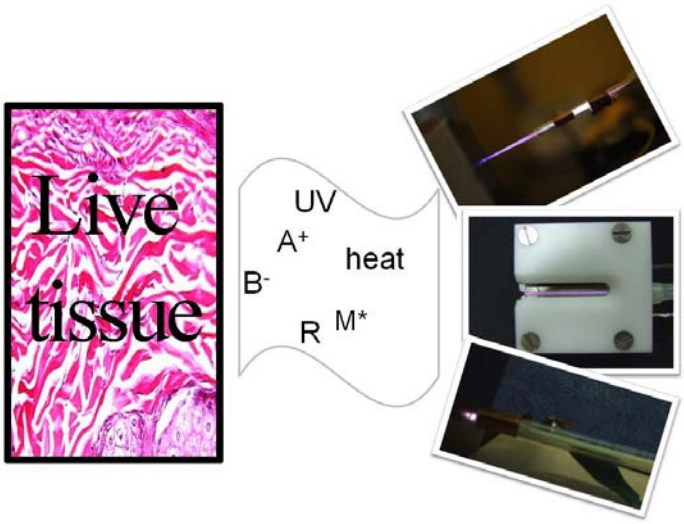

Fig. 2. Photographs of several atmospheric plasma devices that are used in our laboratory for biomedical applications. From the top, a plasma jet, a micro atmospheric pressure plasma jet and a plasma needle are shown.

In our laboratory, low-pressure plasma reactors are accessible that have been used mainly for the treatment of surfaces (textile, polymers, graphene, silicon dioxide surfaces, *etc*.). Atmospheric pressure non-equilibrium plasmas that are available include plasma needle, micro atmospheric pressure plasma jet, plasma jet (operating in the plasma bullet mode), corona and dielectric barrier discharge.

Our principal plasma device that was used to date in the studies of plasma medicine is the plasma needle, which was first applied for the treatment of mammalian cells reported in 2003.[28] The operating power was low and the frequency of the driving current was 13.56 MHz in atmosphere of helium. The plasma needle can be used for the treatment of small areas covered by cells. The plasma needle at higher power kills cells, usually causing necrosis, but at smaller powers either apoptosis may be induced or cells could be just separated.

This plasma device was shown to be suitable for bacteria sterilization[20] of bacteria colonies, planktonic samples and bio films. In addition, this source was

2012 Copyright (CC) SCS

shown to be able to destroy cancer cells, affect but to a much lesser degree human stem cells and even cause differentiation of the stem cells.[29]

DIAGNOSTICS OF PLASMAS

In order to determine the pertinent plasma properties and optimize the desired effects, we use several diagnostic methods. In principle, the basic electrical properties are determined by probes (including derivative probes for higher frequencies that have been calibrated to determine the powers delivered to a plasma of less than 1 W). Optical emission spectroscopy is applied with a limited range of interesting effects that may be covered unless time resolved measurements are made. Spatial profiles of emission recorded by an ultra fast ICCD are employed to determine the time dependent anatomy of the discharge. Finally, a mass analyzer with triple differential pumping is employed, which enables sample ions or radicals from atmospheric pressure discharges to be sampled.[30,31]

MECHANISMS

The interactions between a plasma and cells are hard to investigate due to the complexity of both systems. A plasma is a cocktail of active agents (radicals, UV light, heat, ions, electric fields, energetic particles, *etc*.) with strong synergetic effects. The proper diagnostics and optimization of plasma treatment is of vital importance. On the other hand, the biological samples being treated have a complex sub-structure of their own, so plasma usually targets and affects several of them if not all. The character and the selectivity of the interaction are determined by the plasma properties and the structure of the bio-sample. For example, UV light can easily penetrate and reach DNA introducing single and double strand breaks (directly and/or by creating radicals in the vicinity of the DNA).[32] In the case of bacteria, the DNA is in the nucleoid and is circular while the eukaryotic cells have their DNA better protected in the nucleus. The same intensity of UV light exposure can lead to the destruction of bacteria without long-term effects on the eukaryotic cell, which is just one of the examples of the selectivity mechanism. Other examples worth discussing can be drawn from the differences in the surface to volume ratios, the structure of cell walls, the existence of cell enzymes, *etc*.[33] Bacteria have a higher surface to volume ratio meaning that the same dose of plasma exposure can be sufficient for deactivation while no negative effects to surrounding tissue is caused. The cell wall is usually directly exposed to the plasma treatment. Due to ion bombardment (or to the strong electric fields), pores are being created in the cell wall.[34] Through these pores, the cell can exchange its content with the surrounding. The cell content can leak out and cause cell stress and eventually cell death, as often happens. Bacteria cell wall is made of polysaccharides. Eukaryotic cells have walls made of phospholipids. Exposed to the plasma, lipid peroxidation process occurs. In the process of peroxidation of polysaccharides and phospholipids, the presence of water is important as well as

2012 Copyright (CC) SCS

the composition of the media surrounding the cells and the ions play a catalytic role. One of the products of the lipid peroxidation process of the cell wall is the malondialdehyde. Formed at the cell wall by the plasma, malondialdehyde can be transported to the vicinity of DNA where it can introduce DNA mutation.[35] All this shows the indirect effects of the plasma as well as the complexity of the cell reactions. The enzymes are also able to regulate the stress dealt to the cell. They also regulate the cell radical levels, which on the other hand are massively produced by the plasma. The importance of reactive oxygen and nitrogen species through cell redox processes is evidently crucial but not sufficiently understood.[36] Some of the reactive oxygen species are listed in Table I.[37] The balance between the free radicals and the antioxidants is necessary for proper cell functioning. The conclusion is general and valid for plant cells also.[37]

TABLE I. Reactive oxygen species, ROS[37]

Radicals	Non-radicals
Superoxide, $O_2^{\bullet -}$	H_2O_2
Hydroxyl, $OH^{\bullet}$	Hypobromous acid, HOBr
Hydroperoxyl, $HO_2^{\bullet}$ (protonated superoxide)	Hypochlorous acid, HOCl
Carbonate, $CO_2^{\bullet -}$	Ozone, O_3
Peroxyl, $RO_2^{\bullet}$	Singlet oxygen ($O_2{}^1\Delta_g$)
Alkoxyl, $RO^{\bullet}$	Organic peroxides, ROOH
Carbon dioxide radical, $CO_2^{\bullet -}$	Peroxynitrite, ONOO
Singlet $O_2{}^1\Sigma_g^+$	Peroxynitrate, O_2NOO

PARALLELS WITH PLASMA NANOTECHNOLOGIES

Plasmas have been used in top down plasma technologies for many years, especially through synergistic process of plasma etching that is presently massively used in production with resolutions of 32 nm. Several plasma applications in nanotechnology may be associated with medicine. These include coating of biocompatible thin films, functionalization of surfaces to allow binding of bactericidal nanoparticles of TiO_2 or silver, thus allowing the development of germ free clothes for surgeons and other medical personnel.[38–45]

Furthermore, a more direct parallel lies in the fact that most plasma medical processes are very local over areas that are small parts of a cell and thus compatible with nano-dimensions. Besides the plasma needle and micro atmospheric pressure plasma jet, the capillary microplasmas used for nanostructuring have similar potentials for biomedical applications.[46,47] In a similar way, non-equilibrium plasmas are used to achieve thermodynamically unlikely structures/effects and in the same way surfaces are bombarded by a cocktail of ions and neutrals, electrons, chemically active radicals and are subjected to the effects of local fields. Finally, the need for atmospheric pressure for plasma medicine is also a

2012 Copyright (CC) SCS

motivating factor for the development of cheaper nano-technologies not employing expensive vacuum procedures. Thus, the development of plasma medicine may be associated with the advances in non-equilibrium plasmas for micro (nano) electronics that have occurred over the past two decades.

CONCLUSIONS

Recent advances in plasma medical applications have left very little doubt that this application will be the main driving force for the future developments of non-equilibrium collisional plasmas. The main trick in achieving the non-equilibrium operation and no gas heating is the control of the electron multiplication. For this purpose, inhomogeneous fields (corona), dielectric barrier, RF and pulsed operation and breakdown in rare gas flow may be employed.

Plasma medicine is a new and fast developing field of both medicine and plasma physics, introduced in the last decade. The non-thermal atmospheric pressure plasmas were recently used for the treatment of diverse thermo sensitive biological samples.

Acknowledgements. This research was supported by the Ministry of Education, Science and Technological Development of the Republic of Serbia, under the contract numbers ON171037 and III41011.

И З В О Д

ПРИМЕНА НЕРАВНОТЕЖНЕ ПЛАЗМЕ У МЕДИЦИНИ

ЗОРАН Љ. ПЕТРОВИЋ[1], НЕВЕНА ПУАЧ[1], ГОРДАНА МАЛОВИЋ[1], САША ЛАЗОВИЋ[1], ДЕЈАН МАЛЕТИЋ[1], МАЈА МИЛЕТИЋ[2], СЛАВКО МОЈСИЛОВИЋ[2], ПАВЛЕ МИЛЕНКОВИЋ[2] и ДИАНА БУГАРСКИ[3]

[1]Институт за физику, Универзитет у Београду, Прегревица 118, 11080 Земун, [2]Стоматолошки факултет, Универзитет у Београду, Др Суботића 8, Београд и [3]Институт за медицинска истраживања, Универзитет у Београду, Др Суботића-старијег 4, Београд

У овом раду дат је преглед примене плазме у медицини, повезаност са нанотехнологијама и резултате на овом пољу које је постигла наша група. Посебан проблем у плазма медицини је развој извора плазме који би радили у неравнотежним условима на атмосферском притиску и у смеши гасова каква је у атмосфери уз занемарљиво грејање гаса и са жељеним карактеристикама које се могу подешавати по жељи. Наша истраживања су показала да се контрола присуства радикала и других хемијски активних честица као што су реактивне кисеоничне честице (ROS) и/или NO, може користити за контролу клијања семенки. У исто време је доказано за посебно конструисану плазма иглу да може ефикасно да стерилише не само колоније бактерија већ и планктонске узорке (микроорганизме заштићене водом) па и биофилмове. На крају, ми смо показали да плазма може да индукује диференцијацију матичних ћелија. Неравнотежна плазма се може користити за детекцију разних специфичних маркера у медицини. На пример масена спектроскопија на бази измене протона може да се користи за детекцију испаривих органских једињења без њихове дисоцијације и на тај начин се може остварити тренутна детекција маркера за бројне болести из даха.

(Примљено 20. октобра, ревидирано 10. децембра 2012)

2012 Copyright (CC) SCS

REFERENCES

1. M. A. Lieberman, A. J. Lichtenberg *Principles of Plasma Discharge and Materials Processing*,Wiley, Hoboken, NJ, 2005
2. T. Makabe, Z. L. Petrović, *Plasma electronics: applications in microelectronic device fabrication*, Taylor and Francis, New York, 2006
3. M. G. Kong, G. Kroesen, G. Morfill, T. Nosenko, T. Shimizu, J. Van Dijk, J. L. Zimmermann, *New J. Phys.* **11** (2009) 115012
4. K. Ostrikov, U. Cvelbar, A. B. Murphy, *J. Phys. D: Appl. Phys.* **44** (2011) 174001
5. Z. Lj. Petrović, B. Radjenović, M. Radmilović-Rađenović, in *Proceedings 26th International Conference on Microelectronics MIEL, the Production of Integrated Circuits and Surface Modification of Materials*, Niš, Serbia, 2008, p. 19
6. K. D. Weltmann, Th. Von Woedtke, *Eur. Phys. J. Appl. Phys.* **55** (2011) 13807
7. J. Heinlin, G. Isbary, W. Stolz, G. Morfill, M. Landthaler, T. Shimizu, B. Steffes, T. Nosenko, J. L. Zimmermann, S. Karrer, *J. Eur. Acad. Dermatol.* **25** (2011) 1
8. R. Sensenig, S. Kalghatgi, E. Cerchar, G. Fridman, A. Shereshevsky, B. Torabi, K. Priya Arjunan, E. Podolsky, A. Fridman, G. Friedman, J. Azizkhan-Clifford, A. D. Brooks, *Ann. Biomed. Eng.* **39** (2011) 674
9. R. Wang, H. Zhou, P. Sun, H. Wu, J. Pan, W Zhu, J Zhang, J Fang, *Plasma Med.* **1** (2011) 143
10. *Non-equilibrium air plasmas at atmospheric pressure*, K. H. Becker, U. Kogelschatz, K. H. Schoenbach, R. J. Barker, Eds., Taylor & Francis, New York, 2004,
11. *Plasma for bio-decontamination, medicine and food security*, Z. Machala, K. Hensel, Y. Akishev, Eds., Springer, Dordrecht, The Netherlands, 2012
12. Z. L. Petrović, N. Puač, S. Lazović, D. Maletić, K. Spasić, G. Malović, *J. Phys. Conf. Ser.* **356** (2012) 012001
13. H. F. Winters, J. W. Coburn, *J. Vac. Sci. Technol., B* **3** (1985) 1376
14. T. Makabe, T. Yagisawa, *Plasma Sources Sci. Technol.* **18** (2009) 014016
15. S. Manola, Z. Lj. Petrović, R. M. Jankov, in *Proceedings of 16th SPIG XVI Summer School and International Symposium on the Physics of Ionized Gases*, Belgrade, 1993, p. 285
16. W. Bovie, H. Cushing, *Surg. Gynecol. Obstet.* **47** (1928) 751
17. J. Sessler, H. D. Becker, I. Flesch, K. E. Grund, *J. Cancer. Res. Clin. Oncol.* **121** (1995) 235
18. M. Laroussi, G. S. Sayler, B. B. Glascock, B. Mccurdy, M. E. Pearce, N. G. Bright, C. M. Malott, *IEEE Trans. Plasma Sci.* **27** (1999) 34
19. G. Fridman, A. D. Brooks, M. Balasubramanian, A. Fridman, A. Gutsol, V. N. Vasilets, H. Ayan, G. Friedman, *Plasma Processes Polym.* **4** (2007) 370
20. S. Lazović, N. Puač, M. Miletić, D. Pavlica, M. Jovanović, D. Bugarski, S. Mojsilović, D. Maletić, G. Malović, P. Milenković, Z. L. Petrović, *New J. Phys.* **12** (2010) 083037
21. S. A. Ermolaeva, A. F. Varfolomeev, M. Y. Chernukha, D. S. Yurov, M. M. Vasiliev, A. A. Kaminskaya, M. M. Moisenovich, J. M. Romanova, A. N. Murashev, I. Selezneva , T. Shimizu, E. V. Sysolyatina, I. A. Shaginyan, O. F. Petrov, E. I. Mayevsky, V. E. Fortov, G. E. Morfill, B. S. Naroditsky, A. L. Gintsburg, *J. Med. Microbiol.* **60** (2011) 75
22. J. Heinlin, G. Morfill, M. Landthaler, W. Stolz, G. Isbary, J. L. Zimmermann, T. Shimizu, S. Karrer, *J. Dtsch. Dermatol. Ges.* **8** (2010) 968

2012 Copyright (CC) SCS

23. G. Fridman, G. Friedman, A. Gutsol, A. B. Shekhter, V. N. Vasilets, A. Fridman, *Plasma Processes Polym.* **5** (2008) 5033
24. G. Fridman, A. Shereshevsky, M. M. Jost, A. D. Brooks, A. Fridman, A. Gutsol, V. Vasilets, G. Friedman, *Plasma Chem. Plasma Process.* **27** (2007) 163
25. K. Schwarz, W. Filipiak, A. Amann, *J. Breath Res.* **3** (2009) 027002
26. A. Wehinger, A. Schmid, S. Mechtcheriakov, M. Ledochowski, C. Grabmer, G. A. Gastl, A. Amann, *Int. J. Mass Spectrom*. **265** (2007) 49
27. D. Smith, P. Španěl, A. A. Fryer, F. Hanna, G. A. A. Ferns, *J. Breath Res.* **5** (2011) 022001ss
28. E. Stoffels, I. E. Kieft, R. E. J. Sladek, *J. Phys., D* **36** (2003) 2908
29. M. Miletić, S. Mojsilović, I. Okić Đorđević, D. Maletić, N. Puač, S. Lazović, G. Malović, P. Milenković, Z. Petrović, D. Bugarski, unpublished results
30. S. Lazović, N. Puač, G. Malović, A. Đorđević, Z. L., Petrović *Chem. Listy* **102** (2008) 1383
31. G. Malović, N. Puač, S. Lazović, Z. Petrović, *Plasma Sources Sci. Technol.* **19** (2010) 034014
32. D. O' Connell, L. J. Cox, W. B. Hyland, S. J. Mcmahon, S. Reuter, W. G. Graham, T. Gans, F. J. Currell, *Appl. Phys. Lett.* **98** (2011) 043701
33. D. Dobrynin, G. Fridman, G. Friedman, A. Fridman, *New J. Phys.* **11** (2009) 115020
34. K. H. Schoenbach, F. E. Peterkin, R. W. Alden, S. J Beebe. *IEEE Trans. Plasma. Sci.* **25** (1997) 284
35. L. J. Marnett, *Mutat. Res.* **424** (1999) 83
36. D. B. Graves, *J. Phys., D* **45** (2012) 263001
37. B. Halliwell, *Plant Physiol.* **141** (2006) 312
38. X. Liu, P. K. Chu, C. Ding, *Mat. Sci. Eng., R* **70** (2010) 275
39. P. Uhlmanna, L. Ionov, N. Houbenov, M. Nitschke, K. Grundke, M. Motornov, S. Minko, M. Stamma, *Prog. Org. Coat.* **55** (2006) 168
40. U. Cvelbar, M. Modic, J. Kovač, S. Lazović, G. Filipič, D. Vujošević, I. Junkar, K. Eleršič, S. P. Brühl, C. Canal, T. Belmonte, M. Mozetič, *Surf. Coat. Technol.* **211** (2012) 200
41. U. Cvelbar, Z. Chen, I. Levchenko, R. M. Sheetz, J. B. Jasinski, M. Menon, M. K. Sunkar, K.(Ken) Ostrikov, *Chem. Commun.* **48** (2012) 11070
42. U. Cvelbar, Z. Chen, M. K. Sunkara, M. Mozetič, *Small* **4** (2008) 1610
43. K. (Ken) Ostrikov, U. Cvelbar, A. B Murphy, *J. Phys. D: Appl. Phys.* **44** (2011) 174001
44. G Arnoult, T Belmonte, F Kosior, M Dossot, G Henrion, *J. Phys., D* **44** (2011) 174022
45. M. Hiramatsu, M. Hori *Carbon Nanowalls: Synthesis and Emerging Applications* Springer, Wein, 2009
46. A. C. Bose, Y. Shimizu, D. Mariotti, T. Sasaki, K. Terashima, N. Koshizaki, *Nanotechnol.* **17** (2006) 5976
47. Y. Shimizu, T. Sasaki, A. C. Bose, K. Terashima, N. Koshizaki, *Surf. Coat. Tech.* **200** (2006) 4251.

2012 Copyright (CC) SCS

Journal of the Serbian Chemical Society
JSCS-info@shd.org.rs • www.shd.org.rs/JSCS

J. Serb. Chem. Soc. *77* (12) 1701–1707 (2012)
JSCS–4382

UDC 533.9+666.293.35+678.031–036.7:
621.3.004.12:539.24
Original scientific paper

Plasma etching of polystyrene latex particles for the preparation of graphene oxide nanowalls

LUCA VALENTINI* and SILVIA BITTOLO BON

Università di Perugia, Dipartimento di Ingegneria Civile e Ambientale, Strada di Pentima 4, INSTM, UdR Perugia, 05100 Terni, Italy

(Received 22 October 2012)

Abstract: Graphene oxide nanowalls were prepared by casting an aqueous dispersion of polystyrene latex particles onto a graphene oxide film followed by tetrafluoromethane plasma etching. Mild plasma etching conditions allowed the oxygen functional groups on the graphene oxide nanowalls to be retained. It was found that exposure to a xenon light source of such graphene oxide nanowalls coated with a gold thin film results in an increase in the electrical conductivity.

Keywords: nanostructures; etching; electrical properties characterization; electrical conductivity.

INTRODUCTION

The optoelectronic properties of graphene have attracted substantial interest because graphene can absorb light and turn it into a photocurrent over a wide range of the electromagnetic spectrum, from the UV to the visible and infrared regimes.[1] A photocurrent response at graphene–metal contacts was reported by various groups, and the origin of such a photocurrent generation was discussed.[2] Graphene oxide (GO), namely a layered material produced by the oxidation of graphite, has been widely exploited but graphene oxide is electrically insulating and requires further reduction steps to generate a photocurrent signal.[3]

One possible way of overcoming these restrictions is to utilize metallic nanostructures placed at the metal/carbon interfaces. Light absorbed by such metal nanostructures is converted into surface plasmon resonances that cause a local increase in the temperature inducing a reduction of the GO.[4–6] Instead of producing metallic nanostructures by expensive and time-consuming electron-beam lithographic technique, a cheap and fast method relies on the possibility to utilize polymer nanoparticles deposited onto the graphene oxide surface as mask for the

* Corresponding author. E-mail: mic@unipg.it
doi: 10.2298/JSC121022137V

Available online at shd.org.rs/JSCS/

2012 Copyright (CC) SCS

localized etching of GO layer and then to use such carbon nanowalls for the deposition of a conformal thin metal film.

The fabrication of graphene nanoribbons by utilizing nanosphere lithography in combination with oxygen plasma etching was recently reported.[7] This technique takes advantage of the use of ordered arrays of latex nanospheres as lithographic masks. Instead of the results found by Liu *et al.*[7], when we used polymer nanoparticles for tetrafluoromethane-assisted plasma etching of graphene oxide sheets, it was surprisingly found that this method was capable of fabricating carbon nanowalls.

The polymer nanoparticles served here as a ''sacrificial'' template, protecting the covered graphene oxide from ablation by the plasma. The choice of polymer nanoparticles was motivated by their low cost and the advantage of self-assembled, ordered arrays of nanospheres as lithographic masks, which has long been known to be a low-cost nanofabrication strategy.

In this communication, a novel method consisting of plasma etching of a polystyrene-coated GO surface for the preparation of graphene oxide nanowalls is reported. The effects of the processing on the resulting morphology together with the chemical composition were employed to characterize the graphene structure. In addition, it was found how a simple device consisting of a thin gold film deposited onto such GO nanowalls induces an increase in the electrical current when exposed to light.

EXPERIMENTAL

Graphene oxide was purchased from Cheaptubes (GO; thickness 0.7–1.2 nm estimated by AFM). An aqueous GO solution (1 mg ml^{-1}) was prepared and tip sonicated (750 W, 60 % amplitude) for 1 h to yield a yellow suspension. The solution was transferred to a vial and centrifuged for 30 min at 9000 rpm. The supernatant of the dispersion was carefully extracted and separated from the residual visible at the bottom of the vial. The graphene nanowalls device was prepared as reported in Scheme 1. Al electrodes (1 mm×5 mm) were deposited on a glass substrate by vacuum evaporation with a thickness of 60 nm and space of 0.5 mm. The aqueous GO solution was drop cast onto the Al electrodes. Polystyrene latex particles (Agar Scientific, 10 wt. % dispersion in water with surface-bound sulphate groups as stabilizer, average particle diameter 125 nm) were spin-cast at 500 rpm. The plasma treatment of the samples was realized in a CF_4 plasma with a gas flow rate of 20 sccm min^{-1}. The vacuum of the chamber was set at 0.133 Pa and a 13.56 MHz radiofrequency source with power fixed at 35 W was used to create the plasma on top of the sample. The plasma treatments were performed for 5 and 10 min, keeping the substrate temperature at 25 °C. The surface morphology of the films was investigated by field emission scanning electron microscopy (FE–SEM). Infrared spectroscopy in the 500–4000 cm^{-1} range, in the transmission mode was used to investigate the chemical composition.

Gold was sputtered onto the plasma treated GO films for 40 s; the average thickness of the gold films as measured by atomic force microscopy was 12 nm. Electrical characterization was performed using a computer-controlled Keithley 4200 source measure unit. Photocurrent

2012 Copyright (CC) SCS

generation was investigated under exposure of the samples to a solar simulator AM1.5D with an output power of 100 mW cm^{-2}.

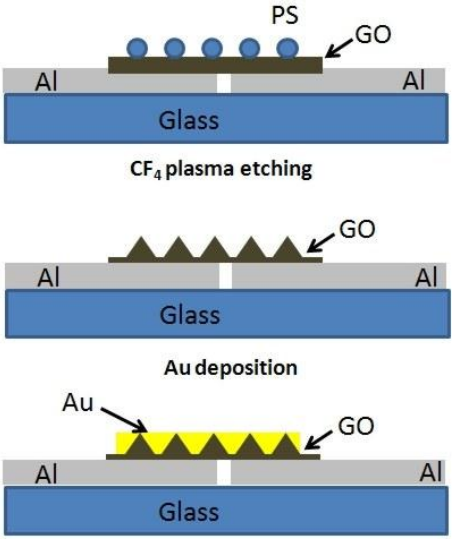

Scheme 1. Schematic presentation of the preparation of GO nanowall devices.

RESULTS AND DISCUSSION

By proper adjustment of the plasma process parameters, a precision control of the obtained nanostructures was achieved; the FE–SEM characterization performed on flat GO (Fig. 1a) and PS latex-coated GO (Fig. 1b) samples showed that after plasma treatment for 5 min, the flat GO morphology was in the form of columnar walls, mainly vertically oriented to the surface of the substrate with the edge having the same dimension of the diameter of the PS latex particles (Figs. 1b and 1c). From Fig. 1c, no trace of residual PS latex particles was found. It was interesting to note that the deposition of gold onto the GO nanowalls did not fill the columnar walls but was conformal to the GO nanowalls (Fig. 1d).

The formation of the GO nanowalls under the nanoparticle masks is due to the anisotropic etching process that has been related to the anisotropic distribution of the plasma ions deflected into the interspacing of the masking nanospheres, as illustrated in Scheme 1. It is expected that the anisotropic etching process plays a role in the anisotropic chemical reactivity of graphene oxide sheet in the reactive plasma etching process.

The most characteristic features in the FTIR spectrum of the GO sample (Fig. 2) are the adsorption bands corresponding to C=O stretching at 1720 cm^{-1} and the sp^2-hybridized C=C in plane stretching at 1629 cm^{-1}.[3] The bands at 3432 and 1390 cm^{-1} are associated, respectively, with the stretching and deformation vibrations of the O−H bond of CO−H; while the band at 1059 cm^{-1} is due to C−O−C in an epoxide group and the signal at about 1246 cm^{-1} could be attri-

2012 Copyright (CC) SCS

buted to C–O epoxide groups.[3] After the plasma treatment, it was observed that the GO nanowalls had retained the same functional groups.

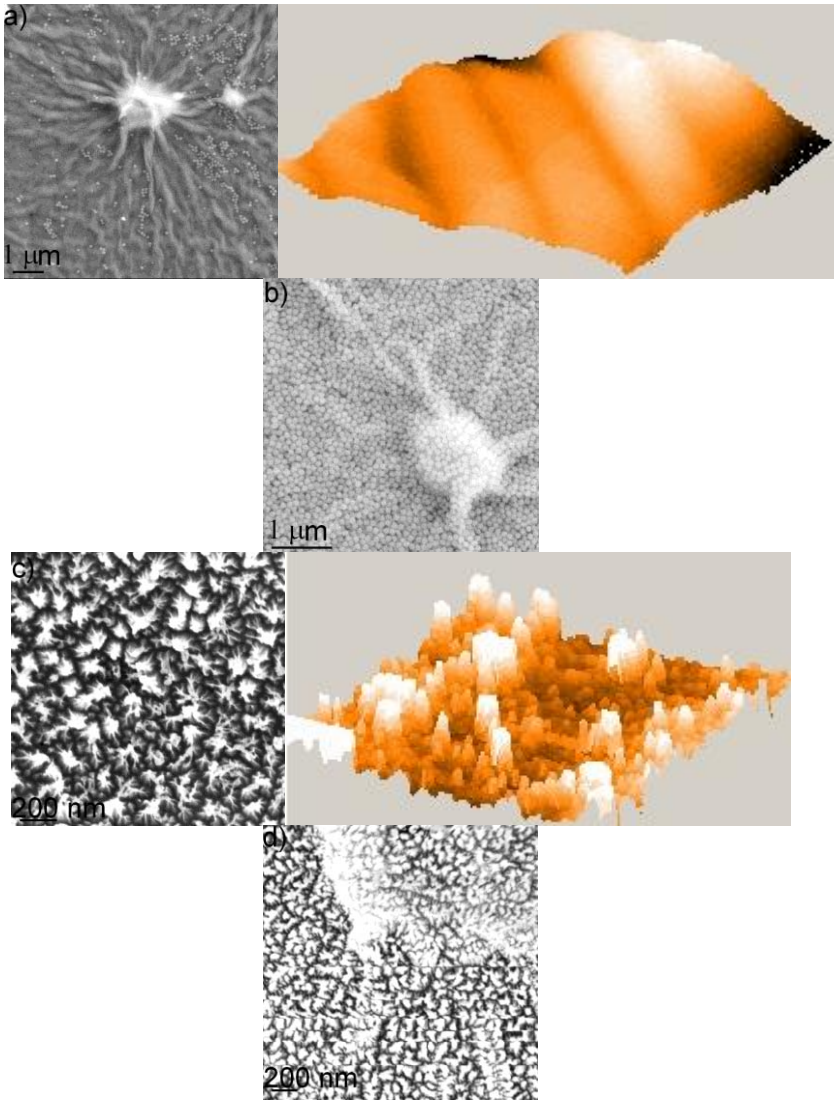

Fig. 1. a) FE–SEM and 3D AFM (500 nm×250 nm) images of GO; b) FE–SEM image of PS latex-coated GO film before plasma treatment and c) FE–SEM and 3D AFM (500 nm×250 nm) images of GO after plasma treatment. d) FE–SEM Image of gold coated GO nanowalls.

GO alone, due to the existence of oxygen-containing groups and its intrinsic high electrical resistance, could not generate a photocurrent signal. The Au film

2012 Copyright (CC) SCS

is very thin and almost transparent to light (Fig. 3a) hence, it could be expected that the GO nanowalls under the gold film are reached by light irradiation, thus allowing the synergic effect of gold sputtered onto such carbon nanostructures to be studied. The current-voltage characteristic of GO nanowalls, as well as of gold coated GO nanowalls, was monitored under illumination. From Figs. 3b and 3c, an increase of the current of the gold-coated GO nanowalls during exposure to light illumination was observed. Uncoated GO nanowalls, as expected (Fig. 3b), did not show a well-defined photocurrent signal when the light was switched "on". Therefore, the photocurrent is attributed to the synergic effect of GO nanowalls and the Au film. The only way to explain these findings could be a deoxygenation that could recover the GO conductivity to some extent.

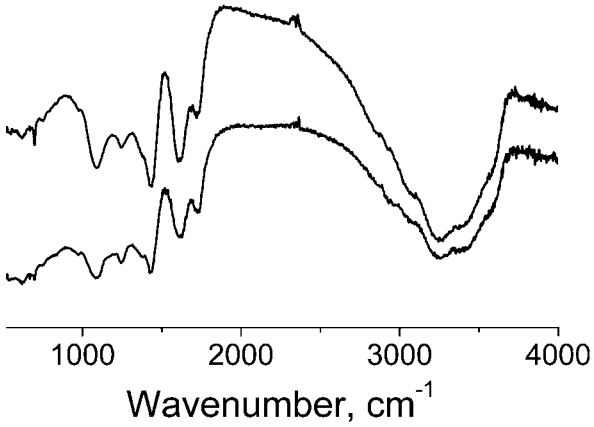

Fig. 2. FTIR Spectra of GO (bottom) and GO nanowalls (top) samples.

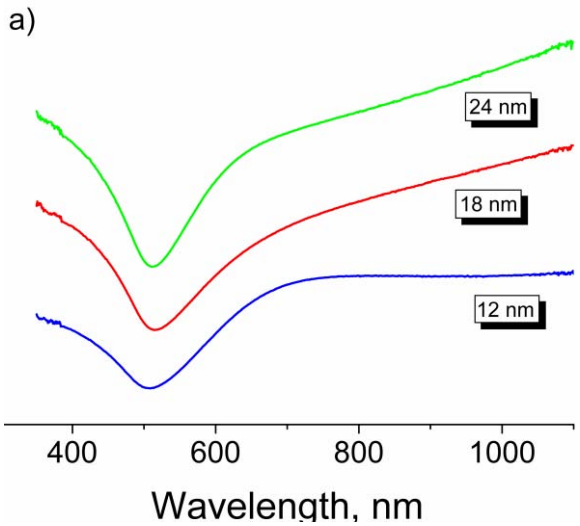

2012 Copyright (CC) SCS

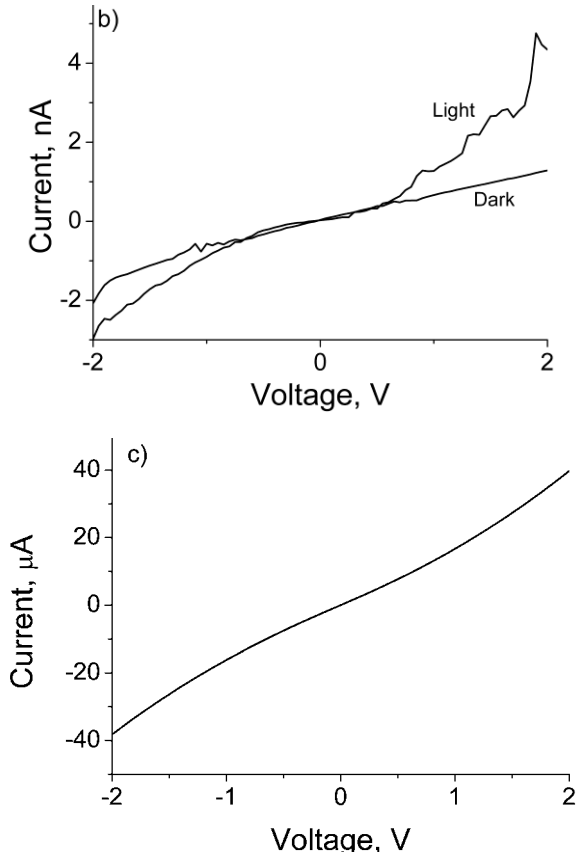

Fig. 3. a) UV–Vis Transmission spectra of sputtered Au films of different thicknesses; b) *I–V* Curves of GO nanowalls under dark and light conditions; c) *I–V* Curve of gold-coated GO nanowalls under light condition.

Recently, the use of metal nanostructures to induce local heating at metal/carbon interfaces was exploited.[4] The surface plasmon resonances in response to the external electromagnetic radiation causes a local increase in the temperature of the metal nanostructures, which could increase the rate of photo-induced deoxygenation of GO. In this study, a photochemical reduction in which the oxygen functional groups of GO decompose by accepting a hot electron from the photo-excited gold is also suggested.[8]

CONCLUSIONS

A polystyrene latex-assisted plasma etching was used as a novel, fast and economical method for preparation of graphene oxide nanowalls. Mild plasma etching was found to leave the oxygen-based functional groups, but led to the formation of carbon nanostructures that when coated with a thin metallic film

2012 Copyright (CC) SCS

become photoresponsive. Photoresponsive carbon–metal interconnect could be important in graphene-based applications.

ИЗВОД

ПЛАЗМА-НАГРИЗАЊЕ ПОЛИСТИРЕНСКИХ ЛАТЕКС ЧЕСТИЦА ЗА ПРИПРЕМУ НАНОЗИДОВА ГРАФЕН-ОКСИДА

LUCA VALENTINI и SILVIA BITTOLO BON

[1]*Università di Perugia, Dipartimento di Ingegneria Civile e Ambientale, Strada di Pentima 4, INSTM, UdR Perugia, 05100 Terni, Italy*

Нанозидови (енгл. *nanowalls*) графен-оксида припремљени су наношењем водене дисперзије полистиренских латекс честица на филмове графен-оксида и накнадним нагризањем тетрафлуорометана у плазми. Благи услови нагризања у плазми омогућавају задржавање кисеоничних функционалних група на зидовима графен-оксида. Уочено је да након излагања зидова графен-оксида превучених танким филмом злата извору ксенонске светлости долази до повећања електричне проводљивости.

(Примљено 22. октобра 2012)

REFERENCES

1. F. Bonaccorso, Z. Sun, T. Hasan, A. C. Ferrari, *Nat. Photonics* **4** (2010) 611
2. E. J. H. Lee, K. Balasubramanian, R. T. Weitz, M. Burghard, K. Kern, *Nat. Nanotechnol.* **3** (2008) 486
3. M. Acik, G. Lee, C. Mattevi, A. Pirkle, R. M. Wallace, M. Chhowalla, *J. Phys. Chem., C* **115** (2011) 19761
4. D. D. Kulkarni, S. Kim, A. G. Fedorov, V. V. Tsukruk, *Adv. Func. Mater.* **22** (2012) 2129
5. T. J. Echtermeyer, L. Britnell, P. K. Jasnos, A. Lombardo, R. V. Gorbachev, A. N. Grigorenko, A. C. Ferrari, *Nat. Commun.* **2** (2011) 458
6. L. Y. Cao, D. N. Barsic, A. R. Guichard, M. L. Brongersma, *Nano Lett.* **7** (2007) 3523
7. L. Liu, Y. Zhang, W. Wang, C. Gu, X. Bai, E. Wang, *Adv. Mater.* **23** (2011) 1246
8. H. Liu, S. Ryu, Z. Chen, M. L. Steigerwald, C. Nuckolls, L. E. Brus, *J. Am. Chem. Soc.* **131** (2009) 17099.

2012 Copyright (CC) SCS

Journal of the Serbian Chemical Society
JSCS-info@shd.org.rs • www.shd.org.rs/JSCS
J. Serb. Chem. Soc. 77 (12) 1709–1722 (2012)
JSCS–4383
UDC 664.644.7–034.21+541.13+542.913:
614.48:61.000.57:620.017:539.24
Original scientific paper

Controlled production of alginate nanocomposites with incorporated silver nanoparticles aimed for biomedical applications

JASMINA STOJKOVSKA, JOVANA ZVICER, ŽELJKA JOVANOVIĆ[#], VESNA MIŠKOVIĆ-STANKOVIĆ[#] and BOJANA OBRADOVIĆ[*#]

Faculty of Technology and Metallurgy, University of Belgrade, Karnegijeva 4, 11000 Belgrade, Serbia

(Received 8 November, revised 15 December 2012)

Abstract: The production of nanocomposite alginate microbeads with electrochemically synthesized silver nanoparticles (AgNPs) based on the electrostatic extrusion technique was investigated with respect to their potentials for utilization in pharmaceutical and biomedical applications. It was shown that electrochemical synthesis of AgNPs results in the reduction of practically all the Ag^+ present in the initial solution, yielding stable Ag/alginate colloid solutions that were demonstrated to be suitable for sterilization, manipulation, and electrostatic extrusion with retention of the AgNPs. The presence of AgNPs in the alginate colloid solutions had negligible effects on the size of the produced Ag/alginate microbeads, which was mainly determined by the electrostatic potential applied during the extrusion. On the other hand, the incorporation of AgNPs within the alginate hydrogel induced slight changes in biomechanical properties of the microbeads determined in a biomimetic bioreactor. Thus, packed beds of nanocomposite Ag/alginate microbeads exhibited a slightly higher dynamic compression modulus as compared to that of control alginate microbeads (154±4 and 141±2 kPa, respectively). On the other hand, the equilibrium unconfined compression modulus was significantly lower for the nanocomposite microbeads as compared to that of the controls (34±2 and 47±1 kPa, respectively).

Keywords: electrochemical synthesis; electrostatic extrusion; sterilization; biomechanical properties.

INTRODUCTION

The antimicrobial properties of silver have been known for centuries, so that silver pots were utilized for water preservation while silver-based compounds

* Corresponding author. E-mail: bojana@tmf.bg.ac.rs
[#] Serbian Chemical Society member.
doi: 10.2298/JSC121108148S

Available online at shd.org.rs/JSCS/

2012 Copyright (CC) SCS

found applications in traditional medicine.[1–3] Today, silver as an antimicrobial agent has gained renewed attention due to the increasing problem of antibiotic-resistant bacterial strains.[4] There is a range of silver-containing medical products such as antimicrobial wound dressings, ointments, and coatings.[5,6] Furthermore, silver nanoparticles (AgNPs) were reported to be even more potent than silver ions acting by attachment and interactions with the bacterial cell membrane, release of Ag^+ ions and, potentially, by penetration into the cell interior.[7] Different methods for the production of AgNPs made them also attractive for exploring possibilities for the development of novel bioactive biomaterials aiming at combining the relevant function of the biomaterial with the antimicrobial properties of the nanoparticles.[5]

However, one of the main problems for utilization of AgNPs is a strong tendency of these nanoparticles to agglomerate due to the large specific surface area and high surface energy. Polymers as capping agents in solutions and as hydrogels were shown to be viable options for achieving nanoparticle stabilization.[8] One of the widely investigated polymers for biomedical applications in general as well as in combinations with AgNPs, is alginate, a natural polysaccharide that easily forms hydrophilic, biocompatible and bioresorbable hydrogels. Alginates are already used in pharmacy and medicine as excipients for drugs, dental impression materials, wound dressings and carriers of drugs and transplanted cells.[9] Supplementation of alginate hydrogels with silver offers the additional feature of antimicrobial activity. Thus, a number of wound dressing products based on alginate fibers with incorporated silver ions have been produced.[10] However, incorporation of AgNPs within alginate solutions and/or hydrogels provides possibilities for controlled and prolonged release of Ag nanoparticles and/or ions and production of variety of formulations with different compositions and forms. AgNPs have been produced in alginate solutions supplemented with silver salts (*e.g.* nitrate, sulfate) by reduction of Ag^+ using sodium borohydride as the reductant,[11–13] by gamma irradiation[14] or simply by heating of the solution where alginate served as both a reducing agent and a stabilizer.[15]

It was recently shown that electrochemical synthesis can also be used for the production of AgNPs in alginate solutions and that the obtained colloid solutions could be further utilized to obtain nanocomposite Ag/alginate hydrogels.[16–18] Electrochemical synthesis is particularly advantageous for potential use in biomedicine and pharmacy due to precise control of particle size achieved by adjusting current density or applied potential and high purity of the obtained nanocomposite hydrogels containing only gelling cations, alginate and AgNPs. Furthermore, nanocomposite hydrogels in the form of microbeads (<1 mm in diameter) are suitable for controlled release of AgNPs and/or ions due to the large specific surface area and short internal diffusion distances. Alginate microbeads

2012 Copyright (CC) SCS

were shown to be suitable for immobilization of variety of cell types, such as insect and mammalian cells[19] as well as brewing yeast cells.[20] It was previously shown that alginate microbeads could also be used for cartilage tissue engineering as supports for chondrogenic cells (*e.g.* bone marrow stromal cells[21,22] and bovine calf chondrocytes[23,24]) coupled with biomimetic bioreactors that imitate physiological conditions in articular cartilage. Supplementation of AgNPs within alginate microbeads could potentially provide an additional feature of prolonged sterility of engineered implants.

One of the techniques for controlled production of uniform hydrogel microbeads is electrostatic droplet generation based on extrusion of an alginate solution under the action of electrostatic forces that disrupt the liquid filament at the capillary/needle tip to form a charged stream of small droplets collected in a gelling bath.[25,26] As Na^+ are exchanged with Ca^{2+} from the gelling solution, the droplets solidify forming microbeads down to 50 μm in diameter.[26,27] The process of electrostatic droplet formation is a complex function of a number of parameters,[28,29] while for a chosen electrode set-up and polymer, the applied electrostatic potential was shown to be the key determinant of the droplet and, consequently, also the microbead size.[28] As the electrostatic potential, U, is increased, the droplet size decreases gradually at first and then sharply at a critical potential value, U_c, after which microscopic charged droplets are formed, the size of which does not vary with further increase in U.[28] Relationship between the applied potential, U, and the droplet radius, r, can be derived by balancing the forces acting on the droplet,[28,29] which for a positively charged needle resulted in:[30]

$$U^2 = \frac{[\ln(4H/r)]^2(c - dr^3)}{2\varepsilon_0} \tag{1}$$

with

$$c = r_0\gamma \tag{2}$$

and

$$d = \frac{2}{3}\rho g \tag{3}$$

where H is the distance between the electrodes (*i.e.*, the needle tip and the surface of the gelling solution), ε_0 is the permittivity of air ($\varepsilon_0 = 8.85\times10^{-12}$ C^2 $N^{-1}m^{-2}$), r_0 is the internal radius of the needle, γ is the surface tension, ρ is the liquid density, and g is the gravitational acceleration. Eqs. (1)–(3) were shown to agree qualitatively with the experimental data.[30]

For potential biomedical utilization of nanocomposite hydrogels, it is required that the production procedure is simple, precisely regulated and scalable, while the final products are pure, sterile and with controlled properties. The aim of this study was to characterize comprehensively the production of nanocompo-

2012 Copyright (CC) SCS

site Ag/alginate microbeads based on electrochemical synthesis of AgNPs in alginate solutions followed by electrostatic extrusion of the obtained colloid solutions. Specifically, the possibilities for sterilization and manipulation of Ag/alginate colloid solutions with retention of AgNPs as well as the production of nanocomposite microbeads regarding the effects of electrostatic extrusion parameters on the microbead size and AgNP concentration were investigated. In addition, the effects of AgNP incorporation in alginate hydrogels on biomechanical properties of packed beds of microbeads were studied in a biomimetic bioreactor with dynamic compression that imitates *in vivo* conditions in native articular cartilage.

EXPERIMENTAL

Materials

Low viscosity sodium alginate (A-2158) was purchased from Sigma (St. Louis, MO). Sodium citrate was bought from Himedia (Mumbai, India), $AgNO_3$ from M. P. Hemija (Belgrade, Serbia), KNO_3 from Centrohem (Stara Pazova, Serbia) and $Ca(NO_3)_2 \cdot 2H_2O$ from Alkaloid (Skopje, Macedonia). Water from Milli-Q system (Millipore, Billerica, MA, USA) was used in all experiments and N_2 gas (Messer Tehnogas a.d., Belgrade, Serbia) was of high purity (99.5 %).

Production of alginate colloid solutions with AgNPs

Sodium alginate solutions with AgNPs were produced by electrochemical synthesis as described previously.[16] Briefly, electrochemical synthesis was performed galvanostatically in an electrochemical cell containing 50 cm^3 of an aqueous solution containing 0.1 M KNO_3, 3.9 mM $AgNO_3$ and 2 % w/v Na-alginate. Two Pt plates functioned as the working and counter electrodes and a saturated calomel electrode (SCE) as a reference electrode using Gamry Reference 600 Potentiostat/Galvanostat/ZRA (Gamry Instruments, Warminster, PA). The synthesis was performed under continuous stirring at the current density of 50 mA cm^{-2} and implementation time of 10 min. N_2 was passed through the solution for 20 min prior to the synthesis, followed by continuous N_2 flow over the solution during the synthesis. Gravimetric analysis showed that the final Ag/alginate colloid solution contained 1.9 % w/v alginate due to slight polymer deposition on the counter electrode.[18]

A series of colloid solutions with different concentrations of AgNPs was obtained by dilution of the initially synthesized colloid solution with 1.9 % w/v Na-alginate solution. Sterilization of the obtained Ag/alginate colloid solutions was realized by transferring the solution into a sterile, covered glass vessel and boiling for 30 min under magnetic stirring.

Production of nanocomposite alginate microbeads with incorporated AgNPs

Sodium alginate colloid solutions with AgNPs were used to produce Ag/alginate microbeads by electrostatic droplet generation as described previously.[16-18] In brief, Ag/alginate colloid solutions with different AgNP concentrations were extruded through a positively charged blunt edge, stainless steel needle (23 gauge) using a 5 or 10 cm^3 syringe and a syringe pump (Racel, Scientific Instruments, Stamford, CT, USA). The electrode distance between the needle tip and the grounded gelling bath (1.5 % w/v $Ca(NO_3)_2 \cdot 2H_2O$) was kept constant in all experiments at 2.5 cm. After extrusion, the microbeads remained in the gelling bath for an additional 30 min in order to complete their gelling, and thereafter were washed in H_2O to remove the residual silver ions. In order to investigate the effects of the extrusion parameters,

2012 Copyright (CC) SCS

the initially synthesized Ag/alginate colloid solution with a silver concentration of 3.9 mM was extruded in two experimental series. In the first experimental series, the applied electrostatic potential was varied in the range 0–7.5 kV at a flowrate of 25.2 cm^3 h^{-1}, while in the second series, the flowrate ranged from 5.1 to 25.2 cm^3 h^{-1} at a constant potential of 6.6 kV. For biomechanical characterization, four experimental series of microbeads were produced at a flowrate of 39.3 cm^3 h^{-1} and an electrostatic potential of 6.8 kV using the initially synthesized Ag/alginate colloid solution (3.9 mM silver concentration), and colloid solutions diluted with 1.9 % w/v Na-alginate to yield silver concentrations of 2 and 1.5 mM, and 1.9 % w/v Na-alginate as a control.

The effects of the electrostatic extrusion on the further reduction of Ag^+ possibly remaining in the alginate solution after the electrochemical synthesis were examined by extrusion of the Ag/alginate colloid solution at different applied electrostatic potentials in the range 0–7.5 kV and measurements of the absorbance at 405 nm.

Characterization of Ag/alginate nanocomposites

UV–Vis Spectroscopy. The presence of AgNPs in alginate colloid solutions and nanocomposite microbeads upon dissolution in 0.05 M sodium citrate (0.1 g of microbeads in 1 cm^3 of sodium citrate) was confirmed using a UV-3100 spectrophotometer (Mapada, Japan). In addition, the possible effects of Na-citrate on the AgNP concentration were examined by measuring the absorbance at a wavelength of 405 nm of a mixture of the initially synthesized Ag/alginate colloid solution (3.9 mM silver concentration) and 0.05 M sodium citrate in the volume ratio 1:9 every 10 min during 1 h.

Silver concentration. The concentration of silver in the Ag/alginate microbeads was determined after oxidation of all the AgNPs by addition of excess concentrated nitric acid (65 %) (10–15 cm^3 of the acid per 1 g of microbeads). Concentration of Ag^+ in the solutions was then determined at a four-digit accuracy by atomic absorption spectrometry (AAS) using a Perkin Elmer 3100 instrument (Perkin Elmer, MA, USA).

Optical microscopy. Diameters of microbeads were determined from measurements of at least 20 microbeads using an optical microscope (Olympus CX41RF, Tokyo, Japan) with the image analysis program "CellA" (Olympus, Tokyo, Japan).

Biomechanical characterization of the Ag/alginate microbeads under bioreactor conditions

Biomechanical properties of packed beds of Ag/alginate microbeads prepared from colloid solutions with silver concentrations of 1.5, 2, and 3.9 mM were investigated in a biomimetic bioreactor with dynamic compression[31] as described previously.[24] Packed beds of 1.9 % w/v Ca-alginate microbeads served as a control. The compression tests were performed simultaneously in 3 cartridges loaded with microbeads (≈0.6 g in each) at 3 mm initial bed height, filled with distilled water and repeated at least 3 times for each microbead group. The tests were performed at 10 % strain in two regimes: at a loading rate of 337.5 μm s^{-1} and at sequential increments of 50-μm displacement every 30 min. Compression and equilibrium unconfined compression moduli were determined from the slopes of the best linear fits of the obtained stress–strain relationships.

RESULTS AND DISCUSSION

Production of alginate colloid solutions with AgNPs

Alginate colloid solutions with AgNPs were successfully produced by electrochemical synthesis as described previously.[16–18] In the present work, the pos-

2012 Copyright (CC) SCS

sibilities for sterilization and dilution of the obtained colloid solution with retention of AgNPs, required for potential biomedical uses, were investigated. The initially synthesized Ag/alginate colloid solution with 3.9 mM concentration of silver was diluted with 1.9 % w/v Na-alginate yielding colloid solutions with different concentrations of AgNPs. Sterilization by boiling for 30 min of the initial and a diluted colloid solution (silver concentration of 1 mM) was shown to stabilize even further the nanoparticles, as indicated by the UV-vis absorption spectra. Specifically, the absorption spectra of all the corresponding samples exhibiting surface plasmon absorption band maxima at the wavelength of ≈405 nm were not significantly different (Fig. 1). Maximal absorbance at this wavelength corresponds to AgNPs with the diameter of about 20 nm based on theoretical predictions of the surface plasmon absorption band for spherical AgNPs suspended in water.[32] Indeed, the diameters of the electrochemically synthesized AgNPs in alginate solutions were in the range 10 to 30 nm as determined previously by transmission electron microscopy.[18] Furthermore, the maximum absorbance value slightly increased by about 10 % upon sterilization, implying a slight further reduction of Ag^+ and/or nanoparticle stabilization (Fig. 1). These results are consistent with the method of AgNP synthesis by reduction of Ag^+ in alginate solutions by heating at 90 °C for 1 h, where alginate was shown to be not only a nanoparticle stabilizer, but also a reducing agent.[15]

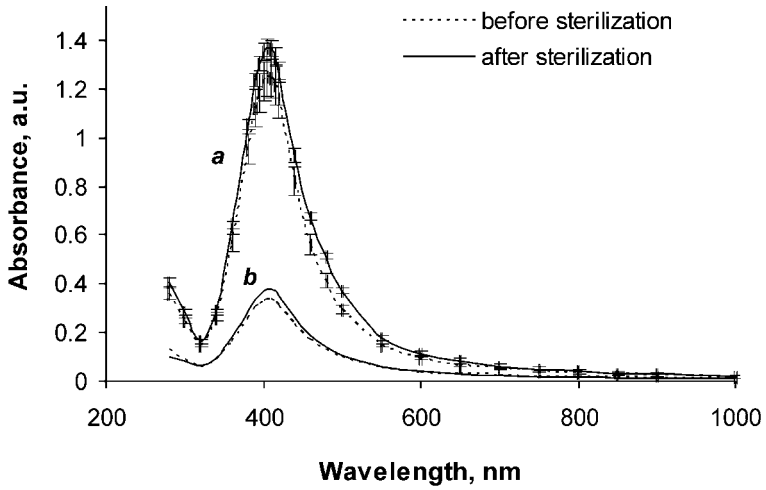

Fig. 1. Absorption spectra of a) initial Ag/alginate colloid solution (3.9 mM silver concentration) and b) 3.9-fold diluted Ag/alginate colloid solution (1 mM silver concentration) before and after sterilization by boiling for 30 min (the data represent the average of $n = 3$; standard deviations (<10 %) are omitted from the graph for data b in order for the spectra to be distinguishable).

2012 Copyright (CC) SCS

Furthermore, dilution of the Ag/alginate colloid solution did not affect the AgNPs as confirmed by the UV-vis spectra that showed unchanged surface plasmon absorption band maxima at ≈405 nm (Fig. 1). In addition, the absorbance values at a wavelength of 405 nm of a series of diluted colloid solutions showed a linear dependence on the concentration of silver nanoparticles/ions ($r^2 > 0.99$), indicating preservation of the AgNPs (Fig. 2).

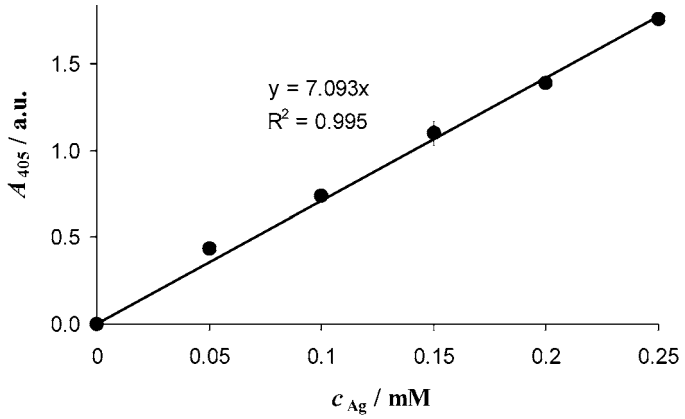

Fig. 2. UV–Vis Spectrometric analysis of Ag/alginate colloid solutions diluted with 1.9 % w/v Na-alginate: absorbance at a wavelength of 405 nm, A_{405}, as a function of the concentration of silver nanoparticles/ions in diluted solutions, c_{Ag} (the data represent an average of $n \geq 3$).

Production of nanocomposite alginate microbeads with incorporated AgNPs

Effects of the electrostatic extrusion parameters. Nanocomposite alginate microbeads with incorporated AgNPs were produced by electrostatic extrusion of Ag/alginate colloid solutions having different silver concentrations. The AgNPs were retained during the microbead production process as revealed by UV–Vis spectrometry as described earlier[18] (Fig. 3, inset). The value of the absorbance maximum positioned at ≈405 nm was even higher for the nanocomposite microbeads as compared to that of the initial colloid solution, implying a higher concentration of AgNPs. In this study, this result and the possibility that Ag^+ ions possibly retained in the Ag/alginate colloid solution were reduced during the electrostatic extrusion process and dilution of the microbeads in sodium citrate were examined. However, the absorbance values at a wavelength of 405 nm determined for Ag/alginate colloid solution extruded at different electrostatic potentials up to 7.5 kV remained constant (1.0±0.1). Moreover, the addition of sodium citrate to Ag/alginate colloid solution was shown to induce negligible effects on the absorbance measured at 405 nm (≈2 %). However, measurements of the concentration of silver nanoparticles/ions in the microbeads by AAS confirmed higher concentrations in the microbeads as compared to the corresponding source Ag/alginate solutions (Fig. 3). It can be seen that concentration of silver nanopar-

2012 Copyright (CC) SCS

ticles/ions in Ag/alginate microbeads was on average ≈20 % higher than that in the corresponding source colloid solution with the exception of the lowest initial concentration of 0.5 mM, for which the measured concentration in the microbeads was significantly lower (0.3±0.1 mM). These results could be explained by the combined effects of mass losses during the extrusion, which were measured in this study to be up to 35 %, and contraction of the alginate gel during gelation, as reported in the literature[33] inducing higher silver concentrations in microbeads as compared to the source colloid solutions. Yet, it should also be noted that some experimental errors are introduced during sampling of the microbeads due to the very rapid water evaporation from the bead surfaces.

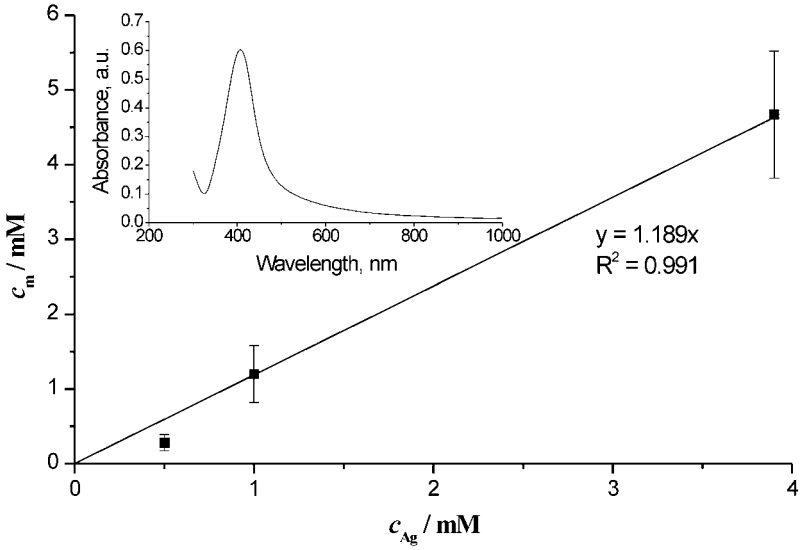

Fig. 3. Concentration of silver nanoparticles/ions in microbeads, c_m, as a function of the concentration in the corresponding source Ag/alginate colloid solutions, c_{Ag}; inset: absorption spectrum of dissolved Ag/alginate microbeads showing the absorbance maximum at a wavelength of ≈405 nm (the data represent an average of $n \geq 3$).

Overall, these results convincingly demonstrate that practically all the initial Ag^+ ions were reduced during the electrochemical synthesis of AgNPs, which were further retained during the electrostatic extrusion.

An investigation of the effects of the electrostatic extrusion parameters on the size of the obtained Ag/alginate microbeads showed the strong effects of the electrostatic potential (Fig. 4). Simultaneously, the effects of the variation of the flowrate, in the investigated experimental range, were negligible (*STD* < 4 %, data not shown). The dependence of the microbead diameter on the applied potential was modeled by Eqs. (1)–(3) using the determined value for the density of the Ag/alginate colloid solution of 1026±2 kg m^{-3} and for the surface tension

2012 Copyright (CC) SCS

of 0.074 N m^{-1},[30] and a needle diameter of 0.337 mm (for a 23 gauge needle). The model predictions were in qualitative agreements with the experimental data (Fig. 4) but predicting a to some extent sharper decrease in the microbead diameter in the region of the critical electrostatic potential (approximately in the range 4–5 kV, Fig. 4). The modeling results could be explained by the hypothesis regarding the surface tension changes during the extrusion process, as reported previously.[30] In the region of applied potentials lower than the critical value ($U < U_c$), the surface tension of the liquid decreases due to repulsion of the charged molecules at the droplet surface that causes a decrease in the droplet diameter as well. However, in the region of the higher potential values ($U > U_c$), the increased liquid velocity may induce an increase in the surface tension and consequently, an increase in the droplet size as compared to the model predictions based on a constant surface tension value, which is consistent with the results presented herein (Fig. 4).

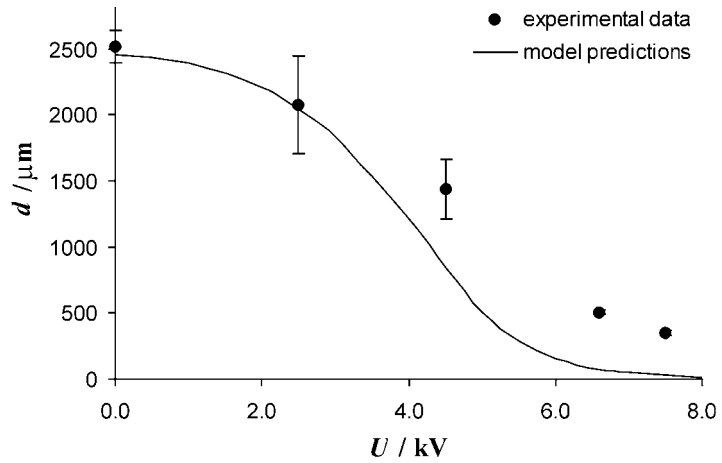

Fig. 4. Diameter of Ag/alginate microbeads as a function of the applied electrostatic potential: experimental data and model predictions.

It should be added that under the same electrostatic extrusion conditions used for production of microbeads for biomechanical characterization, the presence of AgNPs in Ag/alginate colloid solutions in the concentration range up to 3.9 mM did not influence the microbead diameter as compared to the control 1.9 % w/v Na-alginate solution amounting to ≈600 μm (600±40 μm).

Biomechanical characterization of Ag/alginate microbeads under bioreactor conditions

Biomechanical properties of packed beds of nanocomposite microbeads with different concentrations of incorporated AgNPs (1, 1.5 and 3.9 mM concentrations in the source colloid solutions) were examined in a biomimetic bioreactor

2012 Copyright (CC) SCS

while packed bed of 1.9 % w/v Ca-alginate microbeads served as a control. The experiments were performed under dynamic compression at 10 % strain in two regimes: at a loading rate of 337.5 μm s^{-1} and at sequential increments of 50-μm displacement every 30 min. All microbeads exhibited similar approximately linear responses to the dynamic loading although the values determined for the control microbeads were slightly lower than those of Ag/alginate microbeads (Fig. 5a). Values of compression moduli determined from the slopes of the best stress–strain linear fits were 141±2 and 154±4 kPa, for packed beds of the control and of the Ag/alginate microbeads, respectively. On the other hand, the equilibrium stresses determined at sequential strains after 30 min pauses were significantly different for the control and Ag/alginate microbeads (Fig. 5b), yielding equilibrium unconfined compression moduli of 47±1 and 34±2 kPa, respectively.

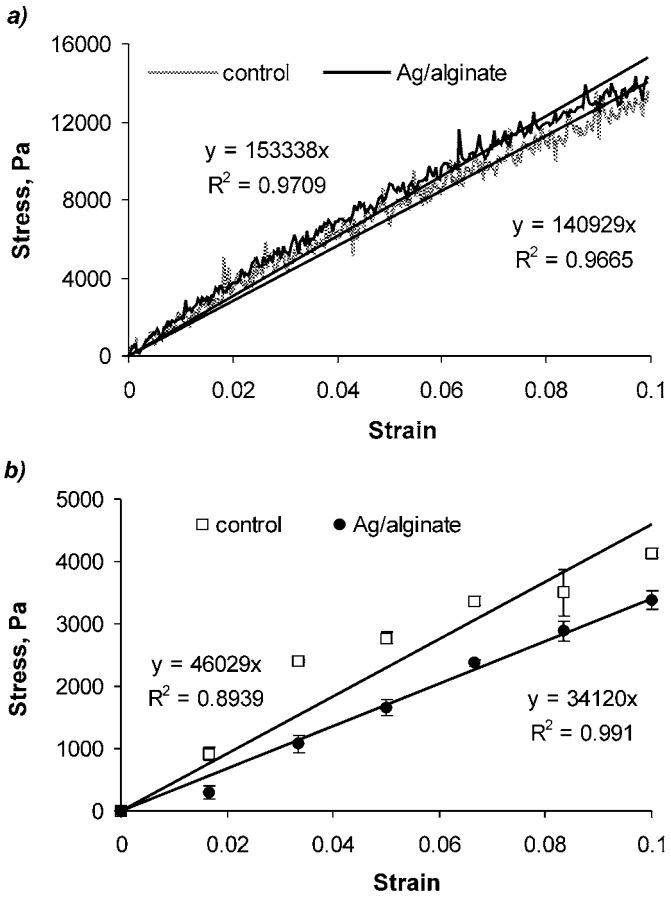

Fig. 5. Stress–strain relationships for packed beds of Ag/alginate and control alginate microbeads: a) at a loading rate of 337.5 μm s^{-1}; b) for sequential increments of 50 μm (the data represent an average of $n = 3$).

2012 Copyright (CC) SCS

The values of compression moduli determined in this study for packed beds of the control alginate microbeads (1.9 % w/v Ca-alginate) were slightly higher than those determined in a previous study for packed beds of 2 % w/v Ca-alginate microbeads (compression modulus of 141±2 *vs.* 111±8 kPa, respectively, and equilibrium unconfined compression modulus of 47±1 *vs*. 32±0.4 kPa, respectively).[24] These result can be attributed to the significantly smaller microbeads used in the present study (600±30 μm) as compared to those used in the previous study (780±30 μm), which is consistent with the influence of entrapped water within a packed bed, as reported previously.[24] It could be assumed that the packed bed of smaller microbeads retains water more efficiently in the smaller interstitial channels, which contributes to the mechanical properties of the bed.

The slight effects of the presence of AgNP on mechanical properties of alginate microbeads are consistent with weak interactions of the nanoparticles with the polymer chains. Thus, the phase transition, thermosensitivity and viscoelasticity of the polymer gel were reported to remain unchanged.[34] The presence of AgNPs in the alginate microbeads apparently induced a slight increase in the dynamic compression modulus but a decrease in the equilibrium unconfined compression modulus (Fig. 5). These results imply that under dynamic conditions, the AgNPs induced a higher retention of water within the hydrogel matrix, while when the hydrogels were provided with time to relax, negative effects of the AgNPs on the hydrogel strength were revealed. In addition, although the influence of the presence of nanoparticle could be distinguished with respect to the control alginate hydrogel, effects of the AgNP concentration in the investigated range (1.5–3.9 mM) could not be perceived. These results are in agreement with reported effects of AgNPs at low concentrations (< 1 wt. %) incorporated within poly(vinyl alcohol) (PVA) hydrogels.[35] Specifically, the addition of AgNPs was shown to induce an abrupt increase in the elastic modulus of the hydrogel, which then remained constant as the AgNP concentration was increased up to 0.8 wt. %. On the contrary, during the stress relaxation, Ag/PVA nanocomposites exhibited reduced stability as compared to pure PVA hydrogels. These results were explained by interactions of nanoparticles with polymer chains inducing immobilization of interfacial regions and enhanced stiffness during loading. However, loading also induced debonding of the nanoparticles, which allowed easier structural rearrangements of polymer chains during the stress relaxation,[35] which is consistent with the lower equilibrium unconfined compression modulus determined in the present study for nanocomposite microbeads as compared to that of the controls.

CONCLUSIONS

Silver nanoparticles were successfully produced in alginate solutions by electrochemical synthesis resulting in stable colloid sols, which were shown in

2012 Copyright (CC) SCS

this study to be suitable for sterilization, dilution and electrostatic extrusion to obtain nanocomposite alginate microbeads. It was demonstrated that practically all Ag^+ added to the alginate solution are reduced during the electrochemical synthesis, indicating the high efficiency of this production method. Furthermore, AgNPs were preserved during manipulation and gelation of the Ag/alginate colloid sol, yielding even higher concentrations in the nanocomposite microbeads by about 20 % as compared to the source colloid solutions. Incorporation of AgNPs in alginate microbeads slightly affected the biomechanical properties of the packed beds determined in a biomimetic bioreactor, strengthening the gel under dynamic compression (by about 9 %) but inducing easier polymer restructuring during relaxation and a lowering of the equilibrium unconfined compression modulus (by about 27 %). Results of these studies imply that Ag/alginate nanocomposite microbeads as well as the production method based on the electrochemical synthesis of AgNPs and electrostatic extrusion of the obtained colloid solutions are suitable for utilization in pharmaceutical and biomedical applications.

Acknowledgement. This work was supported by the Ministry of Education, Science and Technological Development of the Republic of Serbia (Grant III 45019, Eureka E!6749).

И З В О Д

КОНТРОЛИСАНО ДОБИЈАЊЕ АЛГИНАТНИХ НАНОКОМПОЗИТА СА ИНКОРПОРИСАНИМ НАНОЧЕСТИЦАМА СРЕБРА У ЦИЉУ БИОМЕДИЦИНСКЕ ПРИМЕНЕ

ЈАСМИНА СТОЈКОВСКА, ЈОВАНА ЗВИЦЕР, ЖЕЉКА ЈОВАНОВИЋ, ВЕСНА МИШКОВИЋ-СТАНКОВИЋ и БОЈАНА ОБРАДОВИЋ*

Технолошко–металуршки факултет, Универзитет у Београду, Карнегијева 4, 11000 Београд

У овом раду је испитиван процес добијања електростатичком екструзијом нанокомпозитних алгинатних микрочестица са инкорпорисаним електрохемијски синтетисаним наночестицама сребра у погледу потенцијала за примену у фармацији и биомедицини. Показало се да током електрохемијске синтезе наночестица долази до практично потпуне редукције Ag јона присутних у почетном раствору, дајући на тај начин стабилне Ag/алгинатне колоидне растворе. Показано је затим, да су ови раствори погодни за стерилизацију, манипулацију, као и електростатичку екструзију уз задржавање и очување наночестица. Присуство наночестица сребра у колоидним растворима није имало утицај на величину добијених Ag/алгинатних микрочестица која је претежно била одређена вредношћу примењеног електростатичког напона током екструзије. Са друге стране, инкорпорација наночестица сребра унутар алгинатног хидрогела је узроковала мале промене биомеханичких карактеристика које су одређене у биомимичном биореактору. Наиме, модул еластичности пакованих слојева нанокомпозитних Ag/алгинатних микрочестица одређен при динамичкој компресији је био нешто већи него код пакованог слоја контролних алгинатних микрочестица (154±4 и 141±2 kPa, редом) док је равнотежни модул еластичности слојева нанокомпозитних микрочестица био значајно мањи (34±2 и 47±1 kPa, редом).

(Примљено 8. новембра, ревидирано 15. децембра 2012)

2012 Copyright (CC) SCS

REFERENCES

1. R. M. Slawson, M. I. Van Dyke, H. Lee, J. T. Trevors, *Plasmid* **27** (1992) 72
2. R. Bhattacharya, P. Mukherjee, *Adv. Drug Delivery Rev.* **60** (2008) 1289
3. I. Armentano, M. Dottori, E. Fortunati, S. Mattioli, J. M. Kenny, *Polym. Degrad. Stab*. **95** (2010) 2126
4. D. R. Monteiro, L. F. Gorup, A. S. Takamiya, A. C. Ruvollo-Filho, E. R. Camargo, D. B. Barbos, *Int. J. Antimicrob. Agents* **34** (2009) 103
5. A. Travan, C. Pelillo, I. Donati, E. Marsich, M. Benincasa, T. Scarpa, S. Semeraro, G. Turco, R. Gennaro, S. Paoletti, *Biomacromolecules* **10** (2009) 1429
6. S. T. Dubas, S. Wacharanad, P. Potiyaraj, *Colloid. Surf., A* **380** (2011) 25
7. V. K. Sharma, R. A. Yngard, Y. Lin, *Adv. Colloid Interface Sci*. **145** (2009) 83
8. Y. M. Mohan, K. Lee, T. Premkumar, K. E. Geckeler, *Polymer* **48** (2007) 158
9. A. D. Augst, H. J. Kong, D. J. Mooney, *Macromol. Biosci*. **6** (2006) 623
10. Y. Qin, *Int. Wound J.* **2** (2005) 172
11. S. T. Dubas, V. Pimpan, *Mater. Lett*. **62** (2008) 3361
12. S. Y. Seo, G. H. Lee, S. G. Lee, S. Y. Jung, J. O. Lim, J. H. Choi, *Carbohydr. Polym.* **90** (2012) 109
13. P. Marie Arockianathan, S. Sekara, S. Sankara, B. Kumaran, T. P. Sastry, *Carbohydr. Polym.* **90** (2012) 717
14. Y. Liu, S. Chen, L. Zhong, G. Wu, *Radiat. Phys. Chem*. **78** (2009) 251
15. S. Sharma, P. Sanpui, A. Chattopadhyay, S. S. Ghosh, *RSC Advances* **2** (2012) 5837
16. B. Obradovic, V. Miskovic-Stankovic, Z. Jovanovic, J. Stojkovska, (Faculty of Technology and Metallurgy, University of Belgrade), Serbia, Patent application No. P-2010/ /0499 (2010)
17. B. Obradovic, J. Stojkovska, Z. Jovanovic, V. Miskovic-Stankovic, *J. Mater. Sci. Mater. Med.* **23** (2012) 99
18. Z. Jovanovic, J. Stojkovska, B. Obradovic, V. Miskovic-Stankovic, *Mat. Chem. Phys*. **133** (2012) 182
19. M. F. A. Goosen, E. S. C. Mahmud, A. S. M-Ghafi, H. A. M-Hajri, Y. S. Al-Sinani, B. Bugarski, in *Immobilization of Enzymes and Cells*, G. F. Bickerstaff, Ed., Humana Press, Totowa, NJ, 1997, p. 167
20. V. A. Nedovic, B. Obradovic, I. Leskosek-Cukalovic, G. Vunjak-Novakovic, in *Engineering and Manufacturing for Biotechnology,* P. H. Thonart, M. Hofman, Eds., Kluwer Academic Publisher, Dordrecht, The Netherlands, 2001, p. 277
21. B. Obradovic, D. Bugarski, M. Petakov, G. Jovcic, N. Stojanovic, B. Bugarski, G. Vunjak-Novakovic, in *Progress in Advanced Material Processes,* D. P. Uskokovic, S. K. Milonjic, D. I. Rakovic, Eds., *Mater. Sci. Forum* **453–454** (2004) 549
22. A. Osmokrovic, B. Obradovic, D. Bugarski, B. Bugarski, G. Vunjak-Novakovic, *FME Trans.* **34** (2006) 65
23. B. Obradovic, A. Osmokrovic, B. Bugarski, D. Bugarski, G. Vunjak-Novakovic, in *Research Trends in Contemporary Materials Science*, D. P. Uskokovic, S. K. Milonjic, D. I. Rakovic, Eds., *Mater. Sci. Forum* **555** (2007) 417
24. J. Stojkovska, B. Bugarski, B. Obradovic, *J. Mater. Sci. Mater. Med.* **21** (2010) 2869
25. T. Keshavartz, G. Ramsden, P. Phillips, P. Mussenden, C. Bucke, *Biotech. Tech.* **6** (1992) 445.
26. B. Bugarski, Q. Li, M. F. A. Goosen, *AIChE J.* **40** (1994) 1026

2012 Copyright (CC) SCS

27. V. Manojlovic, J. Djonlagic, B. Obradovic, V. Nedovic, B. Bugarski, *J. Chem. Technol. Biotechnol.* **81** (2006) 505
28. D. Poncelet, V. G. Babak, R. J. Neufeld, M. Goosen, B. Bugarski, *Adv. Colloid Interface Sci*. **79** (1999) 213.
29. D. Poncelet, R. J. Neufield, M. F. A. Goosen, B. Bugarski, V. Babak, *AIChE J*. **45** (1999) 2018
30. B. Bugarski, B. Obradovic, V. A. Nedovic, M. F. A. Goosen, in *Finely dispersed particles: Micro-, Nano-, and Atto-Engineering*, J. P. Hsu, A. Spasic, Eds., CRC Press, Boca Raton, FL, USA, 2006, p. 869
31. M. Petrovic, D. Mitrakovic, B. Bugarski, D. Vonwil, I. Martin, B. Obradovic, *Chem. Ing. Chem. Eng. Q*. **15** (2009) 41
32. A. Slistan-Grijalva, R. Herrera-Urbina, J. F. Rivas-Silva, M. Avalos-Borja, F. F. Castillon-Barraza, A. Posada-Amarillas,. *Physica, E* **27** (2005) 104
33. N. M. Velings, M. M. Mestdagh, *Polym. Gels Network* **3** (1995) 311
34. P. Schexnailder, G. Schmidt, *Colloid Polym. Sci.* **287** (2009) 1
35. Z. H. Mbhele, M. G. Salemane, C. G. C. E. van Sittert, J. M. Nedeljkovic, V. Djokovic, A. S. Luyt, *Chem. Mater.* **15** (2003) 5019.

2012 Copyright (CC) SCS

Journal of the Serbian Chemical Society
JSCS-info@shd.org.rs • www.shd.org.rs/JSCS
J. Serb. Chem. Soc. 77 (12) 1723–1733 (2012)
JSCS–4384
UDC *Chitosan+678.742–.31:67.017:620.01:62–416
Original scientific paper

Processing and nanomechanical properties of chitosan/poly(ethylene oxide) blend films

JELENA D. DJOKIĆ, ALEKSANDAR KOJOVIĆ, DUŠICA STOJANOVIĆ, ALEKSANDAR MARINKOVIĆ#, GORAN VUKOVIĆ, RADOSLAV ALEKSIĆ and PETAR S. USKOKOVIĆ*

Faculty of Technology and Metallurgy, University of Belgrade, Karnegijeva 4, 11120 Belgrade, Serbia

(Received 21 November, revised 10 December 2012)

Abstract: Chitosan-based films have found increasing implementation in a variety of fields, among which are as drug delivery carriers, in the packaging industry and as water purification filters. Therefore, in order to achieve mechanical integrity of such films while preserving processability and biocompatibility, chitosan-based films are fabricated in the forms of blends with poly(ethylene oxide) (PEO). A nano-indentation study was undertaken in order to investigate the nanomechanical properties and surface morphology of chitosan films in blends with various content of PEO. The results of differential scanning calorimetry, water uptake and nano-indentation revealed that films with an 80/20 blend ratio of chitosan/PEO showed the optimal values of reduced modulus and hardness. It appears that the incorporation of the synthetic PEO in chitosan films could lower the manufacturing costs while preserving the mechanical integrity of the films.

Keywords: chitosan; poly(ethylene oxide); polymer blend film; nano-indentation.

INTRODUCTION

The biopolymer chitosan has attracted increased interest in the past few decades due to its biodegradability and non-toxicity,[1] and containing free hydroxyl and amino groups, chitosan shows functional versatility, such as antimicrobial activity,[2] the ability to bind metal ions from solution,[3] and as a drug release carrier.[4] Significant work has been undertaken to fabricate multifunctional materials based on chitosan in the form of films, fibers, beads and hydrogels, which

* Corresponding author. E-mail: puskokovic@tmf.bg.ac.rs
# Serbian Chemical Society member.
doi: 10.2298/JSC121121139D

Available online at shd.org.rs/JSCS/

2012 Copyright (CC) SCS

are designed for use in disease treatment,[5] drug release,[4,6,7] removal of metal ions[3,8–10] as well as for the production of antimicrobial food packaging.[2,11]

Widespread use of chitosan is limited mainly due to its relatively high cost compared to synthetic polymers, yellowish color that occurs over time and poor barrier properties.[12] A practical way to improve these properties and add new functionalities to chitosan-based materials is blending with low production cost synthetic polymers,[13] such as poly(ethylene oxide) (PEO) that improves processability and mechanical properties[14] and does not significantly affect the binding properties of metals from aqueous solutions and the antimicrobial properties of films, while reducing the water vapor permeability of films.[9,10]

The synthetic polymer PEO, which is partially crystalline, biodegradable and soluble in water with the capacity to build hydrogen bonds, is widely used in the pharmaceutical and cosmetic industries, in the manufacture of paint and paper and in biomedical applications. Recently, its use in the fields of polymer membranes, solid electrolytes, hydrogels and pharmaceutical applications as drug carrier have become of interest. However, pure PEO films have relatively poor mechanical and physical properties due to the high solubility of the polymer in water, which limits their applications.[15] These disadvantages are overcome by blending with other polymers, and since synthetic polymers are easy to produce at low costs, blends of natural and synthetic polymers may contribute to the feasibility of blend films. Films based on chitosan and PEO can provide additional functionality compared to the pure polymer films. Chitosan can enhance the mechanical properties and reduce the solubility of PEO in water; PEO may contribute to the formation of colorless flexible films. Conventional mechanical, metal-binding and antibacterial characterization of chitosan/PEO films was thoroughly performed in a series of studies by Zivanovic *et al.*[9,10,15]

However, when chitosan and its blends are used in biomaterial applications, cell/tissue interactions are initiated at the nanoscale level. Nanomechanical properties of chitosan/PEO blends are not known; and as concluded by Majd *et al.*[16] macroscopic mechanical properties do not necessarily convey the nanoscale properties of the material. Nano-indentation testing is used to characterize mechanical properties in fine spatial resolutions of materials such as fine-grained ceramics, polymers and composites, which found wide applications as biomedical implants.[17–21] Given the wide range of applications of chitosan-based materials and its partially crystalline and amorphous composition, nanomechanical information related to chitosan films, and composites reinforced with carbon nanotubes and graphenes were studied using the nano-indentation method.[22–26] Therefore, the aim of this study was to determine the surface nanomechanical properties and the optimal composition of chitosan and PEO blends and of the neat constituents in the form of thick films.

2012 Copyright (CC) SCS

EXPERIMENTAL

A low molecular weight chitosan (Sigma Aldrich) with a deacetylation degree about 81 % (average value from potentiometric titration, FTIR and elemental analysis) and a molecular weight of 154 kDa (Kuhn–Mark–Houwink–Sakurada Equation) and poly(ethylene oxide) (PEO) of molecular weight 600 kDa (ACROS Organics) were used for the fabrication of the polymer blends. The solvent was 2 wt. % acetic acid (Sigma Aldrich). A phosphate buffer was used to adjust the pH value of solution in the swelling experiments. Deionized water (DI) (18 MΩ cm) was used for solution preparation. Methanol (Sigma Aldrich) was used for additional treatment of the dried films and for removal of residual monomer and acetic acid.

Films based on chitosan and PEO were prepared by the dilution technique and the film formation was completed by solvent evaporation. First, the polymers were dissolved in 2 wt. % acetic acid in a way to gain 5 wt. % polymer solutions. The solutions were prepared with different contributions of chitosan and PEO as follows: 100/0, 80/20, 70/30, 50/50, 20/80 and 0/100 (weight ratio: chitosan/PEO). The solutions of certain fractions were mixed on a magnetic stirrer for 24 h at room temperature. Homogenized solutions of the polymers, of total weight of 20 g, were poured into 50-mm diameter Petri dishes. The samples were first dried at 30 °C for 48 h, and then in a vacuum drying oven for 8 h at 40 °C. The dried films were detached from Petri dish and treated for 24 h in water and methanol sequentially to remove any remnants of acetic acid, which could affect the pH that may affect the degradation of the films in contact with water. After treatment with methanol, all the films had retained their previous form and structure. The films were then dried in a vacuum oven under the same conditions as above.

Film thickness (μm) was determined on six films each of which was measured on average five times. For these measurements, we used an electronic digital vernier caliper PRO-Max (Fowler). Thermal properties of chitosan, PEO and their blends were determined by differential scanning calorimetry (DSC Q10, TA Instruments) under a nitrogen atmosphere (50 ml min^{-1}). To determine the melting temperature (T_m), melting enthalpy (ΔH_m) and the degree of crystallinity (X_m), samples were heated to 80 °C and kept at 80 °C for 10 min. Then, they were cooled and reheated at a rate of 10 °C min^{-1}. The melting temperatures (T_m) were measured from the second cycle as the temperature at the top of the endothermic peak, T_m(max). The melting enthalpy, ΔH_m, was determined from the area under the endothermic peak.

The static contact angles of chitosan/PEO films were measured using a DSA100 (Kruss). Samples with a circular cross-sectional diameter of 10 mm were placed on the testing board and carefully instilled with a drop of distilled water. The contact wetting angles were measured using a video camera and for each group of samples, the measurements were repeated five times. Adsorption capacity of water was determined by the degree of swelling. Specimens with mass W_0 were immersed in phosphate buffer (pH 7.4). After the desired welling time, the films were taken from the buffer, the water from the surface of the films was removed using filter paper and the weight, W_t, was recorded. The degree of swelling, Q, was calculated from the following equation:

$$Q = \left(\frac{W_t - W_0}{W_0} \right) \times 100 \quad (1)$$

The nano-indentation experiments on neat polymer films and blend films were performed using a Triboscope T950 nanomechanical testing system (Hysitron, Minneapolis, MN) equipped with Berkovich indenter type with an *in situ* imaging mode. The frequently used

2012 Copyright (CC) SCS

power law method, developed by Oliver and Pharr,[27] involves the extrapolation of a tangent to the top of the unloading curve to determine the depth (a combination of elastic and plastic displacement) over which the indenter is in contact with the specimen at the maximum load. A peak load of 2 mN was applied for all samples with a load–hold–unload of 20 s for each segment. Ten indentations were made for each sample and the average values and standard deviations are reported.

RESULTS AND DISCUSSION

DSC is a particularly useful tool to study polymer–polymer miscibility and phase-separated polymer blends. The DSC method in this study was suitable for estimating the degree of phase separation and mixing of the chitosan/PEO polymer blends and determining the change in the degree of crystallinity in the blends compared to pure polymer. The degree of crystallinity of the films (X_m) can be accurately determined from DSC analysis of the samples based on the following equations:

$$\chi_{m,PEO} = \frac{\Delta H_{m,PEO}}{\Delta H^0_{m,PEO}} \quad (2)$$

$$\chi_{m,s} = \frac{\Delta H_{m,s}}{\Delta H^0_{m,PEO}\omega_{PEO}} \quad (3)$$

where $\Delta H_{m,PEO}$ is the melting enthalpy of PEO, $\Delta H_{m,s}$ is the melting enthalpy of PEO in the blends, ω_{PEO} is the mass fraction of PEO in the blends and $\Delta H^0_{m,PEO}$ is the melting enthalpy of 100 % crystalline PEO (213.7 J g^{-1})[28] for PEO of 600 kDa molecular weight. The degree of crystallinity of the PEO, which was calculated according to Eq. (3), was 79 %, whereas those for the other films are given in Table I.

TABLE I. Result of the DSC analysis for chitosan/PEO blends

Sample	Melting temperature T_m / °C	Melting enthalpy ΔH_m / J g^{-1}	Degree of crystallinity X_m / %
CS/PEO–90/10	–	–	–
CS/PEO–80/20	61.99	30.97	43
CS/PEO–50/50	62.65	54.73	51
CS/PEO–20/80	65.23	73.56	72
CS/PEO–0/100	66.82	168.70	79

According to the data presented in Table I, blends with more than 10 wt. % PEO showed an increase in the degree of crystallinity and a decrease in the amount of amorphous phase. The increase of the degree crystallinity with increasing chitosan mass content could be assigned to a decrease in crystal growth because of the restriction of the molecular chain flexibility and the overall mobility of the blend. The progressive increase in the PEO content led to higher

2012 Copyright (CC) SCS

values of T_m and ΔH_m, which is a reflection of the higher content of crystalline PEO in the polymer blend. These changes follow approximately linear trends with the PEO content and the increase of the melting enthalpy and temperature, as well as the degree of crystallinity. These findings point to a certain amount of compatibility between chitosan and PEO due to intermolecular chain formation and primary hydrogen bond formation between the polymer chains. The dependencies of the heat flow on temperature for chitosan/PEO polymer blends with various mass fractions of the starting polymers are shown in Fig. 1. If the polymer blends show a unique melting temperature instead of the individual values for the starting components, and if the melting temperatures and enthalpy shows an increase, a change in the semi-crystalline polymer could be used as proof for the qualitative degree of mixing of the polymers in the chitosan/PEO blends.

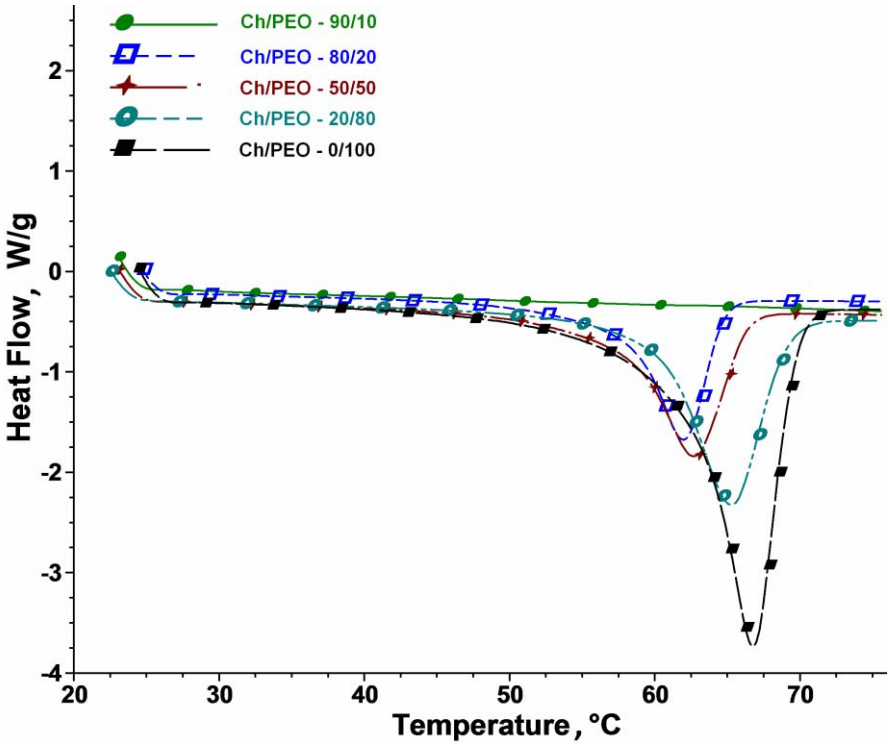

Fig. 1. Heat flow *vs*. temperature curves for chitosan/PEO blends.

PEO is a more hydrophilic polymer than chitosan. A higher content of chitosan in the blend led to water contact angles from 62.5 and 76.3° for 80/20 and 90/10 chitosan/PEO contents, respectively, and up to 81.2° for neat chitosan. It is interesting that the neat PEO films had a high contact angle (79.7°), probably due to their densely packed, low-dimension crystalline film structure, which is in-

2012 Copyright (CC) SCS

soluble and make the film surface rough and hydrophobic. Zivanovic *et al.*[15] revealed that the permeability of water vapor is lower for neat PEO than for films with a lower PEO content in chitosan. With an increased hydrophilic PEO content in chitosan, which in this case was more prone to hydratation, the water contact angle decreased, *i.e.*, the films show more hydrophilic properties – for chitosan/PEO contents of 20/80, 50/50 and 60/40, the contact angle were 59.5, 48.7 and 55.1°, respectively. For these samples, the crystalline PEO does not prevail, but more decisive is that the water-soluble polymer is introduced that increases the hydrophilic nature of the blends. In the samples where the PEO is dominant, the crystalline structure is more decisive than its water solubility.

Water uptake tests were determined through the swelling degree after 200 min (Fig. 2) and 24 h and the results were shown to be in accordance with contact angle tests. Thus, for samples of neat chitosan and the 90/10 and 80/20 chitosan/PEO ample, swelling occurred very rapidly and equilibrium was attained in about 30 min. For 70/30 and 60/40 chitosan/PEO samples, the swelling was also at first very fast, but after 20 min, peaks in the degree of swelling were observed and equilibrium was attained in about 100 min. This could be a consequence of the dissolution of certain amount of PEO that is not bonded to the interpenetrating network and to the formation of surface layer of polymer that is not hydrophilic in the contrast to ones incorporated in the main polymer structure. Although high resistance to water uptake of polymer films may be beneficial for many applications, controlled solubility is required if films are to be used as drug and antiseptic carriers, and, in general, in membrane-like structures.

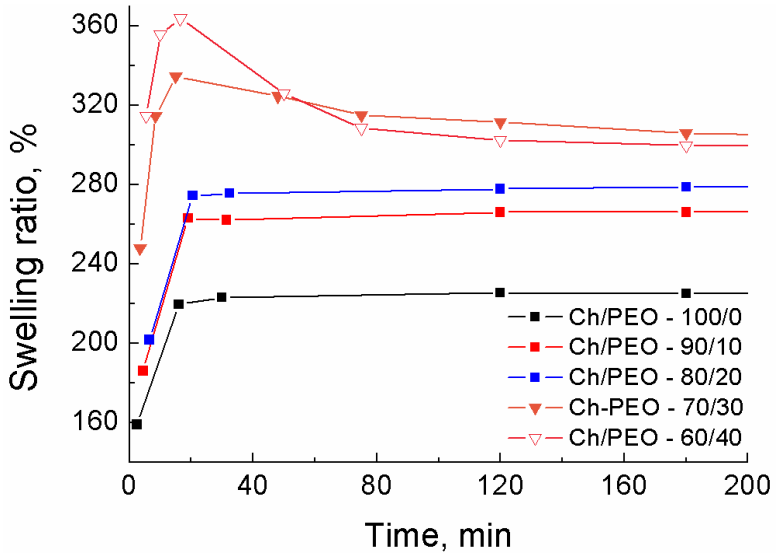

Fig. 2. Water uptake tests recorded during 200 min.

2012 Copyright (CC) SCS

The nano-indentation method was used in this study to determine the reduced modulus and hardness of neat chitosan and PEO, as well as their blends. Typical load–depth profiles of the indents, which were recorded during the indentation of films of neat PEO and the blends with various mass content of chitosan are shown in Fig, 3, which revealed that the smallest resistance to the indentation load was shown by the neat PEO film and the largest resistance was exhibited by the blend film with 80 % of chitosan. After reaching the maximal indentation force, the plateau reveals the hold time of the indenter tip, which was predicted in order to minimize the polymer creep effect.

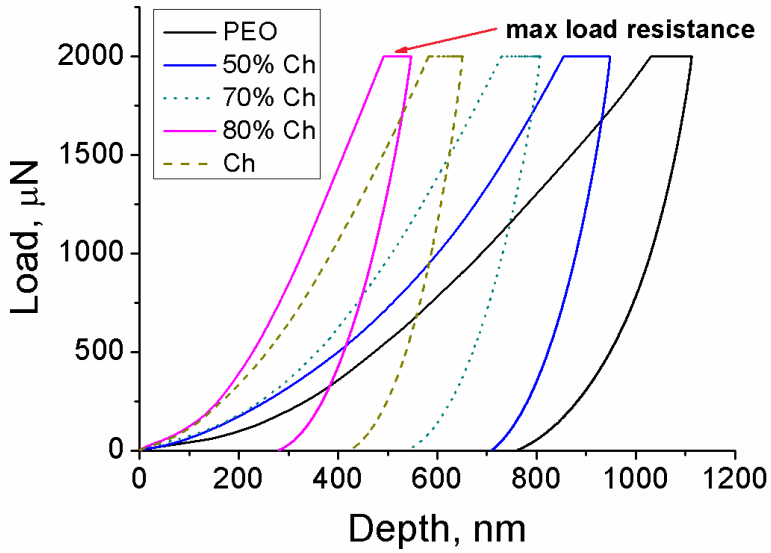

Fig. 3. Representative load–depth curves for chitosan/PEO films with various chitosan contents showing highest load resistivity of the blend film containing 80 wt. % chitosan.

The film thickness varied in the range of 353–409 μm. The indent depth did not exceed 1.1 μm; hence, it is obvious that there was no substrate influence on nano-indentation test results. Therefore, the Oliver–Pharr method appeared suitable to calculate the reduced modulus of elasticity and the hardness values. Increasing PEO content led to a decrease in the film thicknesses. This could be explained by the contractions of the 3D film matrix due to strong interactions of the chitosan and PEO molecules, the increase in crystallinity within the PEO phase and by the fact that the addition of PEO led to a decrease in the blend viscosity.

In situ imaging scans of the indent plastic imprint with the corresponding line scan and median roughness for the blend film with 20 wt. % chitosan are shown in Fig. 4. As an insert, the 3D view of the indent imprint is included in this Figure. The tested films had median surface roughness in the range 0.09–0.14 μm whereby, the greatest roughness was measured for the neat PEO film. With addi-

2012 Copyright (CC) SCS

tion of chitosan, a slight decreasing trend was registered. The samples were not polished prior to testing and the surface roughness was appropriate for the testing procedure. The selected imprint shown in Fig. 4 and the scans for the other samples revealed the absence of micro cracks at the indent corners. Line scans for the selected and the other tested sample show that there are no significant pile-up and sink-in formation of the material deposits at the indent edges. These findings together with the indentation curves without pop-in formations (Fig. 3) give confidence that the material properties derived from the nano-indentation testing could be considered as reliable.

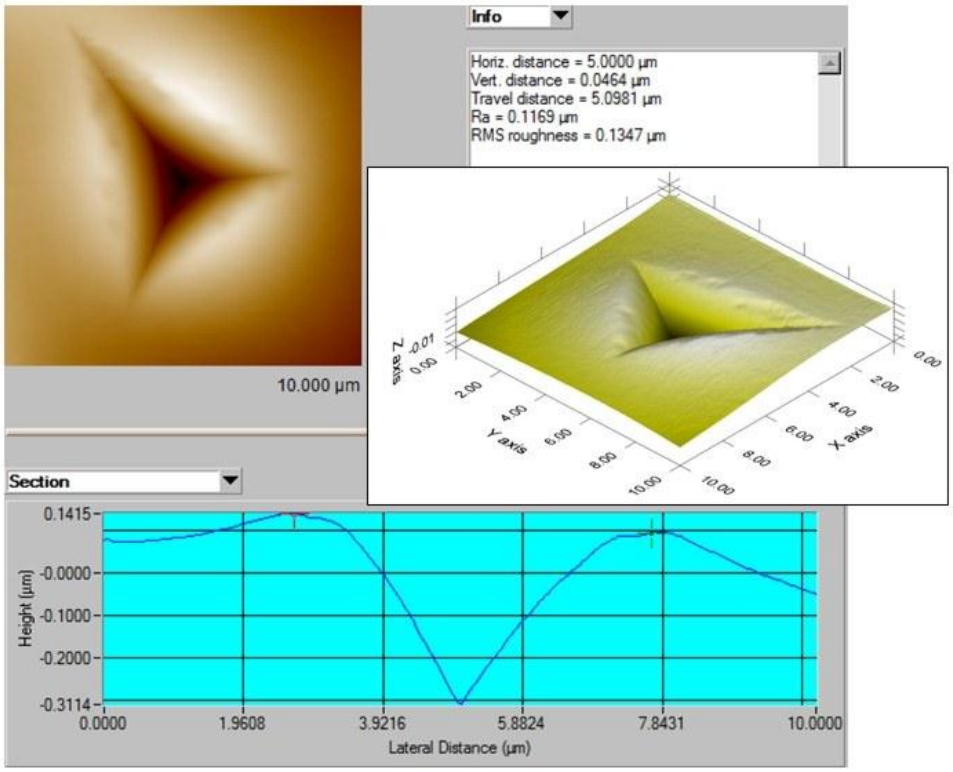

Fig. 4. 2D and 3D view (axis dimensions, µm) of the plastic nano-indentation imprint with the corresponding line scan and median roughness for the blend film with 20 wt. % of chitosan.

The average values with the range of reduced elastic modulus (E_r) and hardness (H) for PEO film samples and the appropriate blends with chitosan, the content of which was varied up to the neat chitosan sample, are shown in Fig. 5. The measured values of E_r and H of neat PEO (1.68 GPa and 0.06 GPa, respectively) are similar to the ones obtained by Nowicki *et al.*,[29] in a study that compared the nanomechanical properties of PEO with poly(vinyl chloride) and poly(acrylic

2012 Copyright (CC) SCS

acid). In the present study, 20 wt. % content of chitosan in the polymer blend led to an increase in E_r and H of about 120 and 165 %, respectively. Additional increases in the chitosan content led to modest changes in the reduced modulus and hardness. The reduced modulus and hardness of the blend increased from 4.15 and 0.19 GPa, respectively, for the blend 70/30 to 6.617 and 0.385 GPa, respectively, for the 80/20 blend. Interestingly, the reduced modulus and hardness were slightly lower for the neat chitosan films (6.57 and 0.336 GPa, respectively). It appears that the optimal configuration for the optimal nanomechanical properties is with a chitosan content of 80 wt. %. The improvement in the mechanical properties with increasing chitosan content could be explained by the addition of the stiffer chitosan phase being more decisive for the mechanical properties than degree of crystallinity of the blend.

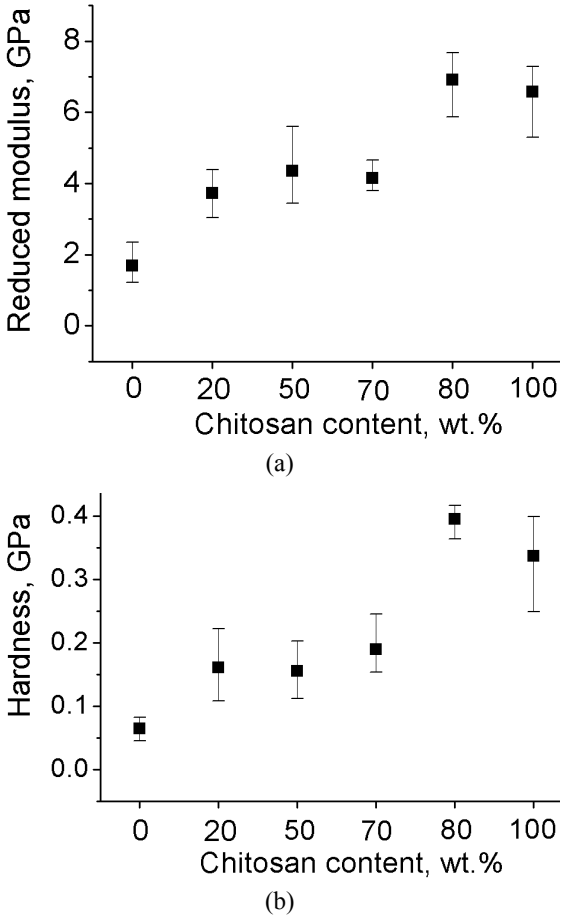

Fig. 5. Average values with error bars of a) the reduced elastic modulus and b) the hardness of blend film samples *vs*. chitosan content (wt. %).

2012 Copyright (CC) SCS

Among other positive features, chitosan materials in various architectures have a significant sorption potential for environmental protection issues as well as favorable antibacterial properties. Despite this, in most material architectures, such as film-like structures, the positive effects of chitosan may be masked if the chitosan molecules are entrapped within the volume of the surrounding material. Li *et al.*[9] argued that an increase in the surface-to-mass ratio of chitosan structures could lead to improved functionalities. In order to increase the efficiency of chitosan and maintain mechanical integrity, further work will be directed towards filters and membranes structured from chitosan nanocomposite fibers reinforced with carbonaceous structures (carbon nanotubes and graphenes) as well as natural fibers from industrial waste.

CONCLUSIONS

For certain applications, just to mention drug or antiseptic carriers and packaging materials, understanding the nanomechanical behavior of chitosan-based films should be considered when designing products. In order to enhance the production feasibility and material processability, substitution of chitosan biopolymer in certain amount by synthetic PEO could reduce the price of the blend films while still maintaining the desired functionalities. Films with 80/20 blend ratio of chitosan/PEO exhibited the best nanomechanical properties, and the trend of the overall nanomechanical results revealed that incorporation of the stiffer chitosan phase is more relevant for positive mechanical properties than the degree of crystallization of blends, which is higher when the PEO is dominant in the film composition.

Acknowledgement. The authors are grateful to the Ministry of Education, Science and Technological Development of the Republic of Serbia for the financial support through the project EUREKA E!5851.

ИЗВОД

ПРОЦЕСИРАЊЕ И НАНОМЕХАНИЧКА СВОЈСТВА ФИЛМА БЛЕНДИ ХИТОЗАН/ПОЛИЕТИЛЕН-ОКСИД

ЈЕЛЕНА Д. ЂОКИЋ, АЛЕКСАНДАР КОЈОВИЋ, ДУШИЦА СТОЈАНОВИЋ, АЛЕКСАНДАР МАРИНКОВИЋ, ГОРАН ВУКОВИЋ, РАДОСЛАВ АЛЕКСИЋ И ПЕТАР С. УСКОКОВИЋ

Технолошко–металуршки факултет Универзитет у Београду, Карнегијева 4, 11120 Београд

Филмови на бази хитозана налазе све ширу примену у разним областима између осталог као носачи лекова, у индустрији амбалаже и као филтери за пречишћавање вода. Да би се постигао механички интегритет оваквих филмова и задржала процесабилност и биокомпатибилност, филмови на бази хитозана припремљени су у форми бленди са полиетилен оксидом (PEO). Студија наноиндентације урађена је у циљу проучавања наномеханичких својстава и површинске морфологије хитозанских филмова у блендама са различитим садржајем PEO. Резултати DSC-а, апсорпције воде и наноиндентације показали су да филмови бленди са односом 80/20 хитозана и PEO поседују оптималне вредности редукованог модула еластичности и тврдоће. Показано је да дода-

2012 Copyright (CC) SCS

вање синтетичког PEO у хитозанске филмове може смањити цену производње и истовремено задржати механички интегритет филмова.

(Примљено 21. новембра, ревидирано 10. децембра 2012)

REFERENCES

1. M. N. V. R. Kumar, R. A. A. Muzzarelli, C. Muzzarelli, H. Sashiwa, A. J. Domb, *Chem. Rev.* **104** (2004) 6017
2. G. J. Tsai, W. H. Su, *J. Food Protect.* **62** (1999) 239
3. A. Gamage, F. Shahidi, *Food Chem.* **104** (2007) 989
4. Z. X. Meng, W. Zheng, L. Li, Y. F. Zheng, *Mater. Chem. Phys.* **125** (2011) 606
5. R. A. A. Muzzarelli, *Carbohydr. Polym.* **76** (2009) 167
6. J. Jin, M. Song, *J. Appl. Polym. Sci.* **102** (2006) 436
7. T. Kean, M. Thanou, *Adv. Drug Delivery Rev.* **62** (2010) 3
8. E. Selmer-Olsen, H. C. Ratnaweera, R. R. Pehrson, *Water. Sci. Tech.* **34** (1996) 33
9. J. Li, S. Zivanovic, P. M. Davidson, K. Kit, *Carbohydr. Polym.* **83** (2011) 375
10. J. Li, S. Zivanovic, P. M. Davidson, K. Kit, *Carbohydr. Polym.* **79** (2010) 786
11. M. Ye, H. Neetoo, H. Chen, *Food Microbiol.* **25** (2008) 260
12. L. Butler, P. J. Vergano, R. F. Testin, J. M. Bunn, J. L. Wiles, *J. Food Sci.* **61** (1996) 953
13. J. R. Fried, *Polymer Science and Technology*, Prentice Hall, New Jersey, USA, 1995, p. 263
14. N. Angelova, N. Manolova, I. Rashkov, V. Maximova, S. Bogdanova, A. Domard, *J. Bioact. Compat. Polym.* **10** (1995) 285
15. S. Zivanovic, J. Li, P. M. Davidson, K. Kit, *Biomacromolecules* **8** (2007) 1505
16. S. Majd, Y. Yuan, S. Mishra, W. O. Haggard, J. D. Bumgardner, *J. Biomed. Mater. Res., B* **90** (2009) 283
17. R. R. Kumar, M. Wang, *Mater. Lett.* **55** (2002) 133
18. K. Park, S. Mishra, G. Lewis, J. Losby, Z. Fan, J. B. Park, *Biomaterials* **25** (2004) 2427
19. V. Nelea, C. Morosanu, M. Iliescu, I. N. Mihailescu, *Surf. Coat. Technol.* **173** (2003) 315
20. P. S. Uskokovic, C. Y. Tang, C. P. Tsui, N. Ignjatovic, D. P. Uskokovic, *J. Eur. Ceram. Soc.* **27** (2007) 1559
21. Y. Tang, P. S. Uskokovic, C. P. Tsui, Dj. Veljovic, R. Petrovic, Dj. Janackovic, *Ceram. Int.* **35** (2009) 2171
22. A. Aryaei, A. H. Jayatissa, A. Champa Jayasuriya, *J. Mech. Behav. Biomed. Mater.* **5** (2012) 82
23. S.-F. Wang, L. Shen, W.-D. Zhang, Y.-J. Tong, *Biomacromolecules* **6** (2005) 3067
24. H. Fan, L. Wang, K. Zhao, N. Li, Z. Shi, Z. Ge, Z. Jin, *Biomacromolecules* **11** (2010) 2345
25. F. Sun, H.-R. Cha, K. E. Bae, S. Hong, J.-M. Kim, S. H. Kim, J. Lee, D. Lee, *Mater. Sci. Eng., A* **528** (2011) 6636
26. T. Wu, Y. Pan, H. Bao, L. Li, *Mater. Chem. Phys.* **129** (2011) 932
27. W. C. Oliver, G. M. Pharr, *J. Mater. Res.* **7** (1992) 1564
28. S. Aminah, M. Noor, A. Ahmad, M. Y. A. Rahman, I. A. T. Talib, *Nat. Sci.* **2** (2010) 190
29. M. Nowicki, A. Richter, B. Wolf, H. Kaczmarek, *Polymer* **44** (2003) 6599.

2012 Copyright (CC) SCS

Journal of the Serbian Chemical Society
JSCS-info@shd.org.rs • www.shd.org.rs/JSCS
J. Serb. Chem. Soc. 77 (12) 1735–1746 (2012)
JSCS–4385
UDC 536.51+546.669–31:547.441–036.7+ 535.37:546.18+539.12
Original scientific paper

Thermographic properties of Eu^{3+}- and Sm^{3+}-doped Lu_2O_3 nanophosphor

VESNA LOJPUR, ŽELJKA ANTIĆ, RADENKA KRSMANOVIĆ, MINA MEDIĆ, MARKO G. NIKOLIĆ and MIROSLAV D. DRAMIĆANIN*

Vinča Institute of Nuclear Sciences, University of Belgrade, P. O. Box 522, 11001 Belgrade, Serbia

(Received 21 October, revised 8 December 2012)

Abstract: Samples of Lu_2O_3:Eu^{3+} (3 at. % Eu) and Lu_2O_3:Sm^{3+} (1 at. % Sm), were prepared *via* the polymer complex solution method using poly(ethylene glycol) as the fuel and as nucleation agent for crystallization process. Knowing that lutetium oxide has high chemical stability and temperature resistance, in this study, the possibility for its application in high-temperature phosphor thermometry was investigated. This non-contact technique uses the thermal dependence of phosphor fluorescence to measure temperature remotely. The structural and morphological properties were investigated by X-ray powder diffraction (XRPD) analysis and transmission electron microscopy (TEM). The obtained results confirmed that this synthesis yields the desired crystalline structure with particle sizes in the range from 30 to 50 nm. Photoluminescence emission measurements were recorded in the temperature range from ambient up to 873 K. The obtained results demonstrated the performance of Eu^{3+}- and Sm^{3+}-doped Lu_2O_3 as high temperature thermographic phosphors of very good sensitivity.

Keywords: Lu_2O_3; Eu^{3+}; Sm^{3+}; thermometry; FIR; luminescence.

INTRODUCTION

Rare-earth luminescent phosphor represents a very important group of materials since they find application in biomedical multicolor imaging, scintillators, high-energy physics, lamps and display devices, *etc.*[1–5] Recently, their application as temperature sensors has become very popular. In order to obtain an optical temperature sensor with appropriate characteristics, it is necessary to choose an adequate optically active ion and a suitable host matrix. Rare earth ions, such as Eu^{3+}, Sm^{3+}, Er^{3+}, Tm^{3+}, Ho^{3+} and Nd^{3+}, are luminescent activators that have coupled energy levels required for application in optical temperature sensors. These ions accommodate easily into a variety of different host materials. It is

* Corresponding author. E-mail: dramican@vinca.rs
doi: 10.2298/JSC121021140L

Available online at shd.org.rs/JSCS/

2012 Copyright (CC) SCS

known that rare-earth sesquioxides are significant host materials due to their good chemical stability, thermal conductivity and high light output. Among them, lutetium oxide Lu_2O_3 represents a promising matrix material because of the high band gap between the valence and conduction bands (≈5.8 eV), high melting point (≈2763 K), very high mass density (≈9.42 g cm^{-3}) and large atomic number ($Z = 71$) that contributes to a high stopping power for ionizing radiation. In addition, Lu_2O_3 has a cubic bixbyite crystalline structure with space group *Ia*-3 which is isostructural with the well-known Y_2O_3 structure.[6–8]

In order to avoid potential problems that could occur during synthesis in the solid phase, such as non-homogeneity, imprecise control of the cation stoichiometry and high processing temperature, it is more convenient to use wet chemical processes, such as hydrothermal synthesis, sol–gel, spray pyrolysis, co-precipitation, combustion synthesis, pulsed vapor deposition, *etc*.[9–15] In this study, the polymer complex solution (PCS) method, which is very simple, fast and cost-effective, was used. The PCS preparation procedure provides powders composed of well crystalline and uniform in size nanoparticles, which is a prerequisite for obtaining high-quality, transparent ceramics. The utility of the polymeric approach comes from the coordination of metal cations onto the poly(ethylene glycol) (PEG) chains during the gelation process, resulting in very low cation mobility. In this way, PCS provides mixing of constituting elements at the atomic level and allows homogeneous control of very small rare earth concentrations, providing in this way, a uniform structure of the materials.[16]

Thermographic phosphors (TPs) are oxides doped with rare earth or transition metal ions that emit visible, infrared or UV radiation upon excitation from an external energy source. Their luminescent properties, such as the positions and widths of the luminescence peaks, the intensities of the luminescence lines and decay lifetimes of luminescence, change with temperature. The fluorescence intensity ratio (FIR) method is based on the intensity ratio between two emission lines or areas in the PL spectrum. This technique is flexible and successful in measuring temperatures where conventional methods employing pyrometry, thermocouples or thermistors, may prove to be unsuitable. The intensity, wavelength or lifetime (duration of light) of the detected emission is used to determine the temperature of a surface. This approach is very precise, simple, non-intrusive with a wide temperature range (from 10 to 2000 K).[17,18]

Using this technique, very good results were previously obtained by measuring and comparing peak intensities and areas in different host matrixes.[19,20] Although, according to the literature, Lu_2O_3 proved itself to be a host material that gives better luminescent properties in comparison to Y_2O_3, it has not been sufficiently studied.[21] Hence, in the present study, Lu_2O_3 doped with either 3 at. % Eu^{3+} or 1 at. % Sm^{3+} prepared by combustion synthesis were elaborated as optical temperature sensors in the range from 293 to 823 K.

2012 Copyright (CC) SCS

EXPERIMENTAL

Lutetium oxide doped with either 3 at. % Eu^{3+} or 1 at. % Sm^{3+} was fabricated by the polymer complex solution method. The starting materials, Lu_2O_3, Eu_2O_3 and Sm_2O_3 (all Alfa Aesar, 99.9 %), were appropriately measured and dissolved in hot nitric acid. To the obtained solutions, PEG (Alfa Aesar, $\overline{M}_w$ = 200) was added in a 1:1 mass ratio to the starting oxides, whereby metal–PEG solutions were formed. The solutions were continuously stirred at 80 °C for a few hours until solid complexes were formed that were subsequently combusted at 800 °C in air for 2 h, giving white powders as the resulting products.

The phase composition was investigated by X-ray powder diffraction analysis (XRPD) on a Philips PW 1050 instrument, using Ni filtered $CuK\alpha_{1,2}$ radiation. The diffraction data were recorded in the 2θ range from 10° to 120° counting for 12 s in each 0.02° step. The microstructure at the local level was analyzed by the TEM technique using a Philips/FEI CM300 electron microscope operating at 300 kV. The photoluminescence spectra were collected under the excitation light of a 450 W xenon lamp on a Fluorolog-3 model FL3-221 (Horiba Jobin-Yvon) spectroflurometer ($\lambda_{exc}(Lu_2O_3{:}Eu)$ = 393 nm and $\lambda_{exc}(Lu_2O_3{:}Sm)$ = 406 nm), elevating the temperature from ambient to 823 K in steps of 50 K.

RESULTS AND DISCUSSION

The X-ray diffraction pattern for the Lu_2O_3:3 at. % Eu sample is shown in Fig. 1. The XRD analysis confirmed that during calcination at 800 °C the sample crystallized in a cubic bixbyte crystal structure with the space group *Ia-3*. The peak positions were indexed according to the JCPDS card No. 12-0728 for the cubic Lu_2O_3 structure. The narrow peaks of high intensities imply good crystallinity of the sample.

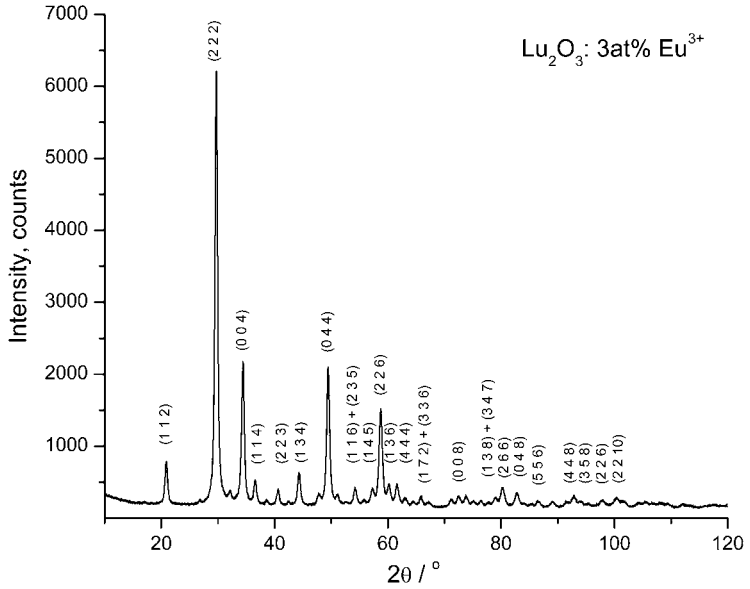

Fig. 1. XRD Pattern of Lu_2O_3:3 at. % Eu^{3+} nanopowder sample with diffraction peaks indexed according to JCPDS card No. 12-0728.

2012 Copyright (CC) SCS

The morphology of Lu_2O_3:3 at. % Eu^{3+} sample analyzed with transmission electron microscopy (TEM) is presented in Fig. 2. The micrograph revealed the presence of agglomerates that consisted of nanoparticles in the range from 30 nm to 50 nm. High-resolution TEM (HR-TEM) showed a good crystalline structure without any irregularities, which are in good agreement with results obtained in the XRD measurements.

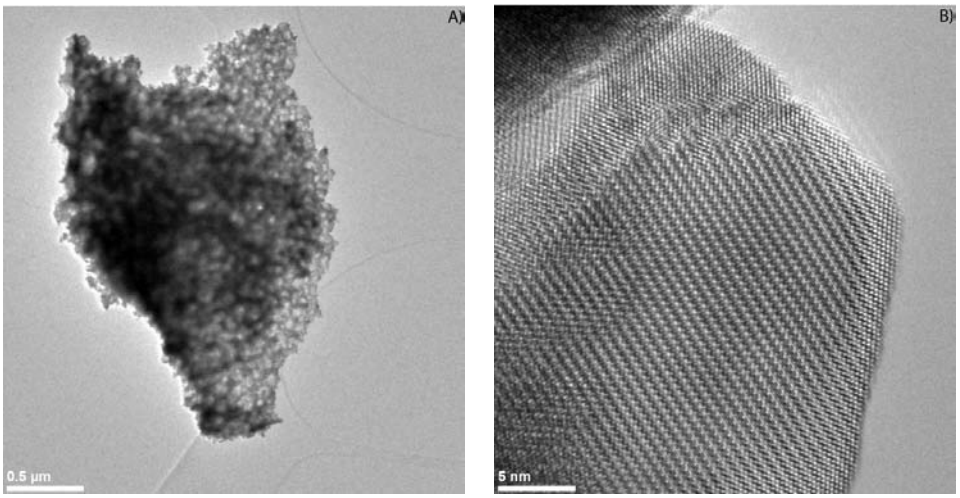

Fig. 2. Bright field image showing agglomerates of the powder sample with particle sizes ranging from 30–50 nm (A) and high-resolution images of constituting nanosized particles (B).

The FIR method is based on the selection of two emission lines from photoluminescent spectra and estimation of the temperature based on the ratio of their intensities. Two lines are considered appropriate for the intensity ratio method if they both have strong emission intensities over the whole temperature range and if their intensity ratio gives high temperature resolution.[22] This approach eliminates a number of errors arising from fluctuations of the excitation light source, temperature changes of excitation bands and non-uniform dopant concentrations. A special case of the FIR measurement technique involves using the fluorescence intensities from two closely spaced, "thermally coupled" energy levels, the relative population of which follows a Boltzmann type population distribution and is dependent on the temperature and the energy gap. Here, the ideal case was used, where the intensity of one of the emission lines is independent of temperature (internal reference); in this way, a calibration between the ratios of emissions is indicative of temperature. The main mechanism behind this phenomenon is thermalization: when two energy levels of the RE activator are closely separated by a difference of approx. 1000 cm^{-1}, the upper level will not emit fluorescence at low temperatures due to the high multi-phonon relaxation that quenches the energy.

2012 Copyright (CC) SCS

With increasing temperature, the upper level becomes more populated and therefore the fluorescence from this level gradually increases at the expense of that of the lower level population.[23] The relative population between the two levels, R, which follows a Boltzmann-type population distribution, is given by:

$$R = \frac{I_{31}}{I_{21}} = C\exp(-\frac{\Delta E}{kT}) \quad (1)$$

where k is the Boltzmann constant, $k = 0.695\,034\,76(63)$ cm^{-1} K^{-1}, and $\Delta E = E_{32}$ is the energy gap between two excited levels (upper $i = 3$, lower $i = 2$, ground $i = 1$).

The rate at which the ratio R changes with temperature represents the sensor sensitivity, S:

$$S = \left|\frac{\mathrm{d}R}{\mathrm{d}T}\right| = R\left(\frac{\Delta E}{kT^2}\right) \quad (2)$$

For Eu^{3+}, temperature could be determined using the FIR technique for the $^5D_1 \rightarrow {}^7F_1$ and $^5D_0 \rightarrow {}^7F_2$ transitions that have separation of approx. 1700 cm^{-1} (Fig. 3a). At higher temperatures, the population of the $^5D_1$ level increases at the expense of the $^5D_0$ level population, causing an enhancement of emission intensity from the $^5D_1 \rightarrow {}^7F_1$ transition. The photoluminescence emission spectra of the (Lu_2O_3):3 at. % Eu^{3+} sample under excitation of 393 nm in the temperature range from 293–823 K are presented in Fig. 3b. Four characteristic emission bands from Eu^{3+} localized at around 580, 593, 611, 656 and 708 nm can be assigned to the $^5D_0 \rightarrow {}^7F_i$ (i = 0, 1, 2, 3 and 4) spin forbidden f–f transitions, respectively. The peak at 533 nm can be assigned to the $^5D_1 \rightarrow {}^7F_1$ transition. Obviously, at higher temperatures, the intensities of the emission band strongly decrease.

Dependence of emission intensities at 533, 580, 593 and 611 nm with temperature for Lu_2O_3:3 at. % Eu^{3+} sample are presented in Fig. 4. It is obvious that the peaks centered at 533, 580 and 593 nm are independent of temperature, while the peak centered at 611 nm gradually decreases with increasing temperature and exhibits a maximum value at 300 K.

The FIR relation was checked by recording the emission spectra at different temperatures from 293 to 823 K and the results are shown in Fig. 5. From the fit of these experimental data according to Eq. (1), the values $C = 3.06$ and $\Delta E =$ $= 1596$ cm^{-1} were found, with a goodness of fit $R^2 = 0.9993$. The maximum sensor sensitivity calculated according to Eq. (2) is approximately 6×10^{-4} K^{-1} at 823 K.

In the case of the Lu_2O_3:1 at. % Sm^{3+} sample, a schematic representation of the characteristic transitions is provided in Fig. 6a. Photoluminescence emission spectra of the sample under excitation of 406 nm in the temperature range from 293–823 K are presented in Fig. 6b. Three emissions at 578, 608 and 656 nm are

2012 Copyright (CC) SCS

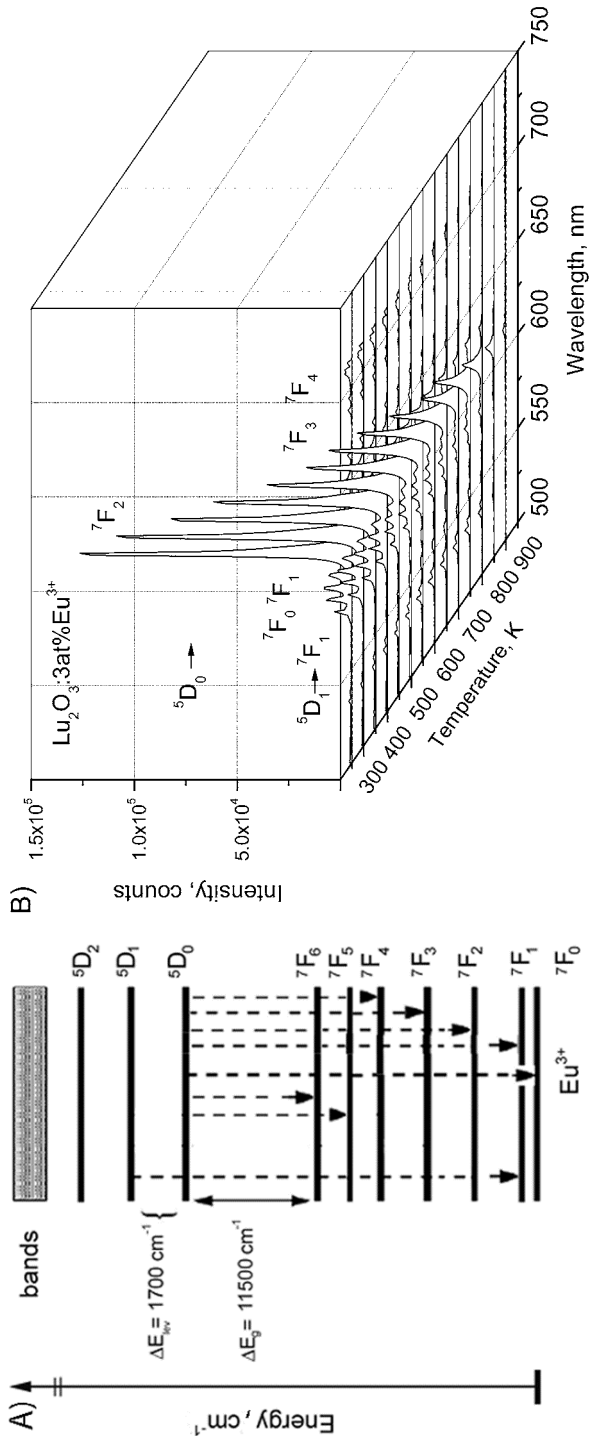

Fig. 3. Energy level diagram for Eu^{3+} (A) and emission spectra at elevated temperatures (B).

2012 Copyright (CC) SCS

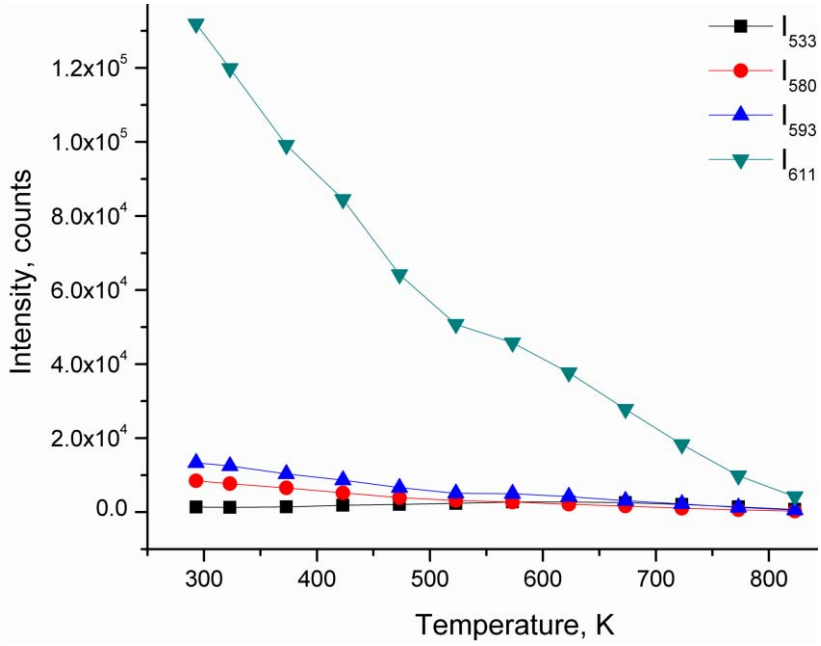

Fig. 4. Temperature dependant variations of the selected peaks' intensity centered at 533, 580, 593 and 611 nm for Lu_2O_3:3 at. % Eu^{3+} sample. The sizes of the symbols represent the error of the measurements.

ascribed to the $^4G_{5/2} \rightarrow {}^6H_{5/2}$, $^6H_{7/2}$, $^6H_{9/2}$ transitions of Sm^{3+}, respectively. As internal reference, the $^4G_{5/2} \rightarrow {}^6H_{5/2}$ transition (emission line at 578 nm) was chosen.

The dependence of the emission intensities at 578, 608, and 656 nm on temperature for Lu_2O_3:1 at. % Sm^{3+} sample are presented in Fig. 7. In this case, the peaks centered at 608 and 656 nm gradually decreased with increasing temperature, while the peak centered at 578 nm showed irregular behavior with changing temperature.

The FIR of the emission at 578 nm relative to the emissions at 608 nm and 656 nm was checked by recording the emission spectra at different temperatures from 293 to 873 K and the results are presented in Fig. 8. From the fit of the obtained experimental data to Eq. (1), values of C = 8.02 and ΔE = 842.8 cm^{-1} were found for $^4G_{5/2} \rightarrow {}^6H_{5/2}$, $^6H_{9/2}$, and C = 4.16, ΔE = 972.4 cm^{-1} for the $^4G_{5/2} \rightarrow {}^6H_{5/2}$, $^6H_{7/2}$ transition ratio, with goodness of fits of 0.9871 and 0.9912, respectively. The maximum sensor sensitivities were approximately 3.6×10^{-3} K^{-1} at about 580 K for the $^4G_{5/2} \rightarrow {}^6H_{5/2}$, $^6H_{9/2}$ ratio and 1.6×10^{-3} K^{-1} at about 700 K for the $^4G_{5/2} \rightarrow {}^6H_{5/2}$, $^6H_{7/2}$ ratio.

2012 Copyright (CC) SCS

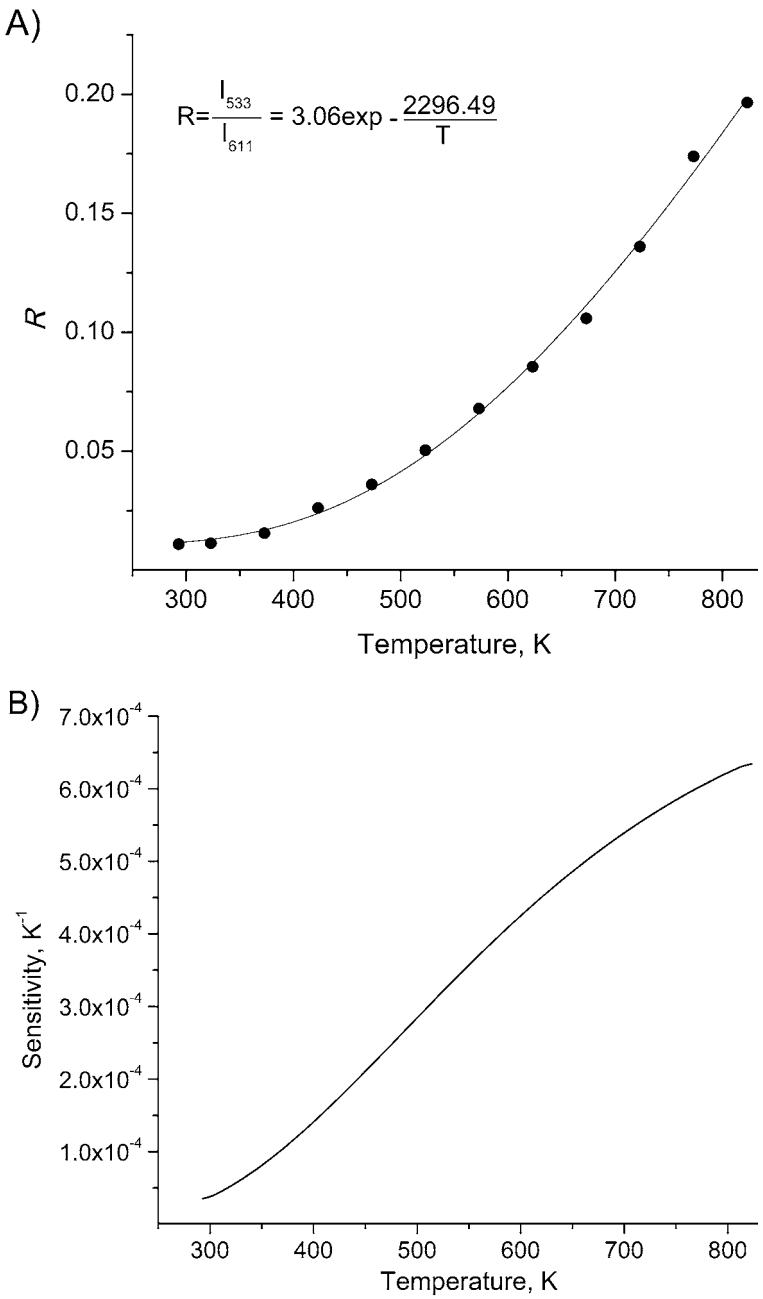

Fig. 5. FIR of the $^5D_1 \rightarrow {}^7F_1$ and $^5D_0 \rightarrow {}^7F_2$ transitions for 3 at. % Eu^{3+} as a function of temperature.

2012 Copyright (CC) SCS

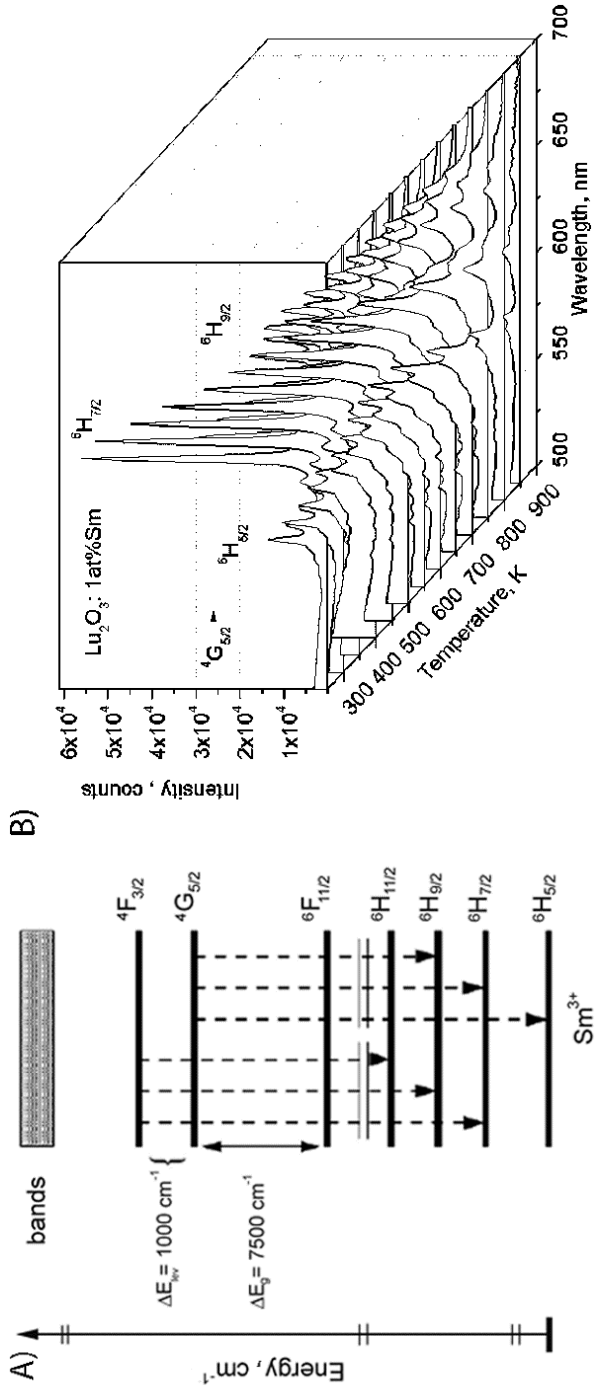

Fig. 6. Energy level diagram for the Sm^{3+} (A) and emission spectra under elevated temperatures (B).

2012 Copyright (CC) SCS

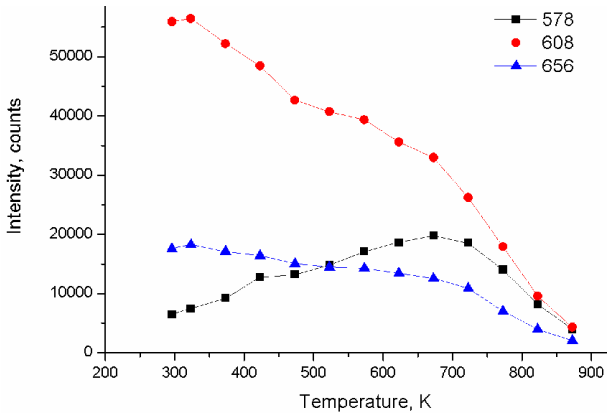

Fig. 7. Temperature dependant variations of the intensity of selected peaks centered at 578, 608 and 656 nm for the Lu_2O_3:1 at. % Sm^{3+} sample. The sizes of the symbols represent the error of the measurements.

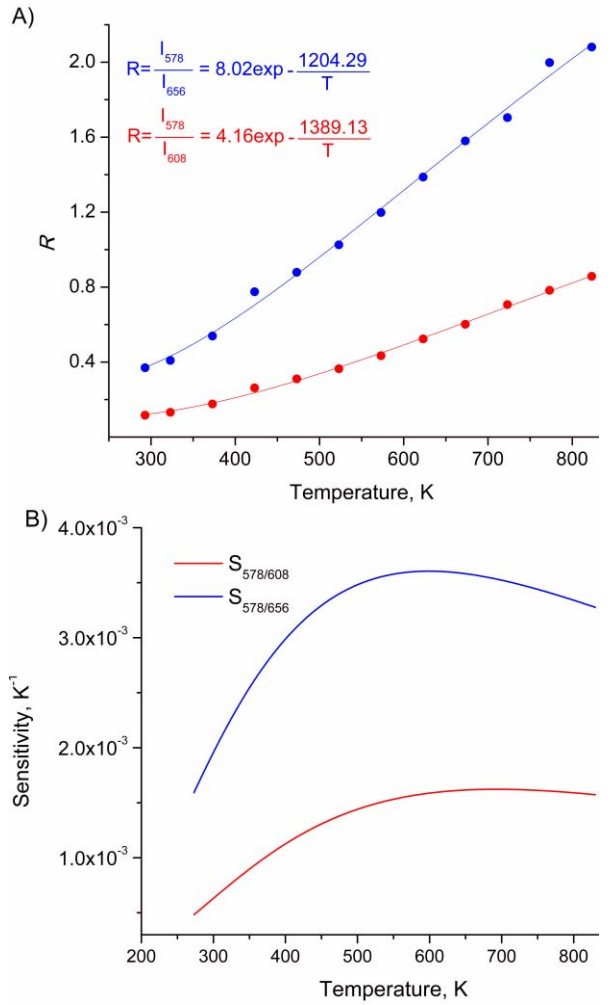

Fig. 8. FIR of the $^4G_{5/2} \rightarrow {}^6H_{5/2}$, $^6H_{9/2}$ and $^4G_{5/2} \rightarrow {}^6H_{5/2}$, $^6H_{7/2}$ transitions for 1 at. % Sm^{3+} as a function of temperature.

2012 Copyright (CC) SCS

CONCLUSION

Lutetium oxide doped with either Eu^{3+} or Sm^{3+} was synthesized *via* the polymer complex solution method. The FIR technique was used to examine potential use of these materials in high-temperature phosphor thermometry. For Eu^{3+}, the emission intensity was monitored with increasing temperature for the main transitions $^5D_1 \rightarrow {}^7F_1$ and $^5D_0 \rightarrow {}^7F_2$, and detected the maximum sensitivity of approximately 6×10^{-4} K^{-1} was detected at 823 K. For the Sm^{3+} ion, the $^4G_{5/2} \rightarrow$ $\rightarrow {}^6H_{5/2}$, $^6H_{9/2}$ and $^4G_{5/2} \rightarrow {}^6H_{5/2}$, $^6H_{7/2}$ emission intensities were tracked and the maximum sensitivities of 3.6×10^{-3} and 1.6×10^{-3} K^{-1} were found at about 580 K and at about 700 K, respectively. Based on these results, it is evident that these materials could be used as temperature sensors at elevated temperatures.

Acknowledgement. This research was financially supported by the Ministry of Education, Science and Technological Development of the Republic of Serbia through Project Numbers 45020 and 171022.

И З В О Д

ТЕРМОГРАФСКА СВОЈСТВА Eu^{3+} И Sm^{3+} ДОПИРАНОГ Lu_2O_3 НАНОФОСФОРА

ВЕСНА ЛОЈПУР, ЖЕЉКА АНТИЋ, РАДЕНКА КРСМАНОВИЋ, МИНА МЕДИЋ, МАРКО Г. НИКОЛИЋ и МИРОСЛАВ Д. ДРАМИЋАНИН

Институт за нуклеарне науке Винча, Универзитет у Београду, п. пр. 522, 11001 Београд

Узорци Lu_2O_3:Eu^{3+} (3 at. % Eu) и Lu_2O_3:Sm^{3+} (1 at. % Sm), су припремљени методом полимерног комплексног раствора уз коришћење полиетилен гликола као горива и нуклеационог агенса за процес кристализације. Узимајући у обзир да лутецијум-оксид има високу хемијску и температурску стабилност, у овом раду истражили смо могућност његове примене за високо-температурску термометрију. Ова термометријска метода је заснована на температурској зависност флуоресценце фосфора. Структурна и морфолошка својства су испитана коришћењем дифракције X зрака и трансмисионе електронске микроскопије. Добијени резултати су потвдили да примењена метода синтезе даје узорке жељене кристалне структуре, са честицама праха пречника од 30 до 50 nm. Фотолуминесцентна мерења су изведена у опсегу од собне темературе до 873 K. Остварени резултати показују да Eu^{3+} и Sm^{3+} допиран Lu_2O_3 има добре перформансе као високо-температурски термографски фосфор.

(Примљено 21. октобра, ревидирано 8. децембра 2012)

REFERENCES

1. E. Zych, M. Wawrzyniak, A. Kossek, J. Trojan-Piegza, L. Kepinski, *J. Alloy. Compd*. **451** (2008) 591
2. M. Xu, W. Zhang, N. Dong, Y. Jiang, Y. Tao, M. Yin, *J. Solid State Chem*. **178** (2005) 477
3. A. Garcia-Murillo, C. Le Luyer, C. Dujardin, T. Martin, C. Garapon, C. Pedrini, J. Mugnier, *Nucl. Ins. Methods, A* **486** (2002) 81
4. H. Wei, Z. Cleary, S. Park, K. Senevirathne, H. Eilers, *J. Alloy. Compd*. **500** (2010) 96
5. H. Guo, X. Yang, T. Xiao, W. Zhang, L. Lou, J. Mugnier, *Appl. Surf. Sci*. **230** (2004) 215
6. A. Martinez, J. Morales, L. A. Diaz-Torres, P. Salas, E. De la Rosa, J. Oliva, H. Desirena, *Mater. Sci. Eng., B* **174** (2010) 164

2012 Copyright (CC) SCS

7. A. N. Gruzintsev, G. A. Emelchenko, Yu. V. Yermolayeva, V. M. Masalov, A. V. Tolmachev, P. Benalloul, C. Barthou, *Phys. Solid State* **53** (2011) 1263
8. L. An, J. Zhang, M. Liu, S. Chen, S. Wang, *Opt. Mater.* **30** (2008) 957
9. M. Kottaisamy, D. Jeyakumar, R. Jagannathan, M. M. Rao, *Mater. Res. Bull.* **31** (1996) 1013
10. P. D. Volanti, V. I. Rosa, C. E. Paris, A. C. Paskocimas, S. P. Pizani, *Opt. Mat.* **31** (2009) 995
11. C. Dujardin, C. Le Luyer, C. Martinet, C. Garapon, J. Mugnier, A. G. Murillo, C. Pedrini, T. Martin, *Nucl. Ins. Methods, A* **537** (2005) 237
12. M. Nichkova, D. Dosev, S. J. Gee, B. D. Hammock, I. M. Kennedy, *Anal. Chem*. **77** (2005) 6864
13. W. Q. Chen, Y. Shi, Q. L. An, W. S. Wang, J. Y. Chen, L. J. Shi, *J. Eur. Ceram. Soc.* **27** (2007) 191
14. S. Cho, H. Lee, C. Moon, J. Kim, J. Park, G. Jeon, R. Lee, S. Nam, *J. Sol–Gel Sci. Technol.* **53** (2010) 171
15. C. Martinet, A. Pillonnet, J. Lancok, C. Garapon, *J. Lumin.* **126** (2010) 807
16. R. Krsmanovic, Z. Antic, B. Bartova, M. D. Dramicanin, *J. Alloy. Compd.* **505** (2010) 224
17. S. A. Wade, S. F. Collins, G. W. Baxter, *J. Appl. Phys.* **94** (2003) 4743
18. S. K. Singh, K. Kumar, B. S. Rai, *Sensor Actuat., A* **149** (2009) 16
19. M. G. Nikolic, D. J. Jovanovic, V. Đordjevic, Z. Antic, R. M. Krsmanovic, M. D. Dramicanin, *Phys. Scr.* **T149** (2012) 014063
20. V. Lojpur, M. Nikolic, L. Mancic, O. Milosevic, M. D. Dramicanin, *Ceram. Int*. **39** (2013) 1129
21. F. Vetrone, J. C. Boyer, J. A. Capobianco, A. Speghini, M. Bettinelli, *J. Phys. Chem., B* **106** (2002) 5622
22. J. Petit, B. Viana, P. Goldner, J. P. Roger, D. Fournier, *J. Appl. Phys.* **108** (2010) 123108
23. L. Liu, Y. Wang, X. Zhang, K. Yang, Y. Bai, C. Huang, Y. Song, *Opt. Commun*. **284** (2011) 1876.

2012 Copyright (CC) SCS

Journal of the Serbian Chemical Society
JSCS-info@shd.org.rs • www.shd.org.rs/JSCS
J. Serb. Chem. Soc. *77* (12) 1747–1757 (2012) UDC 667.2–037+549.514.6:544.526.5+542.92
JSCS–4386 *Original scientific paper*

A study of the photocatalytic degradation of the textile dye CI Basic Yellow 28 in water using a P160 TiO_2-based catalyst

VELJKO DJOKIĆ[1], JELENA VUJOVIĆ[1], ALEKSANDAR MARINKOVIĆ[1#], RADA PETROVIĆ[1], DJORDJE JANAĆKOVIĆ[1], ANTONIJE ONJIA[2] and DUŠAN MIJIN[1*#]

[1]*Faculty of Technology and Metallurgy, University of Belgrade, Karnegijeva 4, P. O. Box 3503, 11120 Belgrade, Serbia and* [2]*Vinča Institute of Nuclear Sciences, University of Belgrade, P. O. Box 522, 11001 Belgrade, Serbia*

(Received 15 November, revised 4 December 2012)

Abstract: The photocatalytic degradation of the synthetic textile dye CI Basic Yellow 28 (BY28) in water, using a recently synthesized P160 TiO_2-based catalyst, under Osram ultra-vitalux® lamp (300 W) light, was studied. The effects of the operational parameters, such as initial concentration of catalyst, initial dye concentration and pH, were studied. The salt effect (NaCl, Na_2CO_3, Na_2SO_4 and $NaNO_3$) was also investigated. It was found that the optimal concentration of catalyst is 2.0 g L^{-1}. A pseudo first-order kinetic model was illustrated using the Langmuir–Hinshelwood mechanism and the adsorption equilibrium constant and the rate constant of the surface reaction were calculated (K_{BY} = 6.126 L mg^{-1} and k_C = 0.272 mg L^{-1} min^{-1}, respectively). The photodegradation rate was higher in weak acidic than in high acidic and alkaline conditions. The presence of CO_3^{2-} ions increased the photodegradation rate while Cl^-, SO_4^{2-} and NO_3^- decreased the reaction rate. The rate of photodegradation of BY28 was measured using UV–Vis spectroscopy.

Keywords: TiO_2; photocatalysis; pseudo first-order kinetic model; Langmuir–Hinshelwood mechanism; salt effect.

INTRODUCTION

Textile and other synthetic dyes are an important source of environmental contamination due to their large production and usage in the textile and other industries. The majority of these dyes are toxic, mostly non-biodegradable and often resistant to destruction by physicochemical methods, such as chemical precipitation and separation of pollutants, coagulation and elimination by adsorption.[1–3] None of these methods is destructive so they only transfer the contami-

* Corresponding author. E-mail: kavur@tmf.bg.ac.rs
# Serbian Chemical Society member.
doi: 10.2298/JSC121015130D

Available online at shd.org.rs/JSCS/

2012 Copyright (CC) SCS

nation from one phase to another. Therefore, a new kind of pollution is obtained that requires further treatment.

Advanced oxidation processes (AOPs) provide an effective means of rapidly treating compounds with efficient process control.[4] Among the new oxidation methods, heterogeneous photocatalysis appears as a destructive technology leading to the total mineralization of many organic pollutants,[5–8] following the proposed mechanism:

a) absorption of efficient photons by titania ($h\nu \geq E_g = 3.2$ eV):

$$TiO_2 + h\nu\,(UV) \rightarrow e_{CB}^- + h_{VB}^+ \quad (1)$$

b) oxygen ionosorption:

$$(O_2)_{ads} + e_{CB}^- \rightarrow O_2^{-\cdot} \quad (2)$$

c) formation of $^{\cdot}OH$ by OH^- reaction with photoholes:

$$(H_2O \leftrightarrow H^+ + OH^-)_{ads} + h_{VB}^+ \rightarrow H^+ + {}^{\cdot}OH \quad (3)$$

d) oxidation of the organic reactant *via* successive attacks by $^{\cdot}OH$ radicals:

$$R + {}^{\cdot}OH \rightarrow R^{\cdot} + H_2O \quad (4)$$

e) or by direct reaction with holes:

$$R + h^+ \rightarrow R^{+\cdot} \rightarrow \text{degradation products} \quad (5)$$

As an example of the last process, holes can generate CO_2 according to:

$$RCOO^- + h^+ \rightarrow R^{\cdot} + CO_2 \quad (6)$$

Titanium dioxide is one of the most frequently studied and applied photocatalysts in advanced oxidation processes. Its ability to be activated by means of natural sources (Sun-UV irradiation) as well as its semiconductor properties, chemical and biological inertness, resistance to chemical and photo-induced corrosion, and also its non-toxicity and low price have attracted world wide attention of scientists and engineers for some time.[9] Titanium dioxide can be manufactured using different methods. The most frequently used methods are sol–gel method, hydrothermal processing and gas-phase reaction.[10]

The aim of the present study was to investigate the influence of various parameters on the photocatalytic decomposition of the textile dye CI Basic Yellow 28 in the presence of a recently synthesized P160 TiO_2-based catalyst[11,12] irradiated under an Osram ultra-vitalux® lamp as the light source. CI Basic Yellow 28 dye is a cationic azo dye that can be also be called an azomethine dye (–CH=N–) or hydrazone dye (=N–N(H,R)–) (Fig. 1). The P160 TiO_2-based catalyst was synthesized by a non-hydrolytic sol–gel process.[11,12] The effects of parameters such as initial concentration of catalyst, initial dye concentration, pH and the presence of salts (NaCl, Na_2SO_4, $NaNO_3$ and Na_2CO_3) were studied.

2012 Copyright (CC) SCS

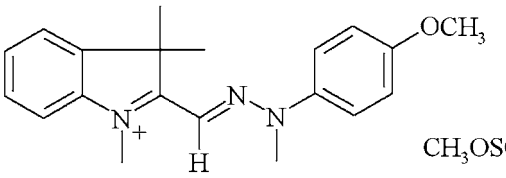

Fig. 1. Structure of CI Basic Yellow 28.

EXPERIMENTAL

Materials

All chemicals used in the investigation were of reagent grade and were used without further purification. Hydrochloric acid, sodium chloride, sodium carbonate, sodium sulfate, sodium nitrate and sodium hydroxide (all *p.a.*) were obtained commercially, mostly from Fluka. P160 TiO_2 was prepared according to a previously procedure published.[11,12] The textile dye, CI Basic Yellow 28, was obtained from Bezema as a gift (commercial name Bezacryl Goldgelb GL 200) and was used without purification. Deionized water was obtained from a Milipore Waters Milli Q purification unit.

Procedures

Irradiations were performed in a glass reactor (cylindrical shape, volume 100.0 mL) with an Osram ultra-vitalux® lamp (mix of lights; UV-A:UV-B = 13.6:3 according to the manufacturer's specifications) placed 500 mm from the surface of the reaction mixture. The photodegradation of BY28 was studied by preparing a solution containing a known concentration of the dye and amount of TiO_2. In a typical experiment, 25 mL of solution was used. Then, the lamp was switched on and during the irradiation, agitation was applied. After an appropriate time of irradiation, as given in the figures, the suspension was sampled. The concentration of dye was determined by UV–Vis spectrophotometer (Shimadzu 1700) at λ_{max} = = 436 nm. After filtration, the pH of the samples was adjusted by the addition of dilute NaOH and HCl and measured using pH meter (PHM 93 reference pH meter, Radiometer Copenhagen, Denmark).

RESULTS AND DISCUSSION

Effect of initial catalyst concentration

The effect of the initial P160 TiO_2 catalyst concentration on the photodegradation rate of BY28 is shown in Fig. 2. The photodegradation rate increased with increasing concentration of photocatalyst, reached the highest value at 2.0 g L^{-1} and subsequently decreased. The explanation for this phenomenon is the fact that when all dye molecules are adsorbed on TiO_2, the addition of larger quantities of TiO_2 would have no effect on the photodegradation efficiency. Above this concentration, light scattering and coagulation of the catalyst particles decreased the reaction rate,[8,13–15] and reduced degradation rate was registered when the concentration of TiO_2 was increased beyond 2.0 g L^{-1}.

The photodegradation efficiency (X) is given by:

$$X = \frac{c_0 - c}{c_0} \tag{7}$$

2012 Copyright (CC) SCS

where c_0 is the initial concentration of BY28 in mg L^{-1}, c is the concentration of BY28 at irradiation time t in mg L^{-1}. The effect of the amount of TiO_2 on the photodegradation efficiency of BY28 at an irradiation time of 0.5 h is shown in Fig. 3. No decolorization was observed if catalyst or irradiation were applied separately. Complete decolorization was observed after 1 hour of irradiation.

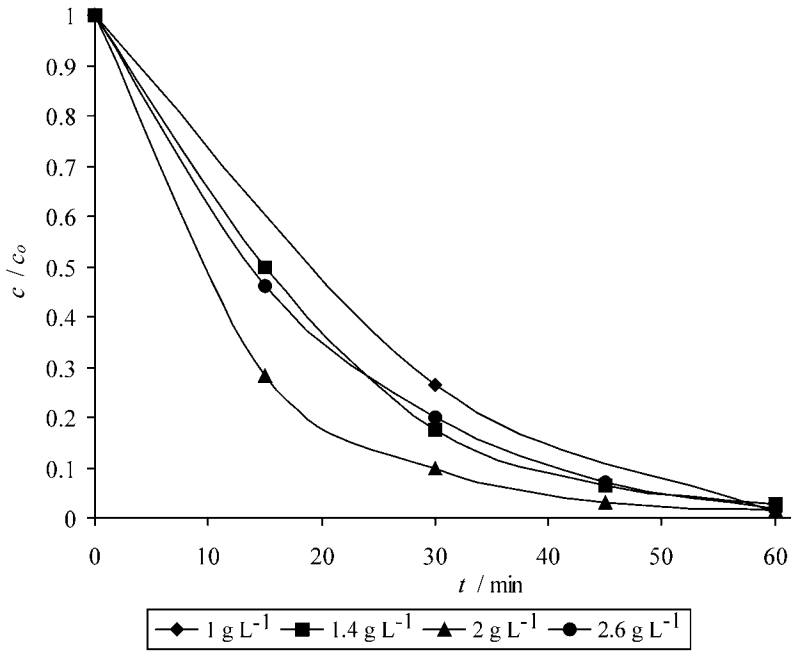

Fig. 2. The effect of the initial concentration of P160 TiO_2 on the photodegradation rate of BY28 (dye concentration = 50 mg L^{-1}).

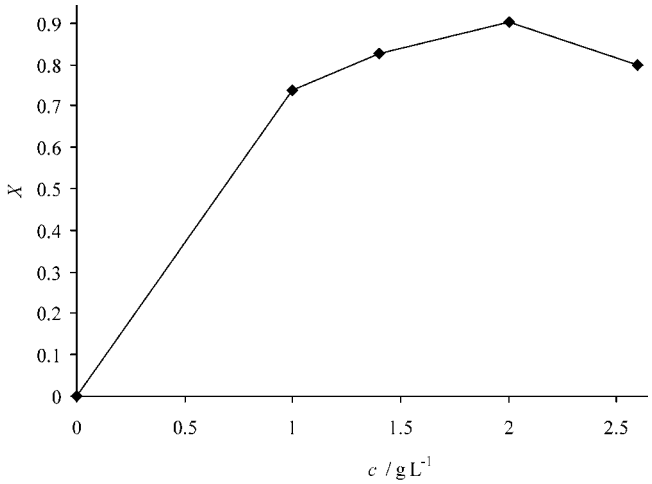

Fig. 3. The effect of the concentration of P160 TiO_2 on the photodegradation efficiency of BY28 at an irradiation time of 0.5 h (dye concentration = 50 mg L^{-1}).

2012 Copyright (CC) SCS

Effect of initial dye concentration

In addition, the effect of the initial dye concentration on the photodegradation rate was studied (Fig. 4). It could be observed that the photodegradation rate of BY28 decreases with increasing initial concentration of dye, since with increasing dye concentration, more and more dye molecules are adsorbed on the surface of the TiO_2. Due to the lack of any direct contact between dye molecules with holes or hydroxyl radicals, inhibition occurred. Increased dye concentration also promotes that the dye molecules adsorb light and hence the photons cannot reach the photocatalyst surface; hence the photodegradation efficiency decreases.[5]

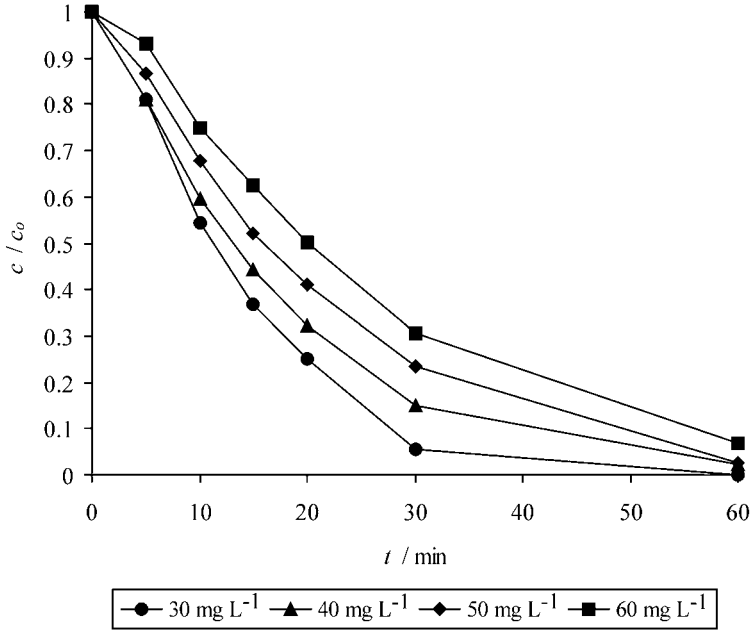

Fig. 4. The effect of the initial dye concentration on the photodegradation rate of BY28 (catalyst concentration = 2.0 g L^{-1}).

The kinetics of the photodegradation rate of most organic contaminants[16] can be well described by pseudo-first order kinetics, which is given by the following equations:

$$\ln\left(\frac{c_0}{c}\right) = kt \tag{8}$$

$$c = c_0 e^{-kt} \tag{9}$$

where c_0, c and t are as given above and k is the pseudo-first order rate constant.

Heterogeneous photocatalytic reaction can be successfully analyzed using the modified Langmuir–Hinshelwood (L–H) kinetic expression.[14,16–18] The rate

2012 Copyright (CC) SCS

of oxidation of BY28 by a surface reaction is proportional to the surface coverage of BY28 on the P160 TiO_2, assuming that BY28 is adsorbed stronger on the catalyst surface than the intermediate products. The effect of the initial BY28 concentration c_0 on the initial BY28 degradation rate r is given in the form of Eqs. (10) and (11):

$$r = \frac{K_{BY} k_C c}{1 + K_{BY} c_0} = kc \tag{10}$$

$$\frac{1}{k} = \frac{1}{K_{BY} k_C} + \frac{c_0}{k_C} \tag{11}$$

where K_{BY}, k_C, and k are the Langmuir–Hinshelwood adsorption equilibrium constant, the rate constant of photodegradation surface reaction and the rate constant of the initial BY28 photodegradation reaction, respectively. At the investigated concentrations, *i.e.*, concentrations up to 60 mg L^{-1}, the applicability of L–H equation for the photocatalytic degradation was confirmed by the linear plot (R = 0.9716) obtained by plotting the reciprocal of the rate constant ($1/k$) against the initial dye concentration c_0 (Fig. 5). The values of K_{BY} and k_C were found to be 6.126 L mg^{-1} and 0.272 mg L^{-1} min^{-1}, respectively.

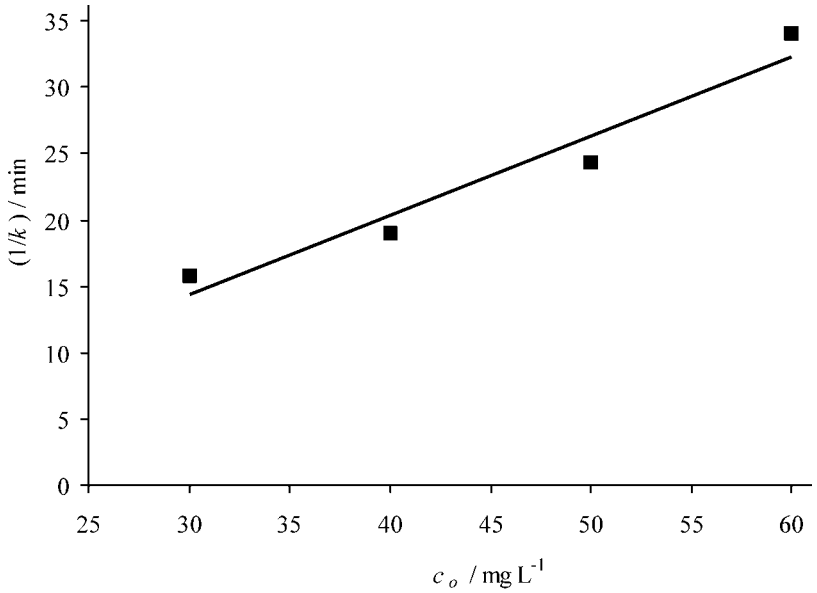

Fig. 5. Linear transformation of the L–H type expression.

Effect of pH

Since pH value has an influence on the rate of photodegradation of some organic compounds in photocatalytic processes,[13,19,20] the photodegradation of

2012 Copyright (CC) SCS

BY28 at four different pH values (3.3, 5.2, 6.7 and 8.7) were studied. The second value is the pH of the pure dye solution in deionized water.

It is known that the amphoteric behavior of most semiconductor oxides influences the surface charge of the photocatalyst. The zero point charge for TiO_2 (pH_{zpc}) is 5.0–6.0, and above this value, the TiO_2 surface is predominantly negatively charged (TiO^-) (Eq. (12)).[18] The surface of the catalyst is positive below pH 6.0, and as the pH decreases, the functional groups are protonated ($TiOH_2^+$), and the proportion of the positively charged surface increases (Eq. (13)):[8]

$$TiOH + OH^- \leftrightarrows TiO^- + H_2O, \; pH > pH_{zpc} \quad (12)$$

$$TiOH + H^+ \leftrightarrows TiOH_2^+, \; pH < pH_{zpc} \quad (13)$$

It was found that the initial photodegradation rate was higher at 5.2 than in more acidic or alkaline solutions (Fig. 6). Since BY28 is cationic dye, one would expect that the reaction rate would be higher at pH values above pH_{zpc} since in this pH range, the TiO_2 surface is negatively charged and the affinity of the dye molecules should be higher, as was reported earlier for TiO_2-Merk Eusolex® T (anatase modification). When TiO_2-Merk Eusolex® T was used, the initial photodegradation rate was highest in alkaline solutions and lowest in acidic solutions.[21] This behavior of the P160 catalyst could be probably be explained by different surface structure obtained by the non-hydrolytic sol–gel process.[12]

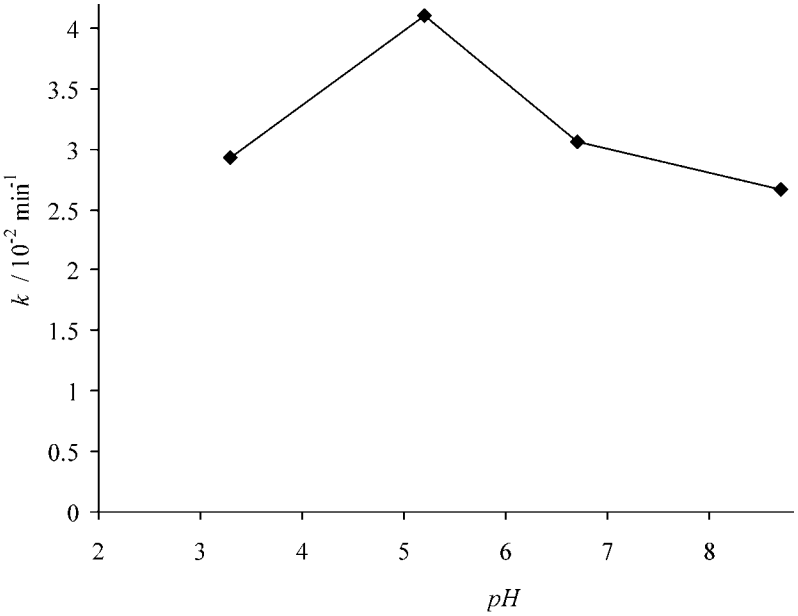

Fig. 6. The effect of pH on the photodegradation rate of BY28 (dye concentration =50 mg L^{-1}, catalyst concentration = 2.0 g L^{-1}).

2012 Copyright (CC) SCS

Salt effect of the photodegradation rate of BY28

Salt effect on photodegradation of organic pollutants was frequently investigated due to the possibility of the adsorption of inorganic anions onto the photocatalyst surface. This adsorption results in decreasing of number of the holes and ·OH radicals, and reaction rate decrease.[14,22] The presence of different inorganic ions (SO_4^{2-}, HSO_4^-, PO_4^{3-}, CO_3^{2-}, HCO_3^-, Cl^-, NO_3^-, *etc*.) present in surface and ground waters leads to decreasing photodegradation effectivity due to their scavenging properties.[22]

The salt effect on the photodegradation of BY28 was studied using sodium salts, *i.e*., sodium chloride, sodium carbonate, sodium sulfate and sodium nitrate (Fig. 7). Sodium chloride along with sectional wastes is usually present in the effluent of textile mills. The decrease of the photodegradation rate of BY28 in the presence of sodium chloride (20 mM) could be explained by the hole scavenging properties of chloride ions:[22]

$$Cl^- + h_{VB}^+ \rightarrow Cl^{\cdot} \quad (14)$$

$$Cl^{\cdot} + Cl^- \rightarrow Cl_2^{-\cdot} \quad (15)$$

The formed chloride anions block the surface sites that are normally available at the TiO_2/dye solution interface for adsorption and electron transfer and so inhibited the degradation process. A similar effect of sodium chloride on the photodegradation rate of BY28 was observed when TiO_2-Merk Eusolex® T was used.[21]

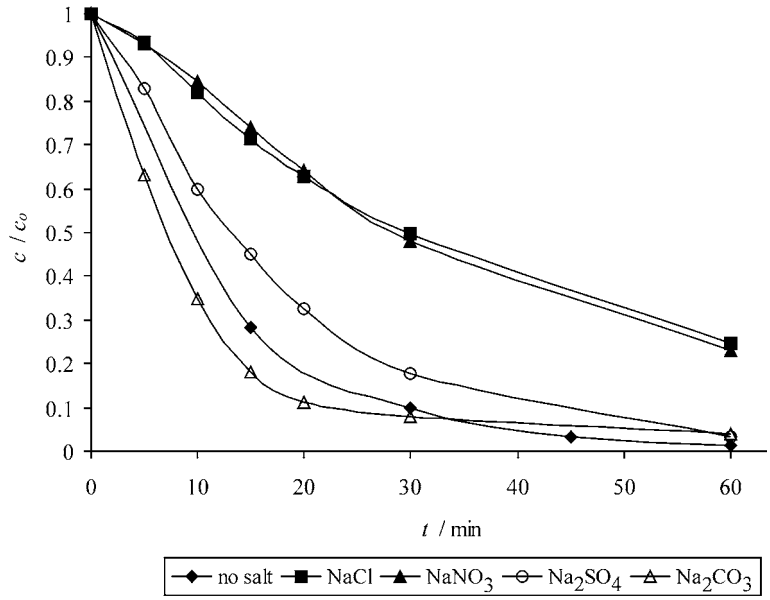

Fig. 7. Salt effect (20 mM) of on the photodegradation rate of BY28 (dye concentration = 50 mg L^{-1}, catalyst concentration = 2.0 g L^{-1}).

2012 Copyright (CC) SCS

Sodium carbonate is mainly used in the textile industry to adjust the pH of the dyeing bath. Therefore, the wastewaters from the textile industry contain considerable amounts of carbonate ions. As can be seen from Fig. 7, the photodegradation in the presence of sodium carbonate (20 mM) was faster in comparison to the reaction in its absence. The obtained results indicate that carbonate ions might favor the formation of OH^- ions, thus promoting the degradation reaction:[23]

$$CO_3^{2-} + H_2O \rightarrow HCO_3^- + OH^- \quad (16)$$

$$HCO_3^- + H_2O \rightarrow H_2CO_3 + OH^- \quad (17)$$

A similar effect of sodium carbonate on the photodegradation rate of BY28 was observed when TiO_2-Merk Eusolex® T was used.[21]

The photodegradation in the presence of sulfate anions was slower in comparison to the reaction without salt. Sulfate anions change the distribution of BY28 between the solution and the P160 TiO_2 surface and/or react with the positive holes (h_{VB}^+) and hydroxyl radicals ($^{\cdot}OH$):[24]

$$SO_4^{2-} + h_{VB}^+ \rightarrow SO_4^{-\bullet} \quad (18)$$

$$SO_4^{2-} + OH^{\bullet} \rightarrow SO_4^{-\cdot} + OH^- \quad (19)$$

The presence of SO_4^{2-} leads to formation of $SO_4^{-\bullet}$, which is less reactive than $^{\bullet}OH$ and h_{VB}^+ and thus the photodegradation rate of BY28 is hindered.

Finally, the effect of sodium nitrate was studied (Fig. 7). Although some authors have reported that nitrate anions can increase the photodegradation rate,[25] in the present study, a strong inhibition of the photodegradation of BY28 was observed due to the possible blockage of the active sites on the TiO_2 surface by nitrates.

CONCLUSIONS

The behavior of recently synthesized P160 TiO_2-based catalyst in the photodegradation of CI Basic Yellow 28 was studied. It was shown that complete decolorization could be achieved in 60 min using a catalyst concentration 2.0 g L^{-1}. The obtained results indicated that the photodegradation rate of BY28 was affected by the initial dye concentration, pH and the presence of salts. The Heterogeneous photocatalytic reaction was analyzed using the modified Langmuir–Hinshelwood kinetic expression, and the rate constant of the photodegradation surface reaction and the rate constant of initial BY28 photodegradation reaction were calculated. The values K_{BY} and k_C were found to be 6.126 L mg^{-1} and 0.272 mg L^{-1} min^{-1}, respectively.

Acknowledgment. The authors are grateful to the Ministry of Education, Science and Technological Development of the Republic of Serbia for financial support through the Projects III 45019 and 172013.

2012 Copyright (CC) SCS

ИЗВОД

ПРОУЧАВАЊЕ ФОТОКАТАЛИТИЧКЕ ДЕГРАДАЦИЈЕ ТЕКСТИЛНЕ БОЈЕ CI BASIC YELLOW 28 У ВОДИ КОРИСТЕЋИ P160 КАТАЛИЗАТОР НА БАЗИ TiO_2

ВЕЉКО ЂОКИЋ[1], ЈЕЛЕНА ВУЈОВИЋ[1], АЛЕКСАНДАР МАРИНКОВИЋ[1], РАДА ПЕТРОВИЋ[1], ЂОРЂЕ ЈАНАЋКОВИЋ[1], АНТОНИЈЕ ОЊИА[2] и ДУШАН МИЈИН[1]

[1]Технолошко–металуршки факултет Универзитета у Београду, Карнегијева 4, Београд и [2]Институт за Нуклеарне науке Винча, Универзитет у Београду, Београд

У раду је проучавана фотокаталитичка деградација синтетске текстилне боје CI Basic Yellow 28 у води, користећи недавно синтетисани катализатор на бази P160 TiO_2, и Osram ultra-vitalux® лампу (300 W). Проучаван је утицај различитих параметара на реакцију, као што су: почетна концентрација катализатора, почетна концентрација боје, присуство соли (NaCl, Na_2CO_3, Na_2SO_4 и $NaNO_3$) и pH. Утврђено је да је оптимална концентрација катализатора 2,0 g L^{-1}. Користећи Langmuir–Hinshelwood механизам одређене су равнотежна адсорпциона константа и константа брзине површинске реакције (K_{BY} = 6,126 L mg^{-1} и k_C = 0,272 mg L^{-1} min^{-1}). Брзина реакције је већа у слабо киселој средини у поређењу са јако киселом или базном средином. Присуство CO_3^{2-} повећава брзину реакције фотодеградације док је Cl^-, SO_4^{2-} и NO_3^- смањују.

(Примљено 15. новембра, ревидирано 4. децембра 2012)

REFERENCES

1. E. Forgacs, T. Cserhati, G. Oros, *Environ. Int.* **30** (2004) 953
2. I. K. Konstantinou, T. A. Albanis, *Appl. Catal., B* **49** (2004) 1
3. A. R. Khataee, M. B. Kasiri, *J. Mol. Catal., A* **328** (2010) 8
4. C. G. da Silva, J. L. Faria, *J. Photochem. Photobiol., A* **155** (2003) 133
5. C. G. da Silva, J. L. Faria, *J. Photochem. Photobiol., A* **162** (2004) 317
6. N. Daneshvar, D. Salari, A. R. Khataee, *J. Photochem. Photobiol., A* **157** (2003) 111
7. M. Karkmaz, E. Puzenat, C. Guillarad, J. M. Herrmann, *Appl. Catal., B* **51** (2004) 183
8. N. Daneshvar, D. Salari, A. R. Khataee, *J. Photochem. Photobiol., A* **162** (2004) 317
9. M. N. Chong, B. Jin, C. W. K. Chow, C. Saint, *Water Res.* **44** (2010) 2997
10. W.-C. Lin, W.-D. Yang, S.-Y. Jheng, *J. Taiwan Inst. Chem. Eng.* **43** (2012) 269
11. N. Tanasković, Ž. Radovanović, V. Đokić, J. Krstić, S. Drmanić, Dj. Janaćković, R. Petrović, *Superlattices Microstuct.* **46** (2009) 217
12. R. Petrović, N. Tanasković, V. Djokić, Ž. Radovanović, I. Janković-Častvan, I. Stamenković, Dj. Janaćković, *Powder Technol.* **219** (2012) 239
13. H. Gupta, S. Tanaka, *Water Sci. Technol.* **31** (1995) 47
14. M. A. Behnajady, N. Modirshahla, R. Hamzavi, *J. Hazard. Mater.* **133** (2006) 226
15. S. Rabindranathan, D. P. Suja, S. Yesodharan, *J. Hazard. Mater.* **102** (2003) 217
16. I. K. Konstantinou, T. A. Albanis, *Appl. Catal., B* **42** (2003) 319
17. N. Daneshvar, S. Aber, M. S. Seyed Dorraji, A. R. Khatae, M. H. Rasoulifard, *Int. J. Chem. Biomol. Eng.* **1** (2008) 24
18. E. Evgenidou, K. Fytianos, I. Poulios, *Appl. Catal., B* **59** (2005) 81
19. G. Wu, X. Liu, D. Wei, J. Fan, L. Wang, *Water Res.* **35** (2001) 3927
20. R. Ameta, P. B. Punjabi, S. C. Ameta, *J. Serb. Chem. Soc.* **76** (2011) 1049
21. D. Mijin, J. Radivojević, P. Jovančić, *Chem. Ind. Chem. Eng. Q.* **13** (2007) 33
22. B. Neppolian, H. C. Choi, S. Sakthivel, B. Arabindoo, V. Murugesan, *Chemosphere* **46** (2002) 1173

2012 Copyright (CC) SCS

23. D. Mijin, M. Savić, S. Perović, A. Smiljanić, O. Glavaški, M. Jovanović, S. Petrović, *Desalination* **249** (2009) 286
24. C. Hu, J. C. Yu, Z. Hao, P. K. Wong, *Appl. Catal., B* **46** (2003) 35
25. H. Y. Zhu, R. Jiang, L. Xiao, Y. H. Chang, Y. J. Guan, X. D. Li, G. M. Zeng. *J. Hazard. Mater.* **169** (2009) 933.

2012 Copyright (CC) SCS

Journal of the Serbian Chemical Society
JSCS-info@shd.org.rs • www.shd.org.rs/JSCS
J. Serb. Chem. Soc. *77* (12) 1759–1773 (2012)
JSCS–4387
UDC 677.12+547.422+547.823:66.081+546.57:615.28
Original scientific paper

Antimicrobial oxidized hemp fibers with incorporated silver particles

JOVANA MILANOVIĆ*, TATJANA MIHAILOVIĆ, KATARINA POPOVIĆ and MIRJANA KOSTIĆ#

Faculty of Technology and Metallurgy, University of Belgrade, Karnegijeva 4, 11120 Belgrade, Serbia

(Received 18 October, revised 10 December 2012)

Abstract: In this study, antimicrobial silver-loaded hemp fibers were prepared by selective TEMPO-mediated oxidation, *i.e.*, oxidation with sodium hypochlorite, catalytic amount of sodium bromide and the 2,2,6,6-tetramethylpiperidine-1-oxy radical (TEMPO), followed by silver sorption from aqueous silver nitrate solution. The most suitable experimental conditions for the selective TEMPO-mediated oxidation were determined by changing the oxidation conditions, *i.e.*, the concentration of sodium hypochlorite and the duration of oxidation. The obtained results showed that the maximum sorption capacity of 0.703 mmol of silver per gram of modified hemp fibers was obtained for the sample oxidized with 9.67 mmol NaClO per gram of fibers for 4 h. SEM Microphotographs of the modified hemp fibers with incorporated silver showed uniformly distributed silver particles on the surface of fibers, with isometric shapes and sizes from 10 to 100 nm, despite the fact that silver was sorbed from an ionic solution. The antibacterial activity of the TEMPO-oxidized hemp fibers with silver particles was confirmed *in vitro* against two strains: *Staphylococcus aureus* (ATCC 25923) and *Escherichia coli* (ATCC 25922), and the antifungal activity against *Candida albicans* (ATCC 24433). The best antimicrobial activity of silver-loaded TEMPO-oxidized hemp fibers was showed against strain *S. aureus*.

Keywords: hemp fibers; TEMPO-mediated oxidation; silver sorption; antimicrobial textile.

INTRODUCTION

Microorganisms are part of everyday life. They join humans in different forms. Especially the skin is home for many of these organisms. On the other hand, textiles are the interface between the skin and the environment and present

* Corresponding author. E-mail: jovana@tmf.bg.ac.rs
# Serbian chemical Society member.
doi: 10.2298/JSC121018143M

Available online at shd.org.rs/JSCS/

2012 Copyright (CC) SCS

the tissue with the longest contact with human skin. Therefore, textiles play a critical role, especially under skin conditions with an increased rate of pathogens infections. Production of materials with antimicrobial properties is constantly increasing. In order to protect customers, fibers with antimicrobial properties should disable the growth or directly destroy many pathogens that cause numerous diseases and infections in hospital environments as well as in daily life.[1,2]

The purpose of this research was to obtain antimicrobial hemp fibers with incorporated silver particles and evaluate their antimicrobial activity against different pathogens. The antimicrobial properties were accomplished by incorporation of silver into modified hemp fibers by chemisorption from aqueous silver nitrate solution. Silver was chosen as the antimicrobial agent because of the unique properties of silver, such as strong inhibitory, odor control, broad and long-term activity, and bacteria are unable to develop resistance to silver, as is the case with antibiotics. These properties, together with high thermal stability and good fabric compatibility, have been established silver as a topical agent in several medical areas of today.[3,4]

Furthermore, hemp fibers possess a range of specific properties, quick absorption of humidity accompanied with quick drying, good thermal and electrical properties, high tenacity, biodegradability and protection against UV radiation, which make them different from other textile fibers.[5] In order to prepare technical (multicellular) hemp fibers for textile applications, *i.e.*, to remove non-cellulosic substances (lignin, pectin, hemicelluloses)[6] and improve the sorption properties of hemp fibers,[7] selective TEMPO-mediated oxidation, *i.e.* oxidation with sodium hypochlorite, a catalytic amount of sodium bromide and the 2,2,6,6-tetramethylpiperidine-1-oxy radical (TEMPO), was applied. TEMPO-mediated oxidation causes the conversion of the C6 primary hydroxyl groups of hemp fibers into carboxyl groups *via* C6 carbonyl groups. The introduced carboxyl groups were used as reactive positions in the further reaction, *i.e.*, for the incorporation of silver ions, because the hydrogen atom present in carboxyl groups can easily be replaced with silver ions. The advantages of this TEMPO-mediated oxidation of polysaccharides are the following: highly regioselective oxidation of the primary hydroxyl groups in polysaccharides to carboxyl groups can be achieved under mild aqueous conditions at around room temperature at pH 10–11.[8,9]

The content of functional groups, moisture sorption and water retention were used to assess the changes in hemp fibers due to the oxidation. The influence of the oxidation conditions on the amount of sorbed silver, and thus on the degree of antimicrobial activity, was also determined. Changes in surface morphology and elemental composition of the TEMPO-oxidized silver-loaded hemp fibers were systematically investigated using Scanning Electron Microscopy–Energy Dispersive X-Ray analysis (SEM–EDX). The antimicrobial activities of silver-loaded hemp fibers against different pathogens: *Staphylococcus aureus* (ATCC 25923),

2012 Copyright (CC) SCS

Escherichia coli (ATCC 25922), and *Candida albicans* (ATCC 24433) were evaluated *in vitro*.

EXPERIMENTAL

Materials

Domestic water-retted long hemp fibers from Bački Brestovac (Serbia) were used in this investigation. The chemical composition of these fibers was *α*-cellulose, 76.10 %; lignin, 8.50 %; hemicelluloses, 11.90 %; pectin, 1.55 %; fats and waxes, 1.60 % and water-solubles, 0.35 %. All chemicals were obtained from commercial sources and were of *p.a.* grade.

Preparation of TEMPO-oxidized hemp fibers

Hemp fibers (10 g) were suspended in water (750 mL) containing TEMPO (0.025 g) and sodium bromide (0.25 g). A 13 % NaClO solution (0, 0.30, 2.42, 4.84 and 9.67 mmol per gram of fibers) was added to the cellulose slurry under continuous stirring.[10] The pH of the slurry at room temperature was maintained at 10.5 by addition of 0.5 M NaOH during 1–4 h. After stirring for the designated time, the oxidation was quenched by addition of ethanol (*ca.* 5 mL). The oxidized hemp fibers were washed thoroughly with water and then with ethanol on filter paper using a Büchner funnel. The thus obtained water-insoluble fractions were then dried at room temperature for 48 h.

Determination of the content of carboxyl groups in the TEMPO-oxidized hemp fibers

The carboxyl groups of the oxidized hemp fibers react with the salts of weaker acids such as calcium acetate, forming a salt of the oxidized cellulose fibers and releasing an equivalent amount of the weaker acid. Based on this and a modification of the calcium acetate method[11] for determining the acidity in modified hemp fibers, the following method of carboxyl group estimation was developed. Hemp fibers (0.5 g) were treated with 0.01 M HCl for 1 h and then washed thoroughly with water. In the next step, 50 mL of distilled water and 30 ml 0.25 M of calcium acetate solution were added to the oxidized hemp fibers. After standing for 2 h with frequent shaking to facilitate completion of the interchange, 30 mL portions of the liquid were titrated with 0.01 M sodium hydroxide using phenolphthalein as indicator.[12]

Determination of the content of carbonyl groups in the TEMPO-oxidized hemp fibers

The content of carbonyl groups in the oxidized hemp fibers was measured according to a method described in the literature.[10,13] The oxidized hemp fibers were further oxidized with sodium chlorite at pH 4−5 to selectively convert the carbonyl groups in the samples to carboxyl ones, and then the total content of carboxyl groups was determined by the calcium acetate method described above. Thus a cellulose slurry with 10 % consistency was prepared and then this slurry (20 g) was added to a mixture containing $NaClO_2$ (1.81 g), 5 M CH_3COOH (20 g), and water (57 mL). Oxidation was performed by stirring the mixture at room temperature for 48 h, followed by washing thoroughly with water and filtration. The carboxyl groups formed by the $NaClO_2$ oxidation were regarded as carbonyl groups present in the original oxidized hemp fibers.

Determination of moisture sorption

Moisture sorption of oxidized hemp fibers was determined according to the standard ASTM D 2654-76, 1976.[14] Fibers were exposed to a standard atmosphere (20±2 °C and 65±2 % relative humidity) for 24 hours (ASTM D 1776-74, 1974).[15] The moisture sorption was calculated as the weight percentage relative to absolute dry material.

2012 Copyright (CC) SCS

Determination of water retention value

The water retention of the hemp fibers was determined by the standard centrifuge method. ASTM D 2402-78, 1978.[16]

Silver sorption by TEMPO oxidized hemp fibers

Silver ions were incorporated into the previously TEMPO-oxidized hemp fibers and control ones by chemisorptions under the following previously optimized conditions:[17] fibers (0.1 g) were immersed in 100 mL of 0.01 mol dm^{-3} $AgNO_3$ solution and shaken at room temperature for 240 min in the dark. The concentration of Ag^+ after sorption was determined by NH_4SCN titration employing $Fe(NH_4)(SO_4)_2$ as an indicator, according to the Volhard Method.[18]

Surface morphology and elemental composition – scanning electron microscopy with energy dispersive X-ray analysis (SEM–EDX)

Investigation of the fiber morphology was investigated by scanning electron microscopy using a JEOL JSM 6610LV microscope operating at 20 kV after sputtering the samples with gold. The elemental composition was analyzed using an INCA Energy 350 Dispersive X-ray Microanalysis System.

Determination of the antimicrobial activity of the silver-loaded TEMPO-oxidized hemp fibers

The agar diffusion test[19] was used to assess the antimicrobial activity of the TEMPO-oxidized hemp fibers with incorporated silver particles. Three test organisms were used: Gram-positive *S. aureus* (ATCC 25923), Gram-negative *E. coli* (ATCC 25922), and the yeast *C. albicans* (ATCC 24433). The agar diffusion test consists in placement of 1.0 cm×1.0 cm samples (0.05 g of parallelized and pressed fibers) onto an agar support inoculated with the test microorganisms and, after 24 h incubation at 37 °C, measuring the width of the zone of inhibition (clear) or suppression (diffuse) of growth against the indicator organisms in comparison to a control sample.

RESULTS AND DISCUSSION

Obtaining silver-loaded hemp fibers

The hemp fibers were first oxidized by TEMPO-mediated oxidation in order to prepare fibers for silver deposition, *i.e.*, to improve the sorption properties by introduction of functional groups, which are necessary for silver sorption. Several oxidations with different concentration of sodium hypochlorite (0.30, 2.42, 4.84 and 9.67 mmol per gram of fibers) and different oxidation time (1–4 h) were investigated. The influences of the oxidation time and concentration of NaClO on the amount of introduced carbonyl and carboxyl functional groups, and silver sorption are shown in Fig. 1.

As can be seen Figs. 1a and 1b, the TEMPO-mediated oxidation with the lowest concentration of NaClO (0.30 mmol per gram of fibers) caused a slight decrease in the content of both the CHO and COOH functional groups, compared with corresponding value for the unmodified hemp fibers. The reason for these decreases could be the consumption of most of the oxidizing agents on oxidation and removal of lignin, hemicelluloses, and other accompanying components in hemp fibers, while the remaining amount of the oxidizing agent was not suffi-

2012 Copyright (CC) SCS

cient to enable significant conversion of hydroxyl groups to carbonyl and further to carboxyl groups.[7]

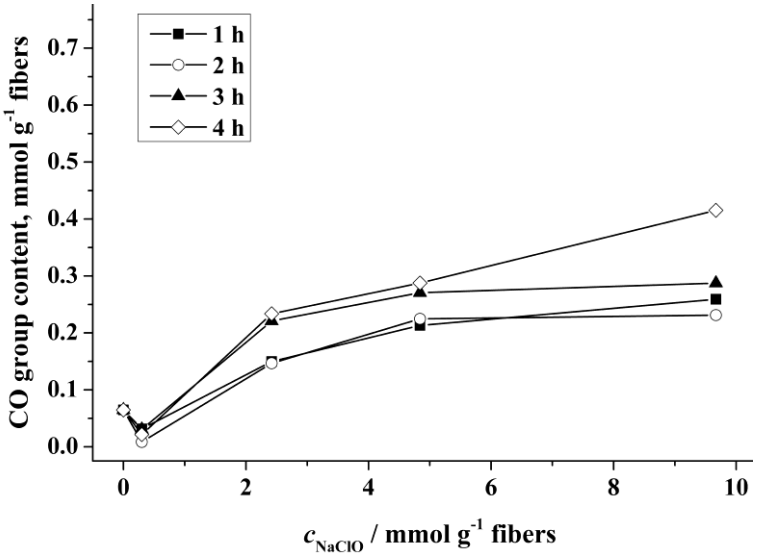

(a)

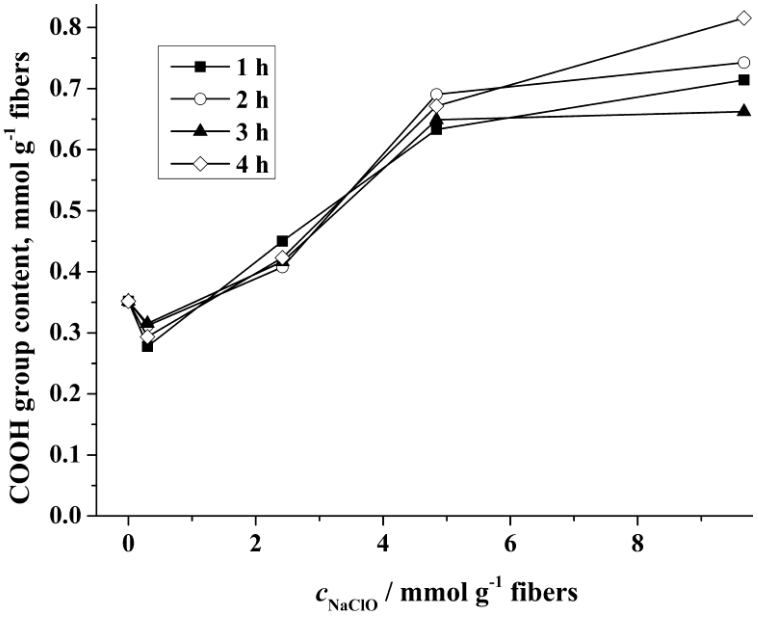

(b)

2012 Copyright (CC) SCS

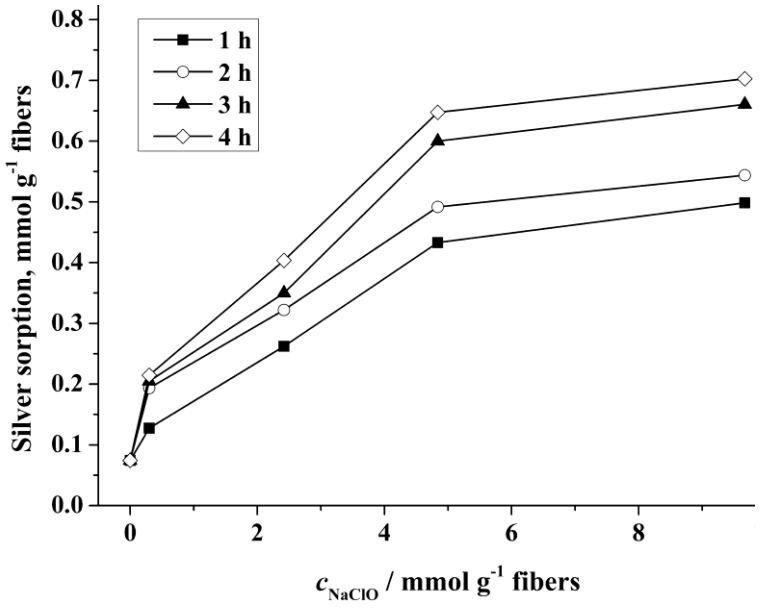

(c)

Fig. 1. Relationship between the amount of NaClO (0.30, 2.42, 4.84, and 9.67 mmol g^{-1} fibers) used in TEMPO-mediated oxidation of hemp fibers and a) carbonyl group content, b) carboxyl group content and c) silver sorption. The oxidations were performed for 1–4 h at room temperature and pH 10.5.

Oxidation in the presence of higher concentrations of NaClO (2.42–9.67 mmol per gram of fibers) led to slight increases in the carbonyl and significant increases in the carboxyl group content. Obtained increase of the content of functional groups is predictable results, because TEMPO-mediated oxidation presents the selective oxidation at C6 of the anhydroglucose units of cellulose to carboxyl groups *via* the intermediate carbonyl stage, finally producing water-soluble polyglucuronic acids. The carboxyl groups introduced by the TEMPO-oxidation are present on the crystal surfaces and in disordered regions of celluloses, without any introduction inside of the cellulose crystallites. The nitroxyl radical affects the oxidation from the alcohol to the carboxyl oxidation state, while the hypobromite generated *in situ* from hypochlorite and bromide performs further oxidation of the carbonyl to the carboxylic acid.[8,9] The maximum carbonyl (0.415 mmol per gram of fibers) and carboxyl group content (0.815 mmol per gram of fibers) were obtained for the hemp fibers oxidized under the most severe conditions (4 h, 9.67 mmol NaClO per gram of fibers).

The hydrophilic carboxyl groups present in the TEMPO-oxidized hemp fibers enable the incorporation of silver, which was realized in the present study from aqueous silver nitrate solution. These groups are reactive sites for the

2012 Copyright (CC) SCS

incorporation of silver and the predicted mechanism is that one COO^- group reacts with one Ag^+ by the ion-exchange process; *i.e.*, by partial cation exchange of H^+ (from the COOH groups) by Ag^+.[20] According to the protocol proposed by Ifuku *et al.*,[21] after the ion-exchange process, reduction of the silver salt on the surface of the TEMPO-oxidized fibers can lead to fine silver particles (Fig. 2).

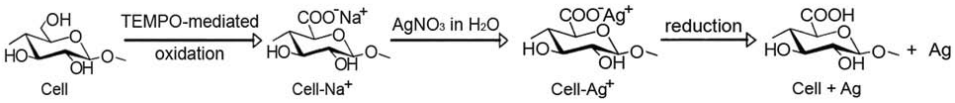

Fig. 2. Synthesis of silver particles on TEMPO-oxidized cellulose fibers.[21]

If Figs. 1b and 1c are compared, it is obvious that in the case of modification with higher concentrations of NaClO (2.42–9.67 mmol per gram of fibers), increases in both the carboxyl group content and silver sorption were obtained. However, for each sample, the number of sorbed silver ions was smaller than the number of introduced hydrophilic carboxyl groups, *i.e.*, $Ag^+ < COO^-$. According to the literature,[22] a difference in the "affinity" of various metal cations for the carboxyl groups of cellulose was noted by Heymann and Rabinov, and examined in detail by Davison. The order of increasing affinity found by this author was $N(CH_3)_4^+ < Li^+ < Na^+ < K^+ < Tl^+ < Ag^+ < Ca^{2+}$, Ba^{2+}. The applied Ca-acetate method[11] for the determination of COOH groups and the stronger affinity of COOH groups for Ca^{2+} than for Ag^+ could be the reason for the obtained result that the number of Ag^+ sorbed was smaller than the number of COO^-.

In spite of the fact that number of silver ions incorporated was smaller than the number of introduced COOH groups for all the TEMPO-oxidized hemp fibers, the amount of silver sorbed increased from 0.1273 to 0.7026 mmol silver per gram of fibers with increasing NaClO concentration used in the oxidation of the hemp fibers. The corresponding value for the unmodified sample is 0.0743 mmol silver per gram of fibers. Additionally, in the case of silver sorption, it was noticed that duration of TEMPO-mediated oxidation had a greater influence on amount of sorbed silver than the reaction time had on the amount of introduced COOH groups. To clarify this statement, the oxidation with 4.84 mmol NaClO per gram of fibers is given as an example. When the modification was performed with 4.84 mmol NaClO per gram of fibers, the amounts of introduced COOH groups were 0.633 and 0.690 mmol per gram of fibers for oxidation times of 1 and 4 h, respectively, while the corresponding silver sorptions increase from 0.433 to 0.648 mmol per gram of fibers, respectively.

All these above-mentioned results infer that, besides the introduced of COOH groups, the TEMPO-mediated oxidation caused other changes in the hemp fibers that had an influence on silver deposition.

2012 Copyright (CC) SCS

During the TEMPO-mediated oxidation, together with the introduction of functional groups, the chemical composition and fibrous morphology of hemp fibers changed, depending on the oxidation conditions. The TEMPO-mediated oxidation removes non-cellulosic substances and makes the hemp fibers finer, cleaner, softer, and more suitable for further processing and textile applications.[9,12,23,24] Changes in the crystallinity and void system (diameter, volume and inner surface of voids)[25] of hemp fibers caused by TEMPO-mediated oxidation affect their sorption properties. In a previous article,[7] the influence of TEMPO-mediated oxidation on the properties of hemp fibers were given in detail. In order to understand the influence of changes in fiber structures and properties caused by TEMPO-mediated oxidation on silver sorption better, the relationship between silver sorption and the sorption properties of TEMPO-oxidized hemp fibers is presented herein. Sorption properties of oxidized hemp fibers were evaluated by determination of water retention power and moisture sorption.

From the correlation between the content of incorporated silver into TEMPO-oxidized hemp fibers and their water retention values (*WRV*) given in Fig. 3, it is obvious that, generally, with increasing water retention values, the silver sorption also increased. Sample oxidized under the most severe conditions (9.67 mmol of NaClO per gram of fibers for 4 h) exhibited maximum values for both, *i.e.*, a sorption capacity for Ag ions of 0.703 mmol per gram of fibers and a *WRV* of 125.41 %. The obtained correlation, *i.e.*, increase in both Ag sorption and *WRV*, can be explained by the fact that when fibers sorb more water, they swell more

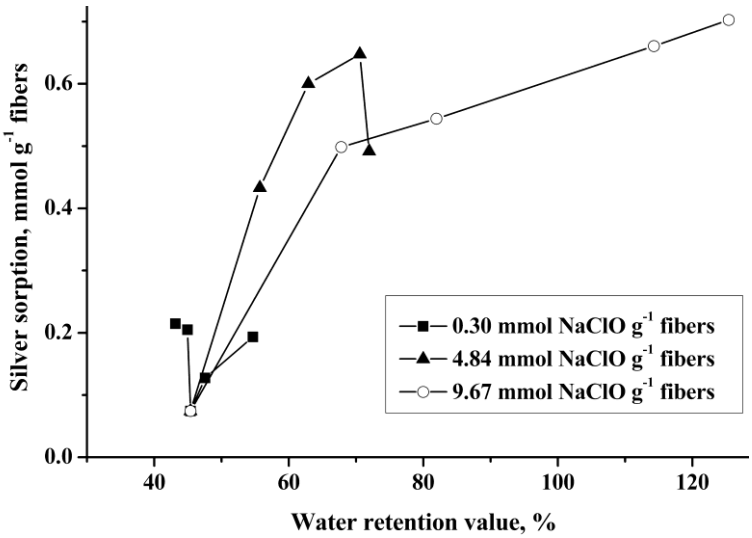

Fig. 3. Relationship between the water retention value, %, and silver sorption, mmol g^{-1}, on TEMPO-oxidized hemp fibers. The oxidations were realized using 0.30–9.67 mmol NaClO g^{-1} fibers, for 1–4 h at room temperature and pH 10.5.

2012 Copyright (CC) SCS

and the fiber structures become "open" and accessible for Ag sorption. Additionally, in the case of hemp fibers, an effective elimination of hydrophobic impurities from the surface of the fibers and morphological changes of the fibers lead to additional water sorption into the fibers, as well as silver ions from aqueous solution.[7] For the samples oxidized with the highest amount of NaClO for 1–4 h, the relationship between the moisture sorption values and the Ag^+ sorption capacity for TEMPO-oxidized hemp fibers is shown in Fig. 4.

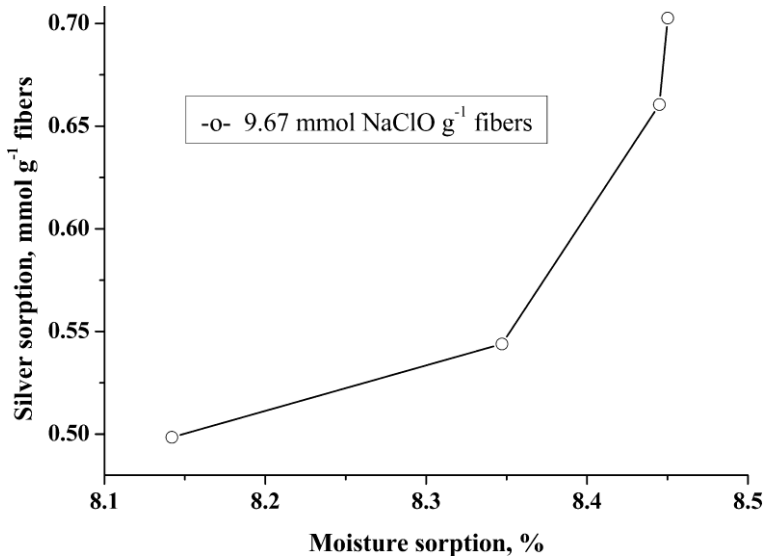

Fig. 4. Relationship between moisture sorption, %, and silver sorption, mmol g^{-1}, by TEMPO-oxidized hemp fibers. The oxidations were performed using 9.67 mmol NaClO g^{-1} fibers for 1–4 h at room temperature and pH 10.5.

The surface morphologies of the TEMPO-oxidized hemp fibers modified with the highest concentration of 9.67 mmol NaClO per gram of fibers for 2 h both without and with loading of Ag^+ were examined by SEM and the obtained microphotographs are presented in Figs. 5a and 5b, respectively. The SEM analysis revealed a large number of small and evenly distributed particles on the surface of the silver-loaded TEMPO-oxidized hemp fibers that were not present before the loading. A careful study of these two samples using the SEM–EDX technique was performed in order to identify elemental composition of the particles. The EDX spectra acquired for the before and after silver loading, presented in Figs. 5c and 5d, respectively, clearly show that the "white dots" present on the surface of the silver-loaded TEMPO-oxidized hemp fibers have strong silver peaks, while no silver observed on the unloaded sample. An EDX analysis over a 2 μm×2 μm area of the silver-loaded sample showed the presence of silver on the

2012 Copyright (CC) SCS

fiber surface in a concentration of about 8 %. Gold peaks (Au) are present in the EDX spectra because the samples were gold-sputtered before SEM analysis.

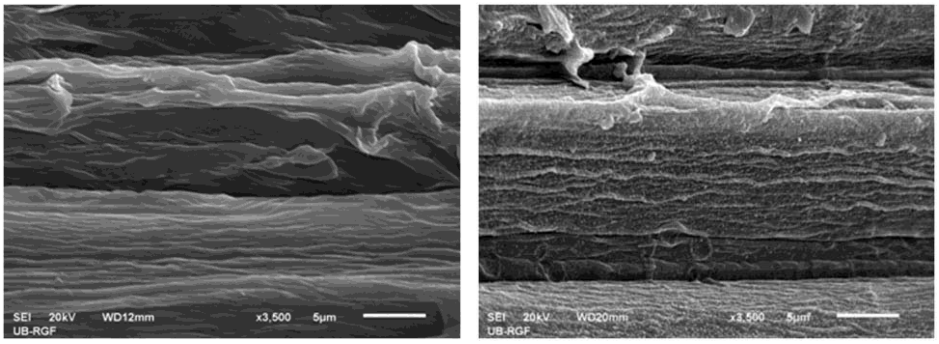

(a) (b)

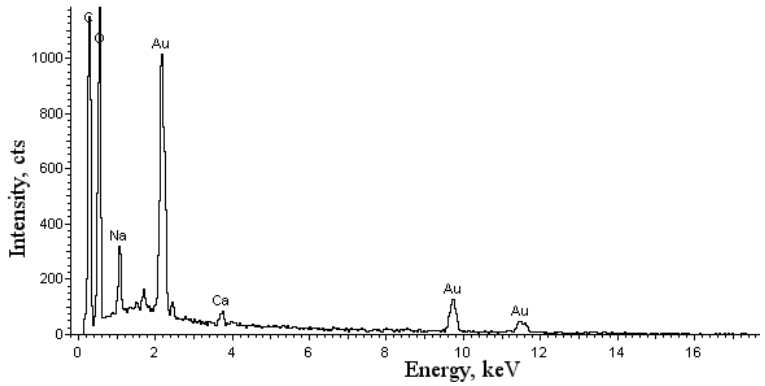

(c)

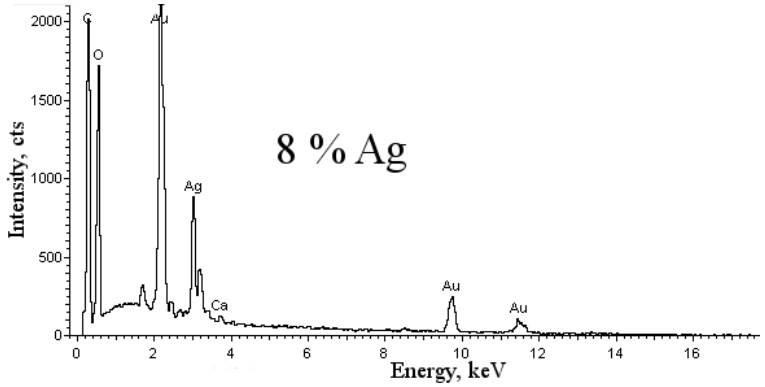

(d)

Fig. 5. SEM Images and EDX spectra of the TEMPO-oxidized hemp fibers modified with 9.67 mmol NaClO g^{-1} fibers for 2 h (a and c) and silver loaded TEMPO-oxidized hemp fibers under the same conditions (b and d). Magnification: 3500×; bar: 5 μm.

2012 Copyright (CC) SCS

SEM Images (Fig. 6) recorded under higher magnification (13000, 50000 and 100000 times) were employed to determine the dimensions of the silver particles. Silver particles, with isometric shapes and sizes ranging from 10 to 100 nm, were uniformly distributed on the surface of the silver-loaded TEMPO-oxidized hemp fibers, despite the fact that the silver deposition was realized from an aqueous silver nitrate solution by the ion-exchange technique, without any subsequent reduction step. According to the literature,[21] cellulose fibers represent unique nanoreactors for *in situ* synthesis of metal nanoparticles from ionic solution using mild reducing agents. This ability of cellulose is the consequence of its specific morphology and available oxygen-rich functional groups on the surface of the fiber. The important role of cellulose and the reducing groups in formation of silver nanoparticles was also demonstrated by Pinto *et al.* and Jiang *et al*.[26,27]

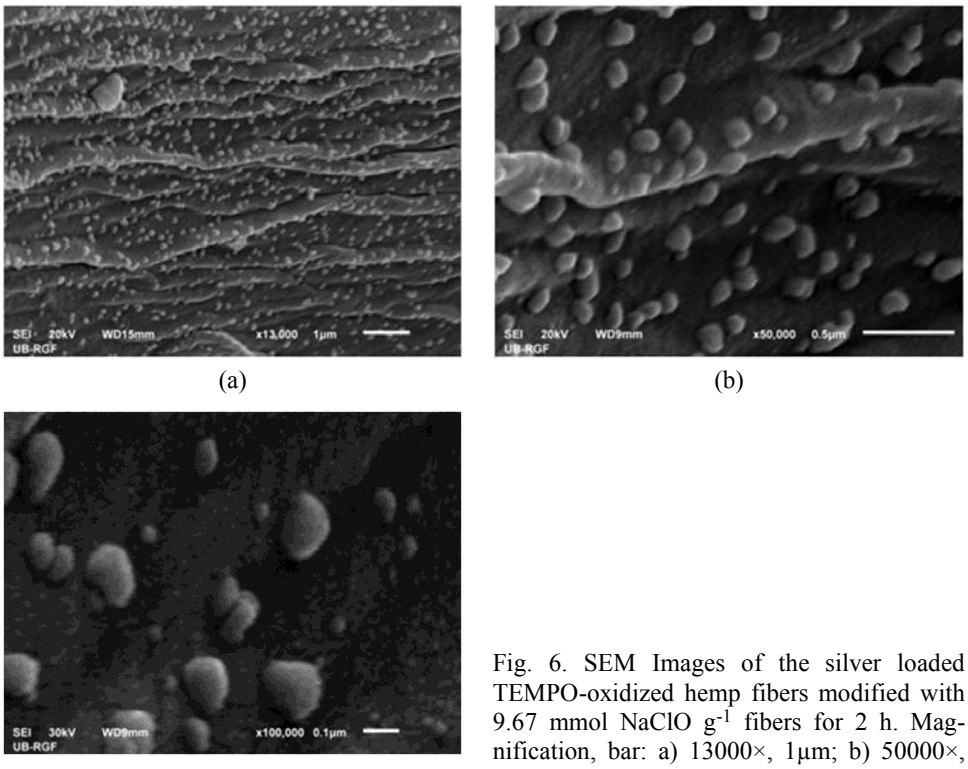

(a) (b)

(c)

Fig. 6. SEM Images of the silver loaded TEMPO-oxidized hemp fibers modified with 9.67 mmol NaClO g^{-1} fibers for 2 h. Magnification, bar: a) 13000×, 1μm; b) 50000×, 0.5μm; c) 100000×, 0.1μm.

In the present study, the direct synthesis and growth of nanoparticles from an ionic solution (without the use of any kind of reducing agent) can be explained by the formation of highly reductive aldehyde groups, as an intermediary product in the TEMPO-oxidation, which were able to reduce silver ions to metallic silver. This statement is supported by the fact that more severe oxidation conditions

2012 Copyright (CC) SCS

resulted in both higher numbers of aldehyde groups (Fig. 1a) and higher amounts of more evenly distributed nanoparticles (Fig. 7). The color of the silver-loaded TEMPO-oxidized hemp fibers changed drastically from cream yellow for oxidized fibers to brown in response to silver particle deposition.

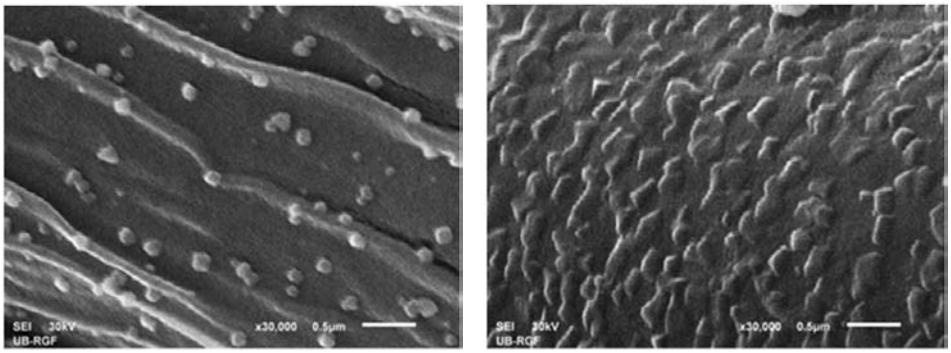

(a) (b)

Fig. 7. SEM Images of the silver loaded TEMPO-oxidized hemp fibers modified with 9.67 mmol NaClO g^{-1} fibers for a) 2 and b) 4 h. Magnification: 30000×; bar: 0.5 μm.

Antimicrobial activity of TEMPO-oxidized hemp fibers with incorporated silver particles

Antibacterial activities of the TEMPO-oxidized hemp fibers with incorporated silver particles were tested against the Gram-positive bacterium *S. aureus* (ATCC 25923) and the Gram-negative bacterium *E. coli* (ATCC 25922), and the antifungal activity was tested against a fungus from the *Candida* family, *C. albicans* (ATCC 24433). From the results presented in Table I, it could be seen that the TEMPO-oxidized hemp fibers with incorporated silver particles generally inhibited the growth of all the tested pathogens. *S. aureus* was more sensitive than strain *E. coli*. For the bacterium *S. aureus*, the silver-loaded hemp fibers containing 0.433 and 0.648 mmol Ag per gram of fibers (entries 7 and 9, in Table I) were the most effective, whereas for the bacterium *E. coli*, the sample with 0.262 mmol Ag per gram of fibers (entry 3) was the most effective. Most of the tested samples showed good antifungal activity against the fungus *C. albicans*. The sample with the maximum amount of sorbed silver (0.703 mmol Ag per gram of fibers) (entry 12) did not show maximum antimicrobial activity against any of the tested microorganisms. The obtained results showed that there was no clear correlation between the amount of sorbed silver and antimicrobial activity. However, the quantity of incorporated silver particles was, in all cases, sufficient to inhibited the growth of tested pathogens, probably because, according to the literature,[28] silver does not attack microorganisms directly; it operates as a catalytic agent and moreover, it is not consumed in this process.

2012 Copyright (CC) SCS

TABLE I. Antimicrobial activity of TEMPO-oxidized hemp fibers with incorporated silver particles

Oxidative conditions			Entry No.	Width of the inhibition zone after 24 h, mm		
c_{NaClO} / mmol g^{-1} of fibers	Reaction time, h	Sorbed silver, mmol per gram of fibers		*S. aureus*	*E. coli*	*C. albicans*
0.00	0	0.074	1	1.0–1.5	1.0–1.5	1.0–1.5
0.30	4	0.214	2	1.0–1.5	1.5	1.0–1.5
2.42	1	0.262	3	2.5–3.0	2.5–3.0	2.5–3.0
	2	0.322	4	3.0	1.0	2.5–3.0
	3	0.350	5	2.5	1.0–1.5	3.0
	4	0.404	6	2.5–3.0	1.0–1.5	3.0
4.84	1	0.433	7	3.5–4.0	1.0–1.5	2.5–3.0
	3	0.600	8	3.0	1.0–1.5	2.5–3.0
	4	0.648	9	4.0	1.5–2.0	3.0–3.5
9.67	1	0.498	10	2.5–3.0	1.0	2.0
	3	0.660	11	2.0	1.0	2.5–3.0
	4	0.703	12	3.0	1.0	2.0

CONCLUSIONS

The introduced hydrophilic carboxyl groups (0.278–0.815 mmol per gram of fibers) and other changes in hemp fibers caused by TEMPO-mediated oxidation influence an increased silver sorption. The amount of sorbed silver onto the modified hemp fibers was in the range 0.214–0.703 mmol per gram of fibers. SEM microphotographs of the modified hemp fibers with sorbed silver showed uniformly distributed silver particles on the surface of the fibers, with isometric shapes and sizes from 10 to 100 nm, and the EDX spectra showed the presence of silver at a concentration of about 8 %. The obtained direct synthesis and growth of nanoparticles from ionic solution (without the use of any kind of reducing agent) could be explained by the formation of highly reductive aldehyde groups, as an intermediary product in the TEMPO-oxidation, which are able to reduce silver ions to metallic silver. The TEMPO-oxidized hemp fibers with sorbed silver showed good antibacterial activity against the tested bacterium strains: *S. aureus* (ATCC 25923) and *E. coli* (ATCC 25922), and the fungus *C. albicans* (ATCC 24433), while the best antimicrobial activity of the silver-loaded TEMPO-oxidized hemp fibers was shown against the Gram-positive bacterium *S. aureus*.

Acknowledgments. This study was supported by the Ministry of Education, Science and Technological Development of the Republic of Serbia (Project OI 172029). The authors also thank ITES Odzaci (Serbia) for supplying the hemp fibers and Aleksandar Pacevski, PhD (Faculty of Mining and Geology, University of Belgrade) for obtaining the SEM images.

2012 Copyright (CC) SCS

ИЗВОД

АНТИМИКРОБНА *TEMPO*-ОКСИДИСАНА ВЛАКНА КОНОПЉЕ СА ИНКОРПОРИСАНИМ ЧЕСТИЦАМА СРЕБРА

ЈОВАНА МИЛАНОВИЋ, ТАТЈАНА МИХАИЛОВИЋ, КАТАРИНА ПОПОВИЋ и МИРЈАНА КОСТИЋ

Технолошко–металуршки факултет, Универзитет у Београду, Karnegijeva 4, 11120 Београд

Циљ овог рада је добијање антимикробних влакана конопље са сорбованим сребром. Модификовање влакана конопље у циљу повећања сорпционих својстава, а тиме и што бољег сорбовања сребра, постигнуто је селективном ТЕМПО-оксидацијом, тј. оксидацијом помоћу катализатора 2,2,6,6-тетраметилпиперидин-1-окси радикала (*TEMPO*) у систему натријум-хипохлорит/натријум-бромид, док је сребро сорбовано из раствора сребро-нитрата. Променом параметара оксидације, тј. концентрације натријум-хипохлорита и времена оксидације, одређени су најпогоднији услови извођења *TEMPO*-оксидације. Добијени резултати показали су да је максимални сорпциони капацитет (0,703 mmol сребра по граму влакна) модификованих влакана конопље добијен код узорка који је оксидисан помоћу 9,67 mmol NaClO по граму целулозе, током 4 сата. SEM микрофотографије модификованих влакана конопоље са сорбованим сребром показале су, на површини влакана, равномерну дистрибуцију честица сребра изометричног облика и нано величине (од 10 до 100 nm), упркос чињеници да је сребро сорбовано из јонског раствора. Антибактеријска активност *TEMPO*-оксидисаних влакана конопље са инкорпорисаним честицама сребра тестирана је *in vitro* на две врсте бактерија: грам-позитивна *Staphylococcus aureus* (ATCC 25923) и грам-негативна *Escherichia coli* (ATCC 25922), док је антифунгална активност испитана према гљивици *Candida albicans* (ATCC 24433). Најбољу антимикробну активност *TEMPO*-оксидисана влакна конопље са инкорпорисаним честицама сребра, показала су према грам-позитивној бактерији *S. aureus*.

(Примљено 18. октобра, ревидирано 10. децембра 2012)

REFERENCES

1. U. C. Hipler, P. Elsner, J. W. Fluhr, in *Biofunctional Textiles and the Skin; Current Problem in Dermatology*, Vol. 33, U. C. Hipler, P. Elsner, Eds., Karger, Basel, 2006, p. 165
2. D. Hofer, in *Biofunctional Textiles and the Skin; Current Problem in Dermatology*, Vol. 33, U. C. Hipler, P. Elsner, Eds., Karger, Basel, 2006, p. 42
3. A. B. G. Lansdown, *in Biofunctional Textiles and the Skin; Current Problem in Dermatology*, Vol. 33, U. C. Hipler, P. Elsner, Eds., Karger, Basel, 2006, p. 17
4. U. Wollina, M. B. Abdel-Nase, S. Verma, in *Biofunctional Textiles and the Skin; Current Problem in Dermatology*, Vol. 33, U. C. Hipler, P. Elsner, Eds., Karger, Basel, 2006, p. 1
5. R. Kozlowski, S. Manys, J. Kozlowska, *Sovremennoe polozhenie u perspektivy na budushchee dlya l'na i pen'ki na rubezhe XX i XXI vekov*, Tezisy dokladov nauchno-prakticheskai konferentsii "Len − na poroge XXI veka". Vologda, Russia, 2000 (in Russian)
6. H. M. Wang, R. Postle, R. W. Kessler, W. Kessler, *Text. Res. J.* **73** (2003) 664
7. J. Milanovic, M. Kostic, P. Milanovic, P. Skundric, *Ind. Eng. Chem. Res*. **51** (2012) 9750
8. P. S. Chang, J. F. Robyt, *J. Carbohydr. Chem.* **15** (1996) 819
9. T. Saito, Y. Okita, T. T. Nge, J. Sugiyama, A. Isogai, *Carbohydr. Polym.* **65** (2006) 435
10. T. Saito, A. Isogai, *Biomacromolecules* **5** (2004) 1983
11. E. C. Yackel, W. O. Kenoyon, *J. Am. Chem. Soc.* **64 (**1942) 121
12. J. Praskalo, M. Kostic, A. Potthast, G. Popov, B. Pejic, P. Skundric, *Carbohydr. Polym.* **77** (2009) 791

2012 Copyright (CC) SCS

13. E. J. Parks, R. L. Hebert, *Tappi. J.* **55** (1972) 1510
14. *ASTM D 2654-76: Moisture Content and Moisture Regain of Textiles*, in *Annual Book of ASTM Standards*, American Society for Testing and Materials, Philadelphia, PA, 1978
15. *ASTM D 1776-74: Conditioning Textiles and Textile Products for Testing*, in *Annual Book of ASTM Standards*, American Society for Testing and Materials, Philadelphia, PA, 1978
16. *ASTM D 2402-78: Standard Test Method for Water Retention of Fibers, Centrifuge Method*, in *Annual Book of ASTM Standards,* American Society for Testing and Materials, Philadelphia, PA, 1978
17. M. M. Kostic, J. Z. Praskalo, S. I. Dimitrijevic, M. V. Baljak, B. M. Pejic, P. D. Skundric, in *Proceedings of the 7th Annual Textile Conference by AUTEX – From Emerging Innovations to Global Business*, Tampere, Finland, 2007, p. 1267
18. P. Patnaik, *Handbook of Environmental Analysis*, Lewis Publishers, CRC Press, Boca Raton, CA, 1997, p. 39
19. B. G. Joiner, in *Bioactive Fibers and Polymers*, J. V. Edwards, L. T. Vigo, Eds., American Chemical Society, Washington DC, 2001, p. 201
20. J. Z. Praskalo-Milanovic, M. M. Kostic, S. I. Dimitrijevic-Brankovic, P. D. Skundric, *J. Appl. Polym. Sci*. **117** (2010) 1772
21. S. Ifuku, T. Manami, M. Minoru, S. Hiroyuki, H. Yano, *Biomacromolecules* **10** (2009) 2714
22. A. M. Sookne, M. Harris, in *Cellulose and Cellulose Derivatives*, Part I, E. Ott, H. M Spurlin, M. W. Grafflin, Eds., Interscience Publishers, New York, 1954, p. 213
23. A. E. de Nooy, A. C. Besemer, H. van Bekkum, *Carbohydr. Res.* **89** (1995) 269
24. Z. Dang, J. Zhang, A. Ragauskas, *Carbohydr. Polym.* **70** (2007) 310
25. T. Kreze, S. Jeler, S. Strnad, *Mater. Res. Innov.* **5** (2002) 277
26. R. J. B. Pinto, P. A. A. P. Marques, C. P. Neto, Y. Trindade, S. Daina, P. Sadocco, *Acta Biomater.* **5** (2009) 2279
27. T. Jiang, L. Liu, J. Yao, *Fibers Polym*. **12** (2011) 620
28. R. L. Davis, S. F. Etris, *Catal. Today* **36** (1997) 107.

2012 Copyright (CC) SCS

Journal of the Serbian Chemical Society
JSCS-info@shd.org.rs • www.shd.org.rs/JSCS
J. Serb. Chem. Soc. 77 (12) 1775–1785 (2012)
JSCS–4388
UDC 661.183.8+539.217+544.02:621.71
Original scientific paper

Effect of cooling rate on the microstructure and porosity of alumina produced by freeze casting

JESÚS M. RODRÍGUEZ-PARRA, RODRIGO MORENO* and MARÍA ISABEL NIETO

Institute of Ceramics and Glass, CSIC, Kelsen 5, 28049 Madrid, Spain

(Received 18 November, revised 3 December 2012)

Abstract: Freeze casting is a well-known shaping technique for the production of materials with directional porosity. One of the major problems is the difficulty to control the cooling rate, thus leading to gradients in pore size and homogeneity. This work deals with the manufacture of alumina ceramics with directional porosity by freeze casting of aqueous suspensions. An experimental set-up was prepared in order to apply different cooling rates. Freeze casting tests were performed with an aqueous alumina suspension after optimization of its rheological behavior. The porosity and microstructural features of the sintered bodies produced under different experimental conditions were studied and analyzed. It was concluded that the cooling rate influences the microstructure while the final temperature has a much lower influence. In addition, microstructural analysis showed that there was a gradient in the directionality of the pores, being lower at the bottom and the top and higher in the central region of the specimens.

Keywords: suspensions; shaping; ceramics; porous materials; alumina; microstructures.

INTRODUCTION

The design of materials with tailored porosity has received increasing attention in the field of porous ceramics, due to the large number of their applications in different technologies.[1–5] Within the available techniques for the manufacture of porous materials, great effort has been devoted to the study of the application of freeze-casting to obtain ceramics with aligned porosity,[6–13] and to establish the influence of different processing variables on the pore size and distribution.

The freeze casting process is based on the fast freezing of a suspension inside a non-porous mould and the subsequent elimination of liquid by sublimation under vacuum conditions. Different liquids have been employed, such as water and camphene,[14,15] which require different freezing temperatures. The obtained

* Corresponding author. E-mail: rmoreno@icv.csic.es
doi: 10.2298/JSC121018132R

Available online at shd.org.rs/JSCS/

2012 Copyright (CC) SCS

porosity is a replica of the frozen liquid; hence, the solid content of the suspensions is directly related to the porosity volumes allowed. When aqueous suspensions are used, it was demonstrated that the presence of a binder is mandatory. Otherwise, the frozen structure formed collapses during sublimation and the pores tend to close.[8]

The most important parameters involved in the process are the freezing temperature, the rate and manner of cooling and the solids content.[6–9,16–23] Cooling temperatures ranging from –20/–80 °C down to liquid nitrogen temperature (–196 °C) are normally used. The solids content determines the volume of the porosity and the pore size.[6,7,9,21,22] There is an optimal range of suspension concentrations required to obtain a handling solid and to avoid microstructure collapse if the solid content is very high.

The parameter that dominantly influences the orientation of the porosity is the cooling procedure.[16–19] Bulk freezing leads to porous materials with a homogeneous distribution of porosities, while it is possible to obtain microstructures with directionally aligned porosities if only the bottom part of suspension is in contact with the freezing agent, so the ice grows in a vertical direction and aligned channels will be obtained after the sublimation process. The cooling process can be performed at a constant temperature or constant cooling rate. When the temperature is maintained constant, the microstructure shows the formation of different oriented colonies with aligned pores, while if the freezing is performed at a constant rate, a porous structure with unidirectional channels is obtained.[8] The size of the ice dendrites is a function of the formation velocity of the ice front;[9] consequently, the rate of freezing determines the size of obtained pores.[16–19]

Poly(vinyl alcohol) (PVA) and glycerol are the most frequently used additives for freezing.[10–12,17,19,24–26] PVA is usually added in concentrations ranging from 2 to 20 wt. %, and it was observed that the dendrites and consequently the pores are finer as the PVA content increases.[12,24] The addition of PVA also transforms the non-interconnected lamellar pores into small and interconnected lamellar pores.[24] Glycerol reduces the volumetric expansion of water and binds to water molecules, reducing the size of the growing ice crystals.[9,25,26] The concentration of glycerol is always related to water, and it is normally added in the range from 10 to 30 wt. %.

In the present work, porous alumina bodies with aligned porosities were shaped by directionally freeze drying at a constant rate of cooling. The influence of freezing rate and freezing temperature on the porosity and microstructure of the sintered alumina specimens was studied and discussed.

EXPERIMENTAL

Commercial α-alumina (Ceralox, Condea HPA05, USA), with an average particle size of 0.4 μm and a specific surface area of 9.5 $m^2 g^{-1}$ was used. The colloidal stability was studied and reported in a previous work, in which the isoelectric point was reported to occur at pH 9

2012 Copyright (CC) SCS

and the effect of polyelectrolyte (an ammonium salt of poly(acrylic acid) (PAA, Duramax D3005, Rohm & Haas, PA, USA) was also studied.[27] This deflocculant is supplied as an aqueous solution with a concentration of 35 wt. % of active matter and has a pH 7–8 and a density of 1.16 g cm^{-3}. The maximum stability was achieved at a concentration of PAA of 0.8 wt. % (*i.e.*, 0.35 wt. % active matter) on a dry solids basis.

Commercial glycerol (Sigma-Aldrich, Germany) was used as a cryoprotector. Concentrated suspensions were prepared to a solids loading of 35 vol. % (*i.e.*, 67 wt. %) by adding 20 wt. % of glycerol (with regard to solids). According to previous studies, these conditions led to good properties in terms of pores volume and size.[19] The suspensions were homogenized during ball milling for 6 h.

The rheological behavior of fresh ball milled suspensions was studied with a rheometer (RS50, Haake, Germany) using a double-cone/plate sensor configuration (DC60/2°, Haake, Germany). The tests were performed under controlled rate (CR) conditions using a three stage program with a linear increase of shear rate from 0 to 1000 s^{-1} in 300 s, a plateau at 1000 s^{-1} for 120 s, and a further decrease to zero shear rate in 300 s. The flow curves of the optimized suspension were measured as a function of ageing time, until 9 days after preparation. The particle size was measured using laser diffraction equipment (Mastersizer S, Malvern, UK) on suspensions diluted to 0.01 g dm^{-3}.

A 22 cm in height copper cylinder was designed as a support for the mould. This mould consisted of a metallic piece on the bottom and plastic walls, in order to allow the transmission of heat from the bottom to the top of the suspension when the copper cylinder was immersed in liquid N_2. A glass fiber matt was used as an isolating component to allow proper control of the cooling rate. Two different devices were used to contain the liquid nitrogen. Firstly, a simple metal container with isolating fibers and polyethylene rings was designed in order to minimize nitrogen loss. Furthermore, the liquid nitrogen was poured in a Dewar vessel supported on a metal box so that the height of the support and hence the cooling rate of the suspension container could be controlled. Temperature control was realized between –200 and 200 °C using a thermocouple (Type T, Watlow No: OKT30B12B, UK) connected to a power source (ITC 503s, Oxford Instruments, UK) where the temperature was revealed. Considering the foreseen cooling procedures (rates), freeze cast samples were dried using a freeze dryer (CRYODOS-50, Telstar, Terrassa, Spain) for 24 h. The condenser temperature was 50 °C and the conditions of the storage camera were 20 °C and 50 Pa. Further characterization was performed for samples prepared at –60 and –90 °C using the Dewar, and at –60 °C in the metallic container. These samples were labeled as –60D, –90D and –60C, respectively.

The green density of freeze cast specimens was measured by the Archimedes method using mercury. The green specimens were sintered at 1500 °C for 2 h in an electric furnace. The sintered specimens were characterized by microstructure observations using a field emission scanning electron microscopy (FE–SEM, (Hitachi S-4700 type I). The porosity was measured by mercury intrusion porosimetry (Poremaster, Quantachrome Corp., USA).

RESULTS AND DISCUSSION

The stability of optimized alumina suspensions (with deflocculant and glycerol) was studied by measuring the flow curves daily until the viscosity started to increase. The flow curves of the fresh suspension and after different ageing times are shown in Fig. 1. The suspensions had a low viscosity until day 7 and were nearly Newtonian. The evolution of the viscosity with time is shown in Fig.

2012 Copyright (CC) SCS

2, from which it can be seen that the viscosity first remained constant and then sharply increased after 9 days.

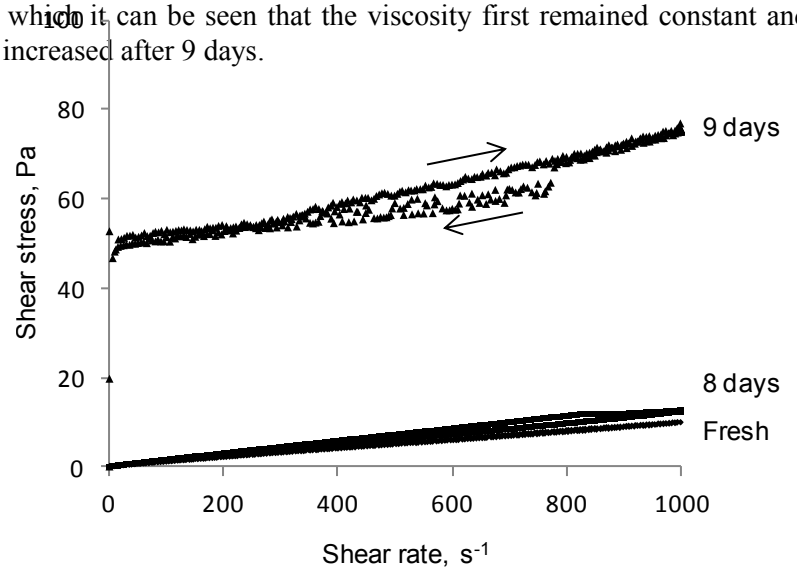

Figure 1. Flow curves of alumina suspensions, just after prepared and after 8 and 9 days ageing.

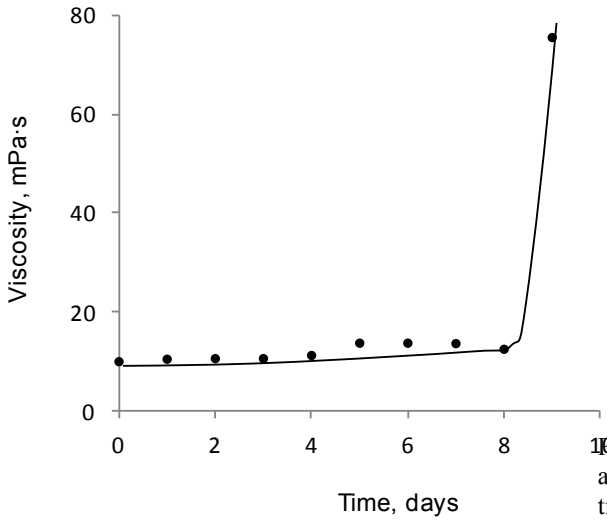

Figure 2. Evolution of viscosity of alumina suspension with ageing time (shear rate, 1000 s^{-1}).

Particle size distribution was measured after dilution of the concentrated suspensions used for the rheological behavior studies. The distribution curve was bimodal with a major contribution of fine particles centered on less than 1 μm with a smaller fraction of the particles having sizes less than 10 μm. There was no change in the size distribution during ageing for a few days, but the coarse fraction seems to increase after that, in agreement with the rheological behavior.

2012 Copyright (CC) SCS

The particle size distributions of fresh suspensions and after 9 days of ageing are shown in Fig. 3.

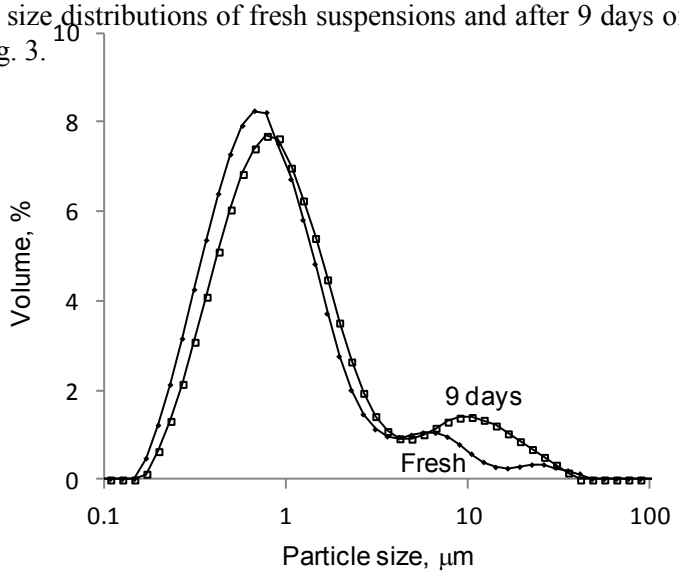

Figure 3. Particle size distribution as measured for the fresh suspension and after 9 days ageing.

Once the stability of the suspensions was ensured, the freezing device was optimized in order to allow for the control of the cooling temperature. Thus, the thermocouple was calibrated by measuring the voltage as a function of temperature in the range from –4.19 to 0.273 mV.

The variations of the temperature with time for the two types of cooling devices described in the experimental section, *i.e.*, the Dewar, and the simple metal container, are shown in Fig. 4. In both cases, the temperature was measured at the top of the metal container, in contact with the suspension, and in the lateral surface of the copper cylinder. It can be seen that the use of a Dewar assured a more homogeneous temperature variation with higher cooling rates and that a lower temperature was reached, as expected. By fitting the curves in the linear range (to –60 °C), calculated rates were 6.8 and 3.4 °C min^{-1} for the Dewar and the metal container, respectively. With this control of temperature, the samples were frozen and dried as described above, giving the samples –60D, –90D and –60C were obtained. The green bodies obtained after freeze-drying for 48 h had densities of 1.63±0.02 g cm^{-3} (*i.e.*, 41 % of theoretical density). These samples were sintered at 1500 °C with a 2-h soaking time.

The data obtained by Hg-porosimetry for the sintered bodies are given in Table I. All samples exhibited macroporosity, which was slightly higher for the samples obtained in the metal container, due to the slower cooling rate. According to Table I, it appears that the cooling rate had no significant effect on the total

2012 Copyright (CC) SCS

pore volume. However, samples cooled in the Dewar had a narrower pore size distribution (Fig. 5), confirming their higher homogeneity.

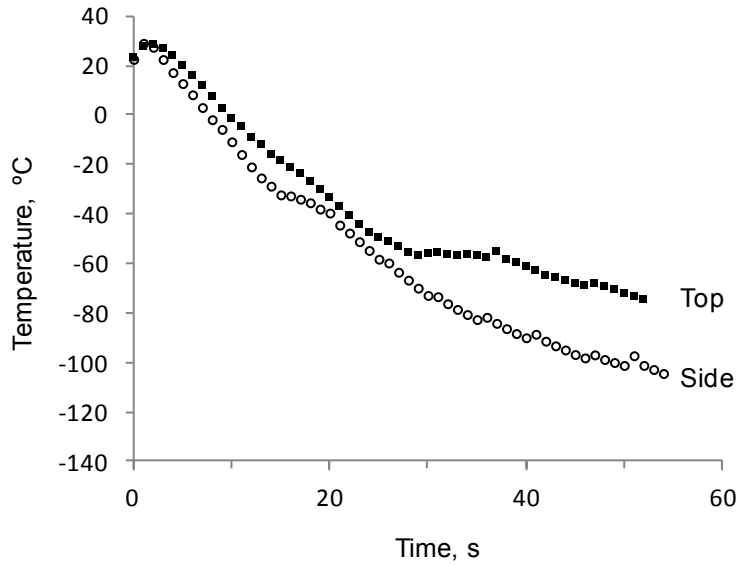

(a)

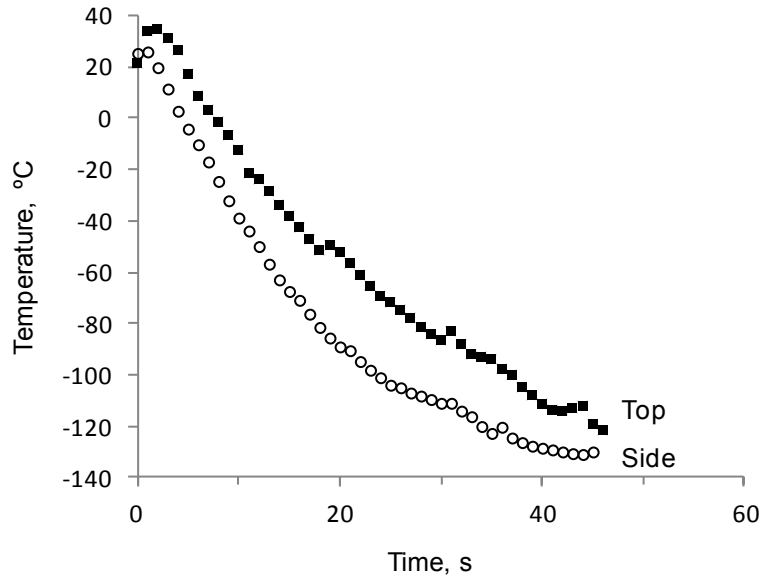

(b)

Figure 4. Variation of temperature with time when cooling with the simple metal container (a), and the Dewar (b). Temperature is measured in both cases at the top of the metal container, in contact with the suspension, and in the lateral surface of the copper cylinder.

2012 Copyright (CC) SCS

Table 1. Density and porosity of the samples obtained at different cooling conditions

Sample	ρ_{green} g cm^{-3}	$\rho_{sintered}$ g cm^{-3}	Pore volume cm^3 g^{-1}	Pore diameter μm	Pore area m^2 g^{-1}
–60C	1.63	2.31	0.17	4.6	0.14
–60D	1.63	2.36	0.15	4.8	0.17
–90D	1.65	2.48	0.15	4.6	0.13

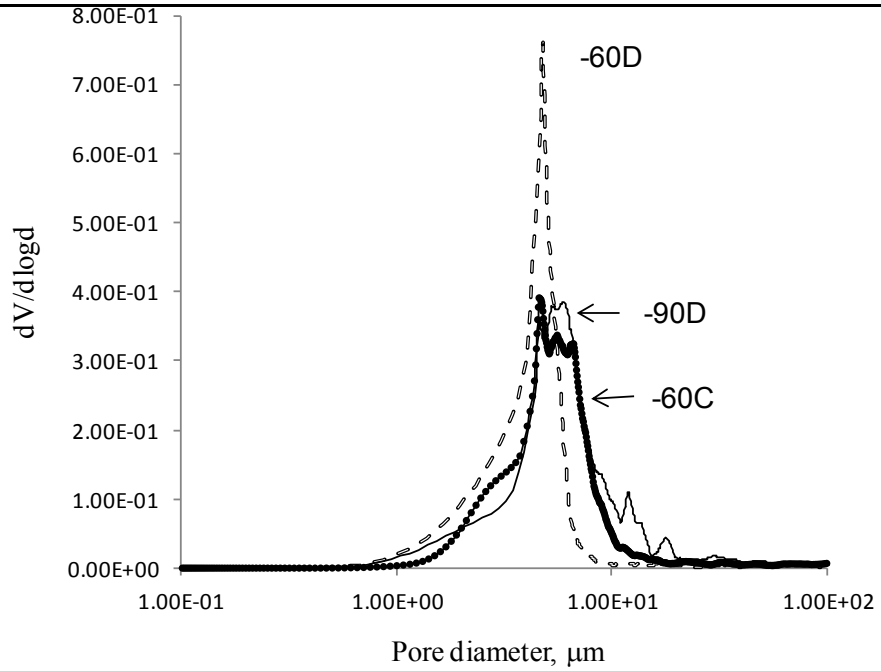

Figure 5. Pore size distribution of sintered alumina samples prepared at the different cooling conditions.

In spite of the similarities in the macroporous structure, SEM observations demonstrated that there were some differences among the variously prepared samples. Low magnification SEM pictures of the three studied samples are shown in Fig. 6. Directional porosity is clear in all samples, but the sample –60D is more homogeneous than –60C, which exhibited lower microstructural uniformity since the areas with directional porosity and dense areas were combined.

SEM observations at higher magnification, Fig. 7, were performed in order to compare the microstructural features of samples prepared under different conditions. Sample –60C revealed a lower degree of directionality and the pores were larger in diameter than those in the other two samples both having rather similar pore sizes and size distributions, which is in good agreement with porosimetry results. Comparing all these microstructures, it was noticed that the cell walls were larger for the sample –60C. This sample, obtained with the lowest cooling rate, revealed characteristics in agreement with results of Deville *et*

2012 Copyright (CC) SCS

al,[8,18] who reported that both the size of the pores and the cell walls were larger if the cooling rate was lower.

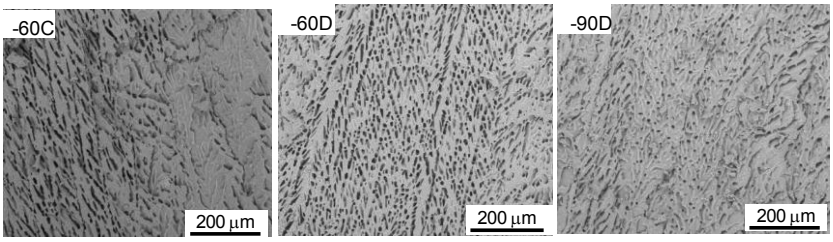

Figure 6. General view of the microstructure of the sintered alumina samples prepared at the different cooling conditions.

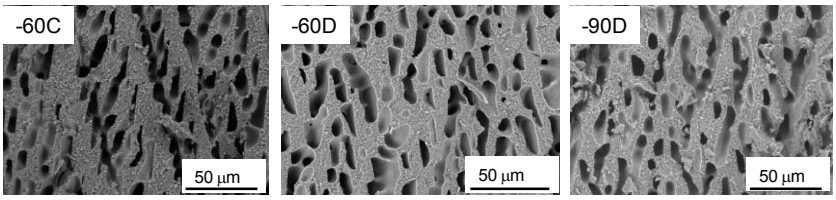

Figure 7. SEM Pictures at high magnification showing the microstructure of the sintered alumina samples studied.

The observation of the cell walls at higher magnifications (Figs. 8 and 9) revealed a well-developed microstructure, with equiaxed grains without exaggerated grain growth and a high densification degree. The materials showed that sintering had been completed to nearly full density, without intergranular porosity and only some pores trapped inside the grains formed by coalescence of smaller grains.

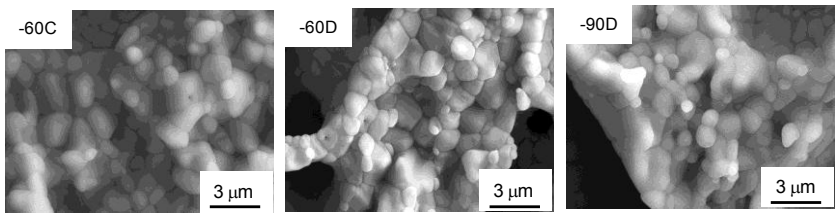

Figure 8. SEM Pictures showing the microstructure of the cross-section of the cell walls for sintered alumina samples prepared at the different cooling conditions.

Another point raised elsewhere[9,18] is the problem related to internal differences in the microstructure of freeze-dried compacts. As reported, irregular heat transfer causes changes in the microstructural features along the sample height, because of the temperature gradients leading to morphological differences in the orientation of the porosity channels formed during ice sublimation. To confirm this

2012 Copyright (CC) SCS

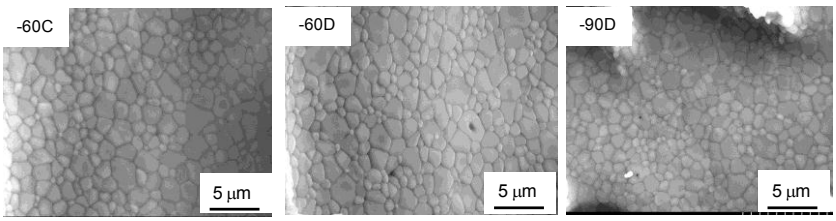

Figure 9. SEM Microstructures of the sintered alumina samples prepared at the different cooling conditions.

aspect, samples were transversally cut to obtain samples from different position along the sample height. The results were similar for all three samples, but sample –60D was selected as a case study. The samples have three regions with different density and porosity, *i.e.*, the sample bottom, in contact with the cooling metallic surface, the central body and top surface, which is the region in contact with air and at the opposite extreme of the cooling surface. Characteristic microstructures of these three regions are shown in Fig. 10. The microstructure at the sample bottom shows randomly distributed pores due to the fast freezing occurring in the vicinity to contact. The central body, which represents the major vo-

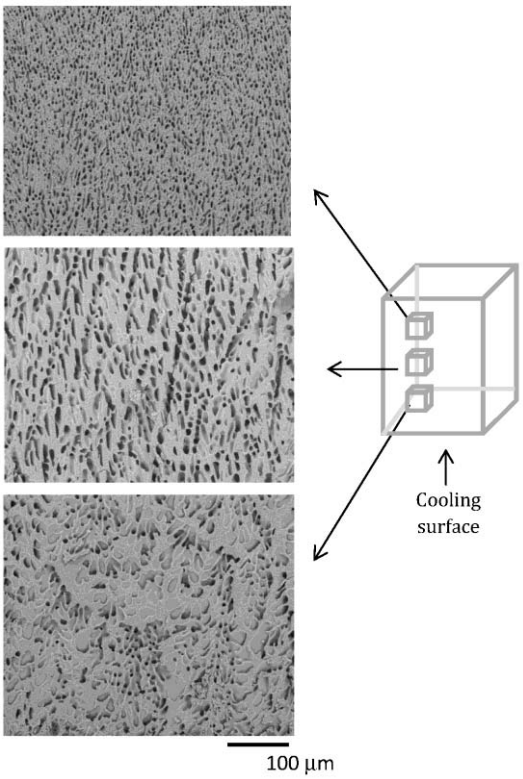

Figure 10. Characteristic SEM microstructures at different heights of freeze cast sintered specimens.

2012 Copyright (CC) SCS

lume of the specimen, showed a higher directionality of the pores and higher uniformity at a macroscopic level. Finally, at the top of the sample, the pore alignment was lower and the size of the pores tended to decrease with respect to those observed in the body.

Summarizing the above results, it could be concluded that the main processing parameter influencing the microstructure is the cooling rate, whereas the temperature itself seems to have a negligible effect if the whole volume of the sample was frozen. Thus, by regulating the cooling rate to a constant value, it would be possible not only to shape materials with aligned porosity, but also to tailor materials with graded porosity in size and alignment.

CONCLUSIONS

Sintered alumina parts with aligned pores were obtained by directional freeze casting. Aqueous alumina suspensions were prepared to solids loadings of 35 vol. % and 20 wt. % of glycerol as a cryoprotector. The suspensions retained stability for at least one week. Control of cooling rate was achieved by an appropriate design of a metal support using either a metal container or a Dewar vessel to obtain different cooling rates. After sintering at 1500 °C, materials with aligned porosity and total volume of pores higher than 40 % were obtained. It was concluded that the cooling rate has a strong influence on the porosity and the microstructure, whereas temperature itself seems to have very low influence.

Acknowledgement. This work was supported by Spanish Ministry of Economy and Competitiveness (MAT2009-14369-C02-01).

ИЗВОД

УТИЦАЈ ТЕМПЕРАТУРЕ ХЛАЂЕЊА НА МИКРОСТРУКТУРУ И ПОРОЗНОСТ ГЛИНИЦЕ ДОБИЈЕНЕ МЕТОДОМ ЛИВЕЊА НА НИСКИМ ТЕМПЕРАТУРАМА

JESÚS M. RODRÍGUEZ-PARRA, RODRIGO MORENO и MARÍA ISABEL NIETO

Institute of Ceramics and Glass, CSIC, Kelsen 5, 28049 Madrid, Spain

Ливење на ниским температурама је добро позната техника обликовања приликом процесирања материјала са контролисаном порозношћу. Један од основних проблема представља контролисање брзине хлађења која проузрокује градијенте величине пора и хомогености. Тема ове студије је процесирање контролисано порозне керамике на бази глинице, полазећи од водених суспензија помоћу технике ливења на ниским температурама. Током експеримента су коришћене различите брзине хлађења. Ливење на ниским температурама је коришћена након оптимизације реолошких својстава водених суспензија глинице. Порозност и микроструктурна својства синтерованих узорака добијених под различитим условима су затим анализирана и проучавана. Закључено је да брзина хлађења у већој мери утиче на микроструктуру од коначне температуре. Микроструктурном анализом је такође показано да је постигнута контрола градијента порозности, у мањој мери при врху и на дну, а у већој мери у централном делу узорака.

(Примљено 18. новембра, ревидирано 3. децембра 2012)

2012 Copyright (CC) SCS

REFERENCES

1. P. Colombo, H. P. Degischer. *Mater. Sci. Technol*. **26** (2010) 1145
2. A. Corma. *Chem. Rev*. **97** (1997) 2373
3. C. Galassi. *J. Eur. Ceram. Soc*. **26** (2006) 2951
4. X. Y. Yang, Y. Li, A. Lemaire, J. G. Yu, B. L. Su. *Pure Appl. Chem*. **81** (2009) 2265
5. T. Ohji, M. Fukushima. *Int. Mater. Rev*. **57** (2012) 115
6. T. Fukasawa, Z. Y. Deng, M. Ando, *J. Am. Ceram. Soc*. **85** (2002) 2151
7. S. W. Sofie. *J. Am. Ceram. Soc*. **90** (2007) 2024
8. S. Deville. *Adv. Eng. Mater*. **10** (2008) 155
9. Y. Chino. D. C. Dunand. *Acta Mater.* **56** (2010) 105
10. K. Lu. *J. Am. Ceram. Soc*. **90** (2007) 3753
11. J. Zou, Y. Zhang, R. Li. *Int. J. Appl. Ceram. Technol*. **8** (2011) 482
12. C. Pekor, B. Groth, I. Nettleship. *J. Am. Ceram. Soc*. **93** (2010) 115
13. L. Qian, H. Zhang. *J. Chem. Technol. Biotechnol*. **86** (2011) 172
14. K. Araki, J. W. Halloran. *J. Am. Ceram. Soc*. **88** (2005) 1108
15. B. H. Yoon, Y. H. Koh, C. S. Park, H. E. Kim. *J. Am. Ceram. Soc*. **90** (2007) 1744
16. D. Koch, L. Andersen, T. Schmedders, G. Grathwohl. *J. Sol–Gel Sci. Technol*. **26** (2003) 149
17. E. Munch, E. Saiz, P. Tomsia, S. Deville. *J. Am. Ceram. Soc*. **92** (2009) 1534
18. S. Deville, E. Saiz, P. Tomsia. *Acta Mater.* **55** (2007) 1965
19. C. Tallon, R. Moreno, M. I. Nieto. *Adv. Appl. Ceram*. **108** (2009) 307
20. L. Qian, A. Ahmed, A. Foster, S. P. Rannard, A. I. Cooper, H. Zhang. *J. Mater. Chem*. **19** (2009) 5212
21. W. Li, K. Lu, J. Y. Walz. *J. Am. Ceram. Soc*. **94** (2011)1256
22. L. Ren, Y. P. Zeng, D. Jiang. *J. Am. Ceram. Soc*. **90** (2007) 3001
23. J. W. Moon, H. J. Hwang, M. Awano, K. Maeda. *Mater. Lett*. **57** (2003) 1428
24. K. H. Zuo, Y. P. Zeng, D. Jiang. *Int. J. Appl. Ceram. Technol*. **5** (2008) 198
25. S. W. Sofie, F. Dogan. *J. Am. Ceram. Soc*. **84** (2001) 1459
26. M. N Rahaman, Q. Fu. *J. Am. Ceram. Soc.* **91** (2008) 4137
27. C. A. Gutierrez, R. Moreno. *J. Mater. Sci.* **35** (2000) 5867.

2012 Copyright (CC) SCS

Journal of the Serbian Chemical Society
JSCS-info@shd.org.rs • www.shd.org.rs/JSCS
J. Serb. Chem. Soc. 77 (12) 1787–1798 (2012)
JSCS–4389
UDC 546.472+549.753.1–36+66.021.1
/.4:57.001.365:615.28–188
Original scientific paper

Biocompatibility and antimicrobial activity of zinc(II)-doped hydroxyapatite, synthesized by a hydrothermal method

ŽELJKO RADOVANOVIĆ[1]*, DJORDJE VELJOVIĆ[1], BOJAN JOKIĆ[1], SUZANA DIMITRIJEVIĆ[1], GORDANA BOGDANOVIĆ[2], VESNA KOJIĆ[2], RADA PETROVIĆ[1] and DJORDJE JANAĆKOVIĆ[1]

[1]*Faculty of Technology and Metallurgy, University of Belgrade, Karnegijeva 4, 11000 Belgrade, Serbia and* [2]*Oncology Institute of Vojvodina, Institutski put 4, 21204 Sremska Kamenica, Serbia*

(Received 19 November, revised 3 December 2012)

Abstract: In order to obtain multifunctional materials with good biocompatibility and antimicrobial effect, hydroxyapatite (HAp) doped with Zn^{2+} was synthesized by a hydrothermal method. Powders with different content of zinc ions were synthesized and compared with undoped HAp to investigate the influence of Zn^{2+} on the antimicrobial activity of HAp. Analyses of undoped and Zn^{2+}-doped powders before and after thermal treatment at 1200 °C were performed by SEM and XRD. The antimicrobial effects of the powders were examined in relation to *Escherichia coli*, *Staphylococcus aureus*, *Pseudomonas aeruginosa* and *Candida albicans* in liquid medium. The results showed that the obtained powders had good antimicrobial activity, but higher antimicrobial activities of the powders doped with Zn^{2+} were observed after annealing at 1200 °C. For powders annealed at 1200 °C, *in vitro* biocompatibility tests: reduction of the tetrazolium salt 3-(4,5-dimethylthazol-2-yl)-2,5-diphenyl tetrazolium bromide (MTT test) and Trypan Blue dye exclusion test (DET test) with MRC-5 fibroblast cells in liquid medium were performed. Based on the MTT and DET tests, it was shown that the powders do not have a significant cytotoxic effect, which was confirmed by SEM analysis of MRC-5 fibroblast cells after their *in vitro* contact with the powders.

Keywords: HAp; Zn; *α*-TCP; biocide; MTT assay; MRC-5.

INTRODUCTION

With the aging of the human population, the need for treatment of skeleton is more pronounced. Synthetic HAp [$Ca_{10}(PO_4)_6(OH)_2$] due to its composition is the most suitable for the mineral phase of human bone and teeth. Biocompatibility and osteoconductivity of HAp are well known and utilized in dentistry

* Corresponding author. E-mail: zradovanovic@tmf.ac.bg.rs
doi: 10.2298/JSC121019131R

Available online at shd.org.rs/JSCS/

2012 Copyright (CC) SCS

and orthopedic surgery to compensate of the damage of teeth and bones.[1–4] HAp is also used for coating metal implants to improve their biocompatibility.[4,5–12] However, during incorporation of filler HAp or HAp-covered implants in the living body, infection by pathogenic microorganisms can appear. To prevent this situation and the need for a second operation, biocidal metal ions or antibiotics are used.[13–16] Use of antibiotics is not suitable because their effect is not last long-lasting and microorganisms can develop resistance. Certain metals, such as silver, copper and zinc, are known to be poisonous to microorganisms. On the other hand, copper and zinc are micronutrients that at low concentrations are necessary for the functioning of many processes in humans, but at large concentrations are toxic.[17–19] The role of zinc in the formation and mineralization of bone is very important, as shown by data from the literature.[20–22]

The synthesis of zinc-doped HAp powders by different methods and the antimicrobial activity and/or structural and morphological characteristics of the obtained powder were investigated in the last decade. Kim *et al*.[23] applied a wet-chemical method to synthesize Zn^{2+}-substituted HAp. In their investigations, no antimicrobial activity of Zn^{2+} substituted HAp against *Escherichia coli* was observed. Chung *et al*.[24] applied a sol–gel method to synthesize Zn^{2+}-doped HAp. In solid-state anti-microbial tests, their Zn^{2+}-doped HAp demonstrated contact microbial inhibition against *Streptococcus mutans*. Ergun *et al*.[25] and Ming'Ou Li *et al*.[26] investigated only the structural and morphological characteristics of Zn^{2+}-doped HAp. The synthesis of Zn^{2+} ion-substituted Hap using a neutralization method was performed by Stanić *et al*.[27] Their investigation confirmed that Zn^{2+}-HAp had a viable cells reduction ability against *E. coli*, *Staphylococcus aureus* and *Candida albicans*.

In the present study, Zn^{2+} ion-doped HAp (0.2 and 0.4 mol % as compared to Ca) powders were hydrothermally synthesized. In order to investigate the influence of Zn^{2+} and phase composition on the antimicrobial activity, Zn-substituted powders were annealed at 1200 °C. The aim of the research was to examine the antimicrobial activity of zinc ions and simultaneously check the cytotoxic effect of zinc ions on MRC-5 fibroblast cells. The antimicrobial activity of Zn^{2+}--doped HAp against different pathogens: *S. aureus* (ATCC 25923), *E. coli* (ATCC 25922), *Pseudomonas aeruginosa* (ATCC 27833) and *C. albicans* (ATCC 24433) was evaluated *in vitro*. The biocompatibility of the Zn-substituted powders was studied by reduction of the tetrazolium salt 3-(4,5-dimethylthazol-2-yl)-2,5-diphenyl tetrazolium bromide (MTT assay) and Trypan Blue dye exclusion test (DET assay) *in vitro* using MRC-5 fibroblast cells.

EXPERIMENTAL

Synthesis of HAp and Zn^{2+}-doped HAp

Synthesis of HAp and Zn^{2+}-doped HAp were performed according to the hydrothermal method described earlier.[28-30] Appropriate quantities of the chemicals: $Ca(NO_3)_2 \cdot 2H_2O$ (Carlo

2012 Copyright (CC) SCS

Erba Reagenti, *p.a.* grade), $Na_2H_2EDTA \cdot 2H_2O$ (Zorka Šabac, *p.a.* grade), $NaH_2PO_4 \cdot 2H_2O$ (Analitika LTD, 99 % pure) and urea (Lach-Ner, 99.5 % pure) and $Zn(NO_3)_2 \cdot 6H_2O$ (Kemika Zagreb, 99 % pure) were dissolved in 1500 mL of distilled water. Doping was performed with 0.2 and 0.4 mol % according to formula (1), with a constant atomic ratio (Ca + Zn)/P = 1.67 to obtain a compound of approximate formula (2):

$$100(Zn/(Zn + Ca)) \quad (1)$$

$$Zn_xCa_{10-x}(PO_4)_6(OH)_2 \ (x = 0.02 \text{ and } 0.04) \quad (2)$$

After dissolution of the chemicals, the dish with the solution was inserted in an autoclave, previously filled with 1500 mL of distilled water. The solution was heated at 160 °C for 3 h. After slow cooling, the obtained suspension (pH ~9.20) was filtered, and the residue was washed with distilled water and dried at 105 °C for 4 h. After drying, the powder was ground in a mortar.

The following dry powders were obtained in this way: HAp, Zn(0.2)HAp and Zn(0.4)HAp. These powders were heated at 1200 °C for 2 h (heating rate 10 °C/min) and ground to obtain HAp12, Zn(0.2)HAp12 and Zn(0.4)HAp12.

Characterization methods

A scanning electron microscope (SEM) JEOL JSM 5800 was used for the morphological characterization of the synthesized powders. Before the SEM analysis, the powders were coated with Au–Pd alloy. SEM analysis of MRC-5 fibroblast cells were performed on scanning microscope Tescan Mira 3 FEG. Before SEM observations, the MRC-5 cells were slowly vacuum dried and then coated with Au–Pd alloy.

X-Ray powder diffraction analysis of the powders was performed on an ITAL Structures APD 2000 instrument using a copper cathode as the X-ray source (λ = 0.15406 nm), in the 2θ angle range from 15 to 65° with a step size of 0.05° s^{-1}.

Antimicrobial test

Quantitative tests of the antimicrobial activity of all the obtained powders against *S. aureus* (ATCC 25923), *E. coli* (ATCC 25922), *P. aeruginosa* (ATCC 27833) and *C. albicans* (ATCC 24433) were performed according to previously described the liquid challenge method in buffer solution.[22] The incubation time was 1 h. The antimicrobial test was performed for both the dry and annealed powders. As a control, a blank sterile potassium hydrogen phosphate buffer solution without sample was used.[22] The test was performed in two series, the one for dry powder and one for the annealed powders.

In vitro *biocompatibility tests*

Cell lines. Tests were performed on the cell line human fibroblasts of lung (MRC-5) that were grown attached to the surface of the flasks (Costar, 25 cm^3) in Eagle's medium modified by Dulbecco (DMEM, Gibco BRL, England) with 4.5 g L^{-1} glucose and 10 % FCS (fetal calf serum, Sigma). The medium contained the antibiotics: penicillin 100 IU mL^{-1} and streptomycin 100 μg ml. The cell line was maintained under standard conditions at 37 °C in an atmosphere of saturated humidity with 5 % CO_2 (Heraeus). They were transplanted twice weekly, whereas in the experiments the logarithmic phase of growth was used between the third and tenth transplantation. Only viable cells were used in the experiments. The number of cells and their viability were determined by the color test rejection with 0.1 % Trypan Blue.[31] The viability of cells used in the experiment was greater than 90 %.

Colorimetric assays with tetrazolium salts (MTT-test).[32] The cells were collected during the logarithmic phase of growth, trypsinized, resuspended and counted in 0.1 % Trypan Blue.

2012 Copyright (CC) SCS

Viable cells were sown at a concentration of $2 \cdot 10^5$ cells mL^{-1} in Petri dishes (50 mm, Center well, Falcon) in which the powders for the analysis were located. Control samples did not contain the investigated powders. Petri dishes with sown cells were thermostated at 37 °C with 5 % CO_2 for 48 h. At the end of the incubation, of the cells were re-sown to fresh medium. Viable cells were sown (5×10^3 cells 100 μL^{-1}) in microtiter plates with 96-well. The plates with sown cells were thermostated at 37 °C with 5 % CO_2 for 48 h, 72 h or 96 h. The MTT solution, prepared just before addition, was added to all the wells of the plate, in a volume of 10 μL per well and incubation was continued for the next 3 h (in the incubator at 37 °C with 5 % CO_2). Upon expiration of 3 h, 100 μL of HCl in 2-propanol (0.04 mol L^{-1}) was added to each well. The absorbance readings was performed immediately after incubation on a microtiter plate reader (Multiscan, MCC/340) at a wavelength of 540 nm with reference to 690 nm. Wells on a plate that contained only medium and MTT but no cells were used as a blank.

The fraction of surviving cells (% *K*) was expressed as a percentage of the control values according to formula (3):

$$\% K = 100 N_s / N_k \quad (3)$$

where N_k is the number of cells in the control sample and N_s is the number of cells with the tested substance.

Trypan Blue dye exclusion test (DET)

The cells were collected during the logarithmic phase of growth, trypsinized, resuspended and counted in 0.1 % Trypan Blue. Viable cells were sown at a concentration of 2×10^5 cells mL^{-1} in Petri dishes (50 mm, Center well, Falcon) in which the powders for the analysis were located. Control samples did not contain the investigated powders. The Petri dishes with sown cells were thermostated at 37 °C with 5 % CO_2 for the next 48 h. At the end of incubation, the cells were counted in the counting chambers after 48, 72 and 96 h using an inverted microscope. A Neubauer chamber was used for counting the cells in four squares. Each square was divided into 16 smaller squares so the total was 64. 100 μL of cells was taken and added to 100 μL of 0.1 % Trypan Blue. After intensive shaking, a few drops were placed on both counting fields of the chambers. Trypan Blue painted dead cells while living cells remain unpainted. The number of cells in 1 mL of suspension (*X*) was calculated using formula (4):

$$X = x \times 10 \times 2 \times 1000 \quad (4)$$

where *x* is the number of cells in 16 squares (the average number of cells in 4×16 squares); 10 is the depth of the chamber; 2 is the dilution factor and 1000 is the volumetric coefficient.

The fraction of surviving cells (% *K*) is expressed as a percentage of the control values, according to formula (3).

Cells preparation for painting

Preparation of the powdered substances. All substances were placed in a serum-free medium (DMEM) so that the concentration was 200 mg mL^{-1}. After 72 h, the medium was filtered (for sterility), 10 % serum was added, so that the medium was used in all the investigated samples except for the control.

The cells were collected during the logarithmic phase of growth, trypsinized, resuspended and counted in 0.1 % Trypan Blue. Viable cells were sown in a Petri dish (50 mm, Center well, Falcon) with a medium that has been tested 72 h with powder at a concentration 2×10^5 cells/ml. The control samples contained no test substance. Petri dishes with sown cells

2012 Copyright (CC) SCS

were thermostated at 37 °C with 5 % CO_2 for 48 h. Painting was performed at the end of the incubation.

RESULTS AND DISCUSSION

The SEM micrographs of the obtained HAp and Zn-doped HAp powders are shown in Fig. 1. The photographs of HAp and Zn(0.2)HAp are similar. Both powders contain mainly spherical particles with a wide size distribution. However, spheres with a diameter of 1 to 2 μm prevail. It can be seen that these spherical particles consisted of a large number of aggregated rod like particles. This is particularly obvious in the case of the spherical particles of the sample Zn(0.4)HAp. Even for this sample, the prevailing sphere diameter is 1 to 2 μm.

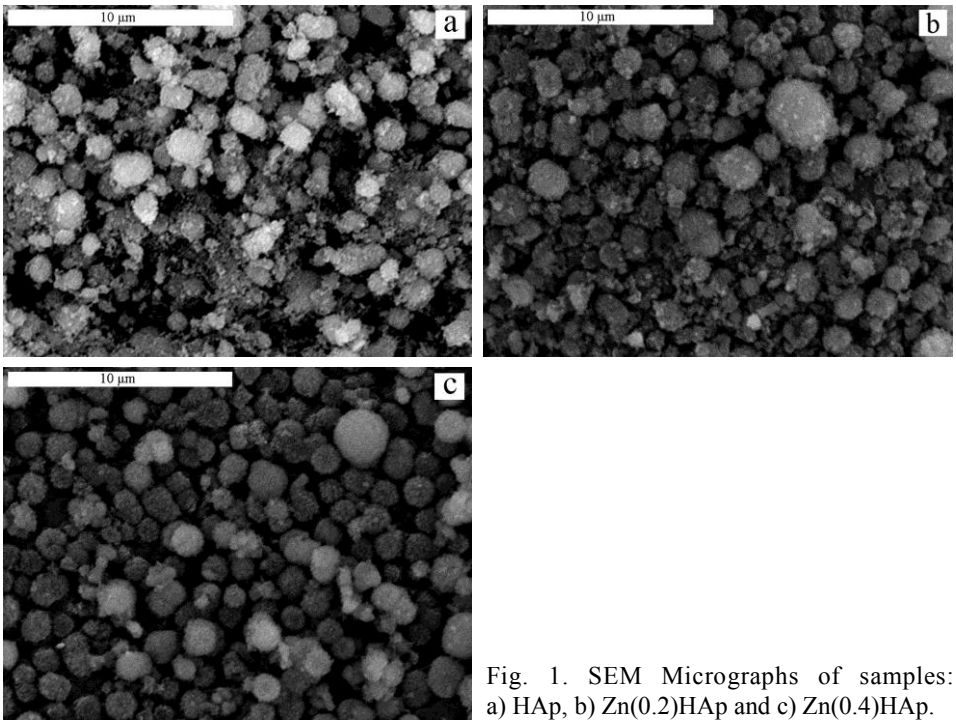

Fig. 1. SEM Micrographs of samples: a) HAp, b) Zn(0.2)HAp and c) Zn(0.4)HAp.

The micrographs of the powders at annealed 1200 °C for 2 h are shown in Fig. 2. Particles merged through the process of neck formation because of annealing can be seen in all cases. Particle size and size distribution were similar for all the samples and it could be concluded that doping of HAp with Zn^{2+}, due to the small concentrations, had no effect on the annealing of the Zn-containing powders.

The XRD diffractograms of the synthesized dry and annealed powders are shown in Fig. 3. The dry HAp and Zn^{2+}-doped HAp powders showed very low crys-

2012 Copyright (CC) SCS

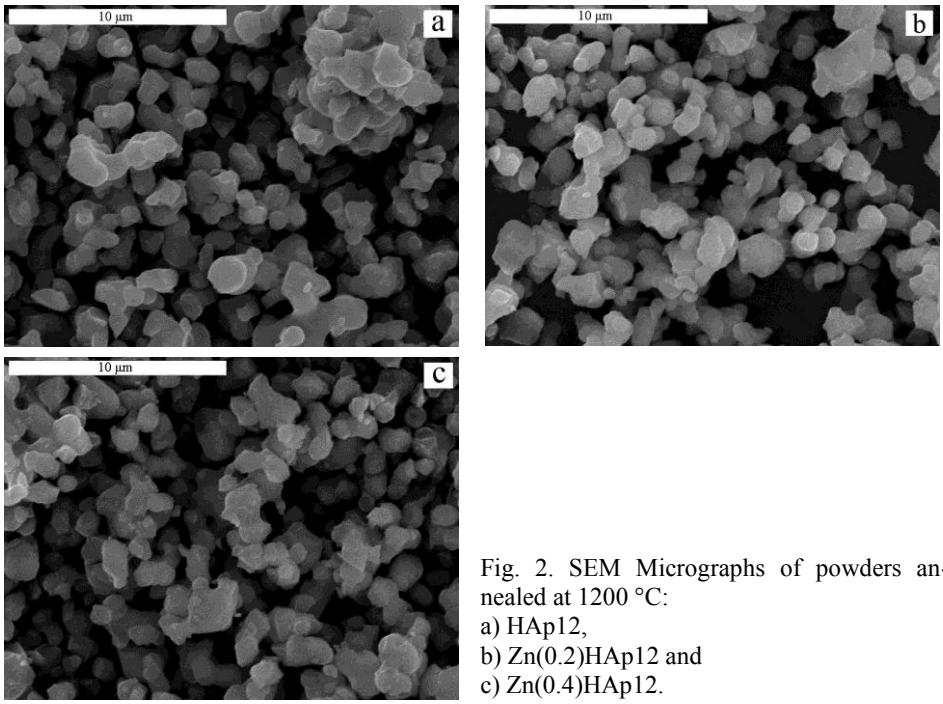

Fig. 2. SEM Micrographs of powders annealed at 1200 °C:
a) HAp12,
b) Zn(0.2)HAp12 and
c) Zn(0.4)HAp12.

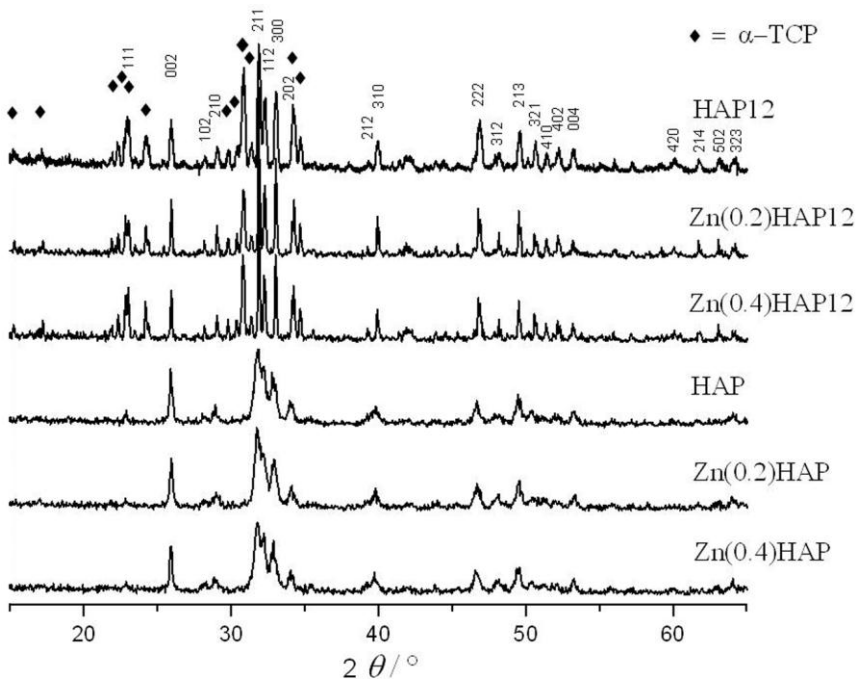

Fig. 3. XRD Patterns of undoped and doped HAp, annealed at 1200 °C and dry powders.

2012 Copyright (CC) SCS

tallinity. Based on ASTM data (Card 9-432), all the peaks present were identified as peaks of hydroxyapatite. These diffraction patterns are very similar, with no clear effect of the doped ions on the diffractograms.

From diffractograms of the annealed powders, it can be seen that HAp was partially transformed to α-TCP. The peaks were identified based on ASTM data (Card 9-432 for HAp and card 09-348 for α-TCP). In Fig. 3, the HAp peaks are marked with the number of the crystal plane. All peaks are sharp, confirming that the annealed samples were well crystallized. Similar to the dry powders, there are not differences between diffractograms of the annealed powders.

The results of the antimicrobial activity of the undoped and Zn^{2+}-doped HAP powders tested against *S. aureus* (ATCC 25923), *E. coli* (ATCC 25922), *P. aeruginosa* (ATCC 27833) and *C. albicans* (ATCC 24433) are given in Table I. The degree of reduction, *R*, was calculated compared to HAp using Eq. (5):

$$R\ (\%) = 100(CFU_{\mathrm{HAp}} - CFU_{\mathrm{Zn-HAp}})/CFU_{\mathrm{HAp}} \quad (5)$$

Comparing the results of antimicrobial activity of dried, doped and undoped powders, it could be concluded that the activity increased with increasing content of Zn ions incorporated in the HAp powders. Undoped HAp powder exhibited the similar antimicrobial activity against all the tested species of microorganism, except against *S. aureus*, which was more susceptible. The most pronounced effects on reduction of all microorganism species were observed using Zn-doped powders annealed at 1200 °C. Probably, the reason for this higher activity lies in the fact that the TCP phase formed during annealing is more soluble than the HAp phase.[3,4,28]

TABLE I. Antimicrobial effect of dry and annealed HAp and Zn^{2+}-doped HAp powder

Sample	*S. aureus*		*E. coli*		*P. aeruginosa*		*C. albicans*	
	No. of colonies	*R* / %	No. of colonies	*R* / %	No. of colonies	*R* / %	No. of colonies	*R* / %
Control	6.0×10^6	–	6.4×10^6	–	1.0×10^7	–	5.4×10^6	–
HAp	2.2×10^4	–	1.9×10^5	–	6.4×10^6	–	1.0×10^6	–
Zn(0.2)HAp	2.2×10^3	90.0	9.1×10^4	52.10	5.3×10^5	91.72	2.9×10^5	71.00
Zn(0.4)HAp	9.6×10^2	95.6	3.6×10^4	81.05	2.0×10^5	96.87	2.8×10^5	72.00
Control	84×10^2	–	636×10^2	–	2.0×10^6	–	1.4×10^6	–
HAp12	253×10^2	–	315×10^2	–	7.0×10^5	–	1.1×10^5	–
Zn(0.2)HAp12	186	99.3	806	97.44	1.9×10^3	99.73	7.2×10^3	93.45
Zn(0.4)HAp12	261	100	1210	96.16	1.0×10^2	99.98	5.7×10^3	94.82

Determination of cells viability was conducted using two types of *in vitro* assays, MTT and DET. In both tests, the cells viability was explored after 48 h, 72 h and 96 h of contact with the powders.

The diagram of the MTT assay (Fig. 4) shows a real increase in the cell viability with the contact time. The numbers of the cells in contact with HAp and

2012 Copyright (CC) SCS

Zn(0.4)HAp12 were about the same, while the cells in contact with powder Zn(0.2)HAp12 had a slightly lower survival rates. After 96 h, the cells showed the same viability as in the control sample, meaning that the powders exhibited no cytotoxic effect on the cells and thus their biocompatibility was demonstrated.

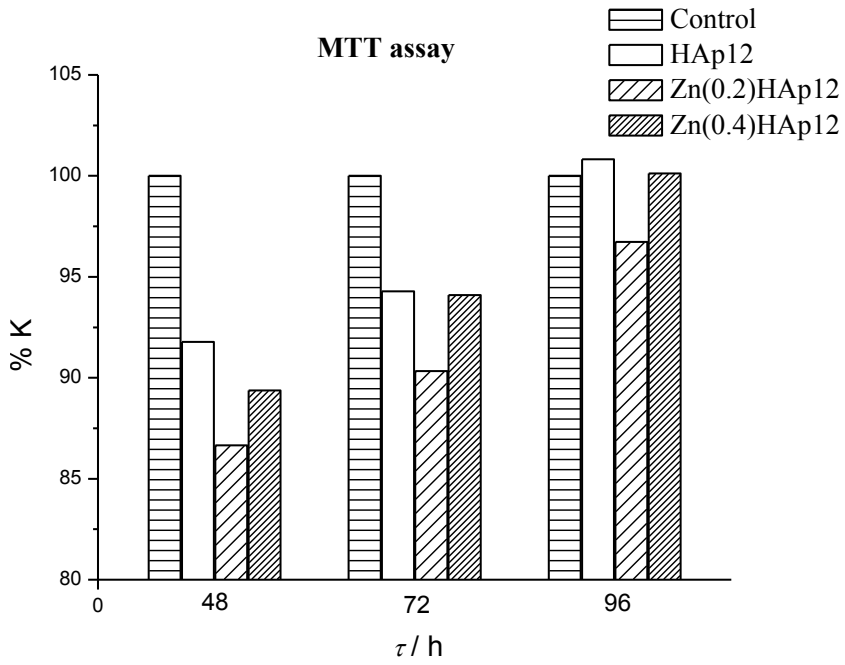

Fig. 4. Fractions of surviving cells in the MTT assay.

DET Test clearly confirmed the results of MTT assay (Fig. 5). The DET assay also showed a gradual increase in cell viability with increasing time of contact of the cells with the powder.

Better viability of cells that were in contact with powder Zn(0.4)HAp12 than with powder Zn(0.2)HAp12 can be explained by their exposure to slightly higher concentrations of Zn^{2+} ions that, as micronutrient, enhanced cells proliferation. Although, there is no significant difference in phase composition (Fig. 3) between undoped and Zn^{2+}-doped HAp, higher proliferation of MRC-5 cells after 96 h in powder extracts of Zn(0.2)HAp12 and Zn(0.4)HAp12 is evident.

Histological analysis of MRC-5 cells that clung to the surface of the Petri dish is shown in Fig. 6. The shape of cells is oval and elongated. It was noted that cytoplasmic extensions were spread from cells that connect to neighboring fibroblast cells. The appearance of the cells is an indication of their preserved viability. This confirmed the results obtained by the MTT and DET assays.

2012 Copyright (CC) SCS

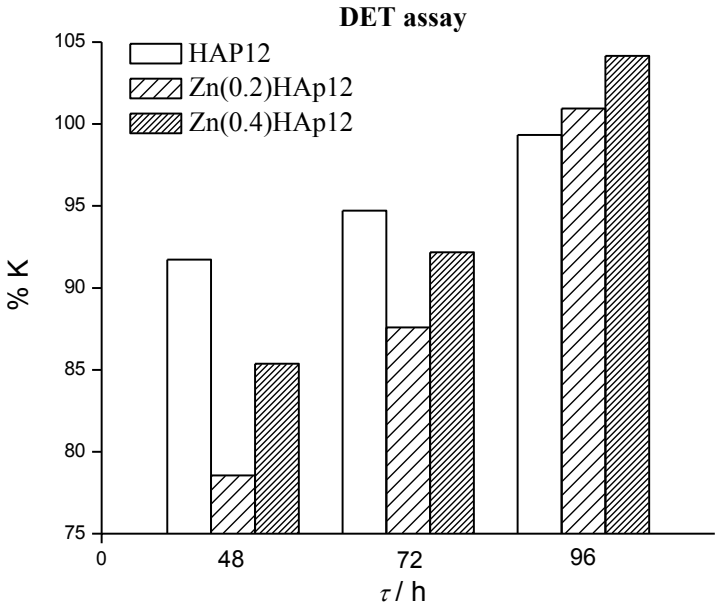

Fig. 5. Fractions of surviving cells in the DET assay.

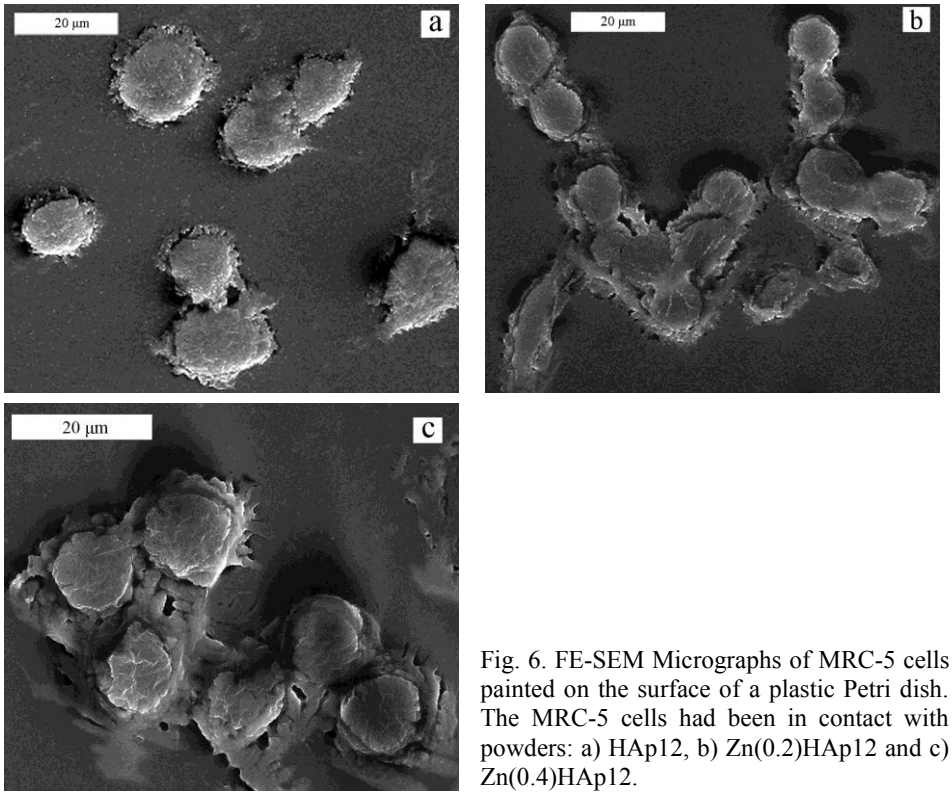

Fig. 6. FE-SEM Micrographs of MRC-5 cells painted on the surface of a plastic Petri dish. The MRC-5 cells had been in contact with powders: a) HAp12, b) Zn(0.2)HAp12 and c) Zn(0.4)HAp12.

2012 Copyright (CC) SCS

CONCLUSIONS

The obtained Zn^{2+}-doped Hap powders had good antimicrobial activities against the pathogenic microorganisms: *S. aureus*, *E. coli*, *P. aeruginosa* and *C. albicans*. The HAp powders with a higher content of Zn^{2+} had a higher degree of reduction of the microorganisms. In addition, the annealed, Zn^{2+}-doped HAp/ /α-TCP powders showed better antimicrobial activity than the dry powders Zn^{2+}--doped Hap powders. The results of the MTT and DET assays showed annealed Zn^{2+}-doped Hap powder clearly exhibited good biocompatibility with fibroblast cells, MRC-5. The viability of the cells was better when in contact with the powder with the higher content of Zn^{2+}. Histological analysis of SEM images of MRC-5 cells confirmed the results of the MTT and DET assays.

Based on previous results, it can be concluded that doping HAp with Zn^{2+}, using a hydrothermal method, results in powders of good biocompatibility with fibroblast cells MRC-5 and antimicrobial activity to pathogenic microorganisms. By annealing of the obtained powders, these properties were enhanced, probably due to partial transformation of HAp to α-TCP, a more soluble phase. The higher content of Zn^{2+} has a pronounced effect against pathogens and as micronutrients improved the proliferation of the fibroblast cells.

Acknowledgement. The authors wish to acknowledge the financial support for this research from the Ministry of Education, Science and Technological Development of the Republic of Serbia through the projects III 45019 and FP7-REGPOT-2009-1 NANOTECH FTM.

ИЗВОД

БИОКОМПАТИБИЛНОСТ И АНТИМИКРОБНА АКТИВНОСТ ХИДРОКСИАПАТИТА СА УГРАЂЕНИМ ЦИНКОМ СИНТЕТИСАНОГ ХИДРОТЕРМАЛНОМ МЕТОДОМ

ЖЕЉКО РАДОВАНОВИЋ[1], ЂОРЂЕ ВЕЉОВИЋ[1], БОЈАН ЈОКИЋ[1], СУЗАНА ДИМИТРИЈЕВИЋ[1], ГОРДАНА БОГДАНОВИЋ[2], ВЕСНА КОЈИЋ[2], РАДА ПЕТРОВИЋ[1] и ЂОРЂЕ ЈАНАЋКОВИЋ[1]

[1]*Технолошко–металуршки факултет, Универзитет у Београду, Карнегијева 4, 11000 Београд и* [2]*Институт за онкологију Војводине, Институтски пут 4, 21204 Сремска Каменица*

У циљу добијања мултифункционалних материјала са добром биокомпатибилношћу и добрим антимикробним дејством, хидроксиапатит (HAp) са уграђеним Zn^{2+} синтетисан је хидротермалном методом. За потребе истраживања утицаја Zn^{2+} на антимикробну активност, синтетисани су HAp прахови са различитим садржајем Zn^{2+} и упоређени са чистим HAp. Чисти прахови и они са уграђеним цинком, пре и после термичког третмана на 1200 °C, анализирани су скенирајућом електронском микроскопијом (SEM) и методом рендгенске дифракције. Антимикробни ефекат прахова испитиван је према сојевима *Escherichia coli*, *Staphylococcus aureus*, *Pseudomonas aeruginosa* и *Candida albicans* у течном медијуму. Антимикробни тест је показао да добијени прахови имају добру антимикробну активност. Побољшана антимикробна активност прахова у које је уграђен Zn^{2+} постигнута је жарењем на 1200 °C. *In vitro* тестови биокомпатибилности, MTT и DET, са MRC-5 фибробластним ћелијама у течном медијуму урађени су за прахове жарене на 1200 °C. На основу MTT и DET тестова закључено је да прахови немају

2012 Copyright (CC) SCS

значајан цитотоксични утицај што је потврђено SEM анализом MRC-5 фибробластних ћелија након њиховог *in vitro* контакта са праховима.

(Примљено 19. новембра, ревидирано 3. децембра 2012)

REFERENCES

1. L. L Hench, *J. Am. Ceram. Soc*. **81** (1998) 1705
2. M. Vallet-Regí, J. M. González-Calbet, *Prog. Solid Stat. Chem*. **32** (2004) 1
3. S. V. Dorozhkin, *Materials* **2** (2009) 399
4. S. V. Dorozhkin, *Biomatter* **1** (2011) 1
5. S. D. Cook, K. A. Thomas, J. F. Kay, M. Jarcho, *Clin. Orthop. Rel. Res*. **232** (1988) 225
6. Y. Nakashima, K. Hayashi, T. Inadome, K. Uenoyama, T. Hara, T. Kanemaru, Y. Sugioka, I. Nodal, *J. Biomed. Mater. Res.* **35** (1997) 287
7. M. Ogiso, M. Yamamura, P. T. Kuo, D. Borgese, T. Matsumoto, *J. Biomed. Mater. Res.* **39** (1998) 364
8. Y. C. Tsui, C. Doyle, T. W. Clyne, *Biomaterials* **19** (1998) 2015
9. D. Tanasković, B. Jokić, G. Socol, A. Popescu, I. N. Mihailescu, R. Petrović, D. Janaćković, *Appl. Surf. Sci*. **254** (2007) 1279
10. M. Roy, A. Bandyopadhyay, S. Bose, *Surf. Coat. Technol*. **205** (2011) 2785
11. R. A. Surmenev, *Surf. Coat. Technol*. **206** (2012) 2035
12. S. Eraković, Dj. Veljović, P. N. Dioufb, T. Stevanović, M. Mitrić, Dj. Janaćković, I. Z. Matić, Z. D. Juranić, V. Mišković-Stanković, *Prog. Org. Coat*. **75** (2012) 275
13. A. Montali, *Injury* **37** (2006) S81
14. F. Chai, J.-C. Hornez, N. Blanchemain, C. Neut, M. Descamps, H. F. Hildebrand, *Biomol. Eng.* **24** (2007) 510
15. X. Ge, Y. Leng, C. Bao, S. L. Xu, R. Wang, F. Ren, *J. Biomed. Mater. Res. A* **95** (2010) 588
16. M. Oner, E. Yetiz, E. Ay, U. Uysal, *Ceram. Int.* **37** (2011) 2117
17. K. M. Hambidge, N. F. Krebs, *J. Nutr.* **137** (2007) 1101
18. A. S. Prasad, *Br. Med. J.* **326** (2003) 409
19. B. R. Stern, R. Bonnie, *J. Toxicol. Environ. Health, Part A* **73** (2010) 114
20. S. L. Hall, H. P. Dimai, J. R. Farley, *Calcif. Tissue Int.* **64** (1999) 163
21. M. Yamaguchi, *Mol. Cell. Biochem*. **338** (2010) 241
22. N. J. Lakhkar, I.-H. Lee, H.-W. Kim, V. Salih, I. B. Wall, J. C. Knowles, *Adv. Drug Deliv. Rev.* (2012), in press, doi:10.1016/j.addr.2012.05.015
23. T. N. Kim, Q. L. Feng, J. O. Kim, J. Wu, H. Wang, G. C. Chen, F. Z. Cui, *J. Mater. Sci. Mater. Med.* **9** (1998) 129
24. R. J. Chung, M. F. Hsieh, K. C. Huang, L. H. Perng, F. I. Chou, T. S. Chin, *J. Sol–Gel Sci. Technol.* **33** (2005) 229
25. C. Ergun, T. J. Webster, R. Bizios, R. H. Doremus, *J. Biomed. Mater. Res.* **59** (2002) 305
26. M.'Ou Li, X. Xiao, R. Liu, C. Chen, L. Huang, *J Mater Sci: Mater Med* **19** (2008) 797
27. V. Stanić, S. Dimitrijević, J. Antić-Stanković, M. Mitrić, B. Jokić, I. B. Plećaš, S. Raičević, *Appl. Surf. Sci*. **256** (2010) 6083
28. B. Jokić, I. Janković-Častvan, Dj. Veljović, R. Petrović, S. Drmanić, Dj. Janaćković, *Key Eng. Mater*. **309** (2006) 821
29. Dj. Janackovic, I. Petrovic-Prelevic, Lj. Kostic-Gvozdenovic, R. Petrovic, V. Jokanovic, D. Uskokovic, *Key Eng. Mater*. **192–195** (2001) 203

2012 Copyright (CC) SCS

30. Dj. Janackovic, I. Jankovic, R. Petrovic, Lj. Kostic-Gvozdenovic, S. Milonjic, D. Uskokovic, *Key Eng. Mater*. **240–242** (2003) 437
31. G. Bogdanović, J. Raletić-Savić, N. Marković, *Arch. Oncol.* **2** (1994) 181
32. T. Mosmann, *J. Immunol. Methods* **65** (1983) 55.

2012 Copyright (CC) SCS

Journal of the Serbian Chemical Society
JSCS-info@shd.org.rs • www.shd.org.rs/JSCS
J. Serb. Chem. Soc. 77 (12) 1799–1806 (2012)
JSCS–4390
UDC 544.478+546.92:661.183.8:66.061+
66.094.3+547.426:539.12
Original scientific paper

Catalyst materials based on plasma-processed alumina nanopowder

ERIKS PALCEVSKIS[1]*, LIDIJA KULIKOVA[1], VERA SERGA[1], ANTONS CVETKOVS[1], SVETLANA CHORNAJA[2], ELINA SPROGE[2] and KONSTANTINS DUBENCOVS[2]

[1]*Institute of Inorganic Chemistry, Riga Technical University, 34 Miera str., Salaspils, LV-2169, Latvia and* [2]*Faculty of Material Science and Applied Chemistry Riga Technical University, 14/24 Azenes str., Riga, LV-1048, Latvia*

(Received 16 November, revised 10 December 2012)

Abstract: A platinum catalyst for glycerol oxidation by molecular oxygen has been developed applying an extractive-pyrolytic method and using, as a support, a fine alumina powder with an average particle size of 30–60 nm processed by plasma technology. The extractive-pyrolytic method (EPM) allows affixing small amounts of catalytic metals (1–5 %) with the particle size ranging from several nanometers to several tens of nanometers onto the surface of the support. The prepared material, 4.8 wt. % platinum on nano-sized alumina, could be used as a catalyst for glycerol oxidation by oxygen with conversions up to 84 %, in order to produce some organic acids (glyceric and lactic acid) with a selectivity of about 60 %.

Keywords: platinum catalyst; extractive-pyrolytic method; glycerol oxidation.

INTRODUCTION

The increasing global demand for biodiesel causes an excess of other important product, glycerol. It is the main by-product in the production of biodiesel fuel with a yield of 10 %. Glycerol is a very useful chemical compound utilized in pharmacy, cosmetics and the food industry, but the demand for glycerol is much smaller than its produced quantity; hence, glycerol utilization is a significant problem.[1,2] Selective oxidation could be one of the preferred methods to convert glycerol to valuable compounds. Using supported Pt, Pd or Au catalysts, glyceric acid, tartronic acid, dihydroxyacetone, glyceraldehyde, glycolic acid, hydroxypyruvic acid, mesoxalic acid and oxalic acid can be produced from glycerol. Glycerol oxidation over these noble metal catalysts by air oxygen is environmentally friendly because the reactions occur in aqueous solutions under low temperatures and pressures, and the catalysts are recyclable.[3,4] Alumina is often used as a

* Corresponding author. E-mail: eriksp@nki.lv
doi: 10.2298/JSC121116147P

Available online at shd.org.rs/JSCS/

2012 Copyright (CC) SCS

support for catalysts containing noble metals. It is known that the particle size of the support influences the obtained metal particle size.[5,6] The activity and selectivity of platinum catalysts loaded on a support in dependence on the size of particles are discussed in some papers,[7,8]

The plasma technology developed at the Institute of Inorganic Chemistry of the Riga Technical University, Riga, Latvia, allows fine oxide powders, including alumina, with an average particle size of 30–60 nm to be produced.[9] Such powders could be used as supports for metal particle catalysts. Fine particles of noble metals (Pt, Pd, Au, *etc*.) on different supports and substrates could be prepared by the developed extractive-pyrolytic method (EPM).[10] Herein, the production of platinum catalysts on nano-sized alumina supports and the test results of glycerol oxidation using the prepared catalyst are described.

EXPERIMENTAL

Characteristics of the support

The plasma technology for the production of nano-sized powders developed at the Institute of Inorganic Chemistry of the Riga Technical University is based on the evaporation of coarse commercially available powders of chemical elements and their compounds and on subsequent condensation of the products to a radio-frequency inductively coupled nitrogen plasma. The experimental equipment and the procedure are described in more detail in the literature.[9] The nano-sized alumina powder for catalyst application was manufactured from 99.7 % pure raw alumina. The alumina powder, as processed (Fig. 1), contains δ- and θ-Al_2O_3 transition crystallographic phases with sphere-shaped particles of an average size of 30–60 nm (the specific surface area is 50 m^2 g^{-1}).[11]

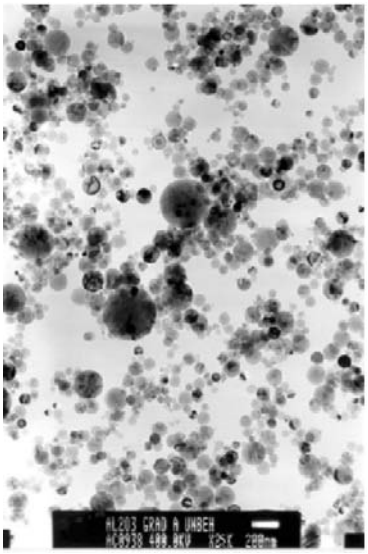

Fig. 1. Micrograph of plasma-processed alumina. Bar = 200 nm.

2012 Copyright (CC) SCS

Materials for EPM and tests of catalytic properties

Platinum powder (≥99.9 %; Aldrich), HCI (35 %) and HNO_3 (65%) (Lachema), *n*-trioctylamine $(C_8H_{17})_3N$ (≥95 %; Fluka) and toluene (analytical grade; Stanchem) were used to produce the precursors. NaOH (reagent grade, Sigma–Aldrich) and oxygen (98 %; AGA SIA) were used to oxidize glycerol (≥98 %; Fluka). DL-Glyceraldehyde dimer (≥97 %; Aldrich), 1,3-dihydroxyacetone dimer (≥97 %; Aldrich), glyceric acid calcium salt hydrate (≥99 %; Fluka), sodium *β*-hydroxypyruvate hydrate (≥97 %; Fluka), lithium lactate (≥97 %; Fluka), tartronic acid (≥98 %; Alfa Aesar), sodium mesoxalate monohydrate (≥98 %; Aldrich), glycolic acid (≥99 %; Acros Organics), glyoxylic acid monohydrate (≥98 %; Aldrich), oxalic acid (98%; Aldrich), acetate standard for IC (1,000 g L^{-1}; Fluka), formate standard for IC (1,000 g L^{-1}; Fluka) were used to analyze the products of glycerol oxidation.

Catalyst preparation

The EPM used to prepare fine metal particles (Pt, Pd, Au, *etc*.) on different supports and substrates was developed at the Institute of Inorganic Chemistry (Riga Technical University). This method allows small amounts of catalytic metals (1–5 %) with particle size ranging from several nanometers to several tens of nanometers to be affixed onto the surface of the support. The main advantages of this method are its simplicity and low costs, and it is possible to apply the method without sophisticated equipment.[10] The method is schematically illustrated in Fig. 2. Previously, a solution of platinum acid hexachloride was prepared. An amount of the platinum powder was dissolved in *aqua regia* and evaporated adding concentrated HCl to the wet salt that was then diluted with 2 M HCl to the necessary concentration (0.5 mol L^{-1}). The organic precursor (extract) was prepared by extracting platinum from the HCI solution using the *n*-trioctylamine $(C_8H_{17})_3N$ solution (1 M) in toluene. The following chemical interaction occurred during the extraction:

$$H_2[PtCl_6]_{(w)} + 2(C_8H_{17})_3N{\cdot}HCl_{(o)} \rightarrow [(C_8H_{17})_3NH]_2PtCl_{6(o)} + 2HCl_{(w)} \quad (1)$$

where the subscripts w and o denote the aqueous phase and organic phase, respectively. As a result, a solution of tri-*n*-octylammonium hexachloroplatinate in toluene was obtained.

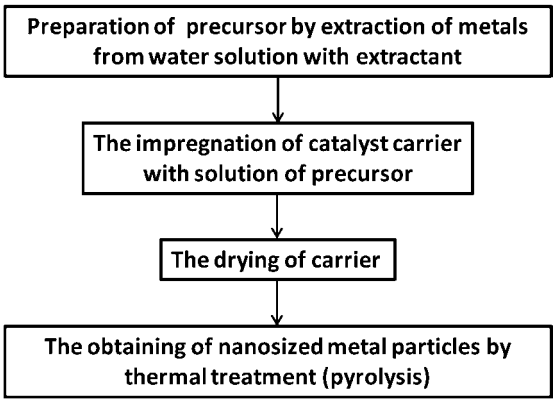

Fig. 2. Processing scheme of catalyst preparation by the extractive-pyrolytic method.

The results of the analysis of the aqueous solution after extraction using a HITACHI 180-50 atomic absorption spectrometer evidenced that the platinum had been completely extracted into the organic phase. Different volumes of the extract were used as the precursor

2012 Copyright (CC) SCS

to impregnate the alumina nanopowder in order to produce catalysts with different platinum contents. After impregnation, the toluene was evaporated by drying at 90–110 °C. The materials were then heated in the air from room temperature to 300, 400 or 500 °C at a rate of 10 °C min^{-1}. The time of thermal treatment at these temperatures was varied from 5 to 120 min. The lowest temperature to ensure the complete decomposition of the precursor without contamination of the catalyst with organic pyrolysis products was 300 °C. This was established by recording the IR spectra of the produced materials.

The phase composition of the prepared catalysts was determined by XRD analysis using a D-8 Advance (Bruker AXS) diffractometer with CuK_α radiation (λ = 1.5418 Å). The average crystallite size of platinum was computed from the (111) peak width by the Scherrer method. TEM investigations were performed using a JEM-1230 operating at 100 kV. The chemical composition of the prepared materials was determined by an X-ray fluorescence spectrometer S4 Pioneer (Bruker AXS).

Testing of the catalysts

Glycerol was oxidized by molecular oxygen in the presence of the catalysts in an alkaline medium in a thermostated slurry bubble column reactor operated in a batch mode. The oxidation was performed as follows: during thermostating (10 min), the required quantities of the dry catalyst, distilled water and an aqueous 3.0 M glycerol solution were fed into the reactor. The supply of oxygen into the reactor was turned on and the required volume of aqueous 5.0 M sodium hydroxide solution was added. The oxidation process started as soon as sodium hydroxide was added. The reaction conditions to test the catalyst were chosen based on preliminary experiments and are were the following: the initial glycerol concentration 0.3 M, the concentration of sodium hydroxide 1.5 M, the glycerol/Pt molar ratio 300 mol mol^{-1}, the reaction temperature 60 °C, the reactions time 7 h, the oxygen pressure 1 atm, and the rate of oxygen flow 300 cm^3 min^{-1}. In order to determine the concentration of the reaction products, liquid samples were collected periodically from the reaction mixture in certain time intervals.

The reaction mixture was analyzed in a Waters 2487 high performance liquid chromatograph (HPLC) equipped with ultraviolet (UV 210 nm) and refractive index detectors. The possible products were identified by comparing with original samples.

RESULTS AND DISCUSSION

Dependence of the platinum particle size on processing parameters

The microscopic studies of the samples showed (Figs. 1 and 3) that it is impossible to identify the platinum particles correctly in the presence of alumina nanoparticles, since the metal particles and the carrier particles are difficult to distinguish. The XRD phase analysis of the platinum-containing composites showed that the peaks for Pt overlap, at least partially, with those of the carrier at all diffraction angles, which makes it difficult to determine precisely the mean size of platinum crystallites when the content of the metal in the composite was small (≤2.4 wt. %) (Fig. 4). Therefore, the average crystallite size was determined only for the composites containing 4.8 wt. % Pt using the most intensive peak (111).

The most important parameters of the catalyst preparation affecting the platinum crystallite size are the thermal treatment (pyrolysis) temperature and du-

2012 Copyright (CC) SCS

ration. The results of investigations of the catalyst with 4.8 wt. % Pt testify that increasing the thermal treatment temperature and treatment duration leads to enlargement of the average crystallite size (Figs. 5 and 6).

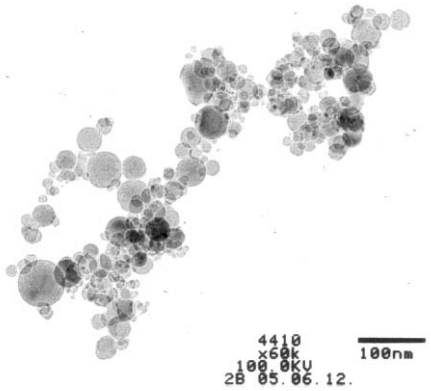

Fig. 3. Micrograph of the 2.4 % Pt catalyst on nano-sized alumina.

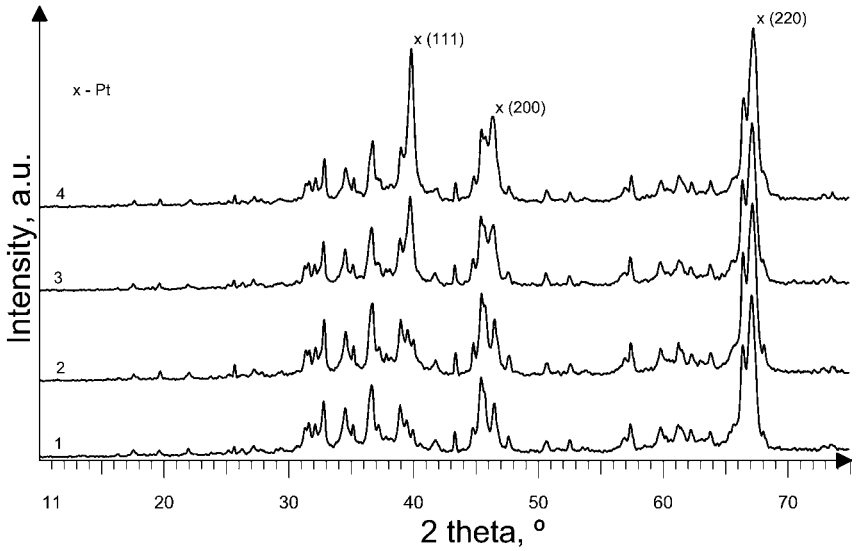

Fig. 4. XRD Patterns of plasma-processed alumina and catalyst powders, 1 – alumina nanopowder as processed, 2 – 1.2 wt. % platinum; 3 – 2.4 wt. % platinum, and 4 – 4.8 wt. % platinum on nano-sized alumina. Thermal treatment temperature 300 °C, treatment time 5 min.

Influence of catalyst synthesis parameters on glycerol oxidation

The obtained catalyst samples were tested for use in the process of glycerol oxidation. From Table I, it can be seen that the 4.8 % platinum-containing catalyst prepared at the lowest pyrolysis temperature 300 °C and having the smallest

2012 Copyright (CC) SCS

average crystallite size demonstrates the highest activity (in terms of glycerol conversion) and selectivity to glyceric acid. Increasing the pyrolysis temperature from 300 to 500 °C decreased both the glycerol conversion from 75 to 22 % and the selectivity to glyceric acid from 53 to 15%. It is important to note that the catalysts prepared at a higher thermal treatment temperature exhibit very good selectivity to lactic acid, which attained 65–67 %. The data in Table II show that the increase of thermal treatment duration from 5 to 120 min led to an increase in catalyst activity. The glycerol conversion increased in this case by 9 %. The catalysts with a thermal treatment time of 120 min are more selective to glyceric acid, but their selectivity to other products is similar and low (<20 %).

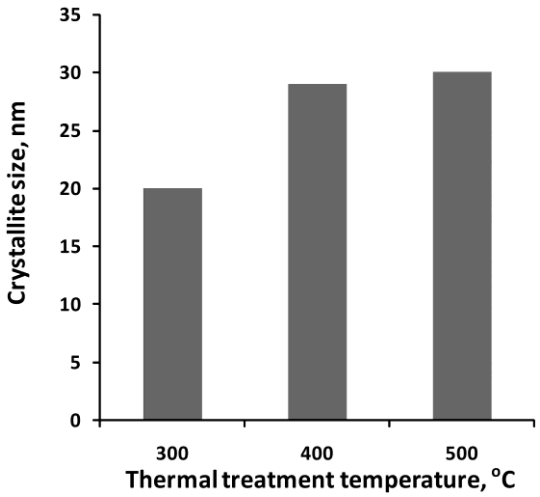

Fig. 5. Influence of the thermal treatment temperature on the average crystallite size of the platinum particles. Thermal treatment time 5 min. Catalysts with 4.8 wt. % Pt.

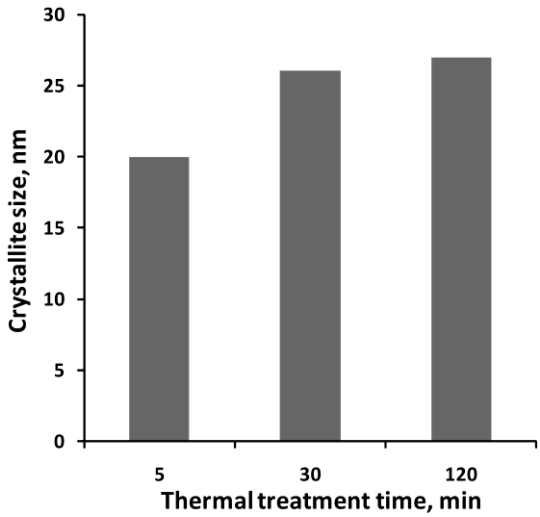

Fig. 6. The average platinum crystallite size *vs*. the pyrolysis time. Thermal treatment temperature 300 °C. Catalysts with 4.8 wt. % Pt.

2012 Copyright (CC) SCS

TABLE I. Glycerol oxidation *vs*. the thermal treatment (pyrolysis) temperature, the treatment time was 5 min; GLYA – glyceric acid, TART – tartronic acid, LACT – lactic acid, GLYC – glycolic acid, OXAL – oxalic acid, FORM – formic acid

Pyrolysis temperature, °C	Glycerol conversion, %	Selectivity, mol %					
		GLYA	TART	LACT	GLYC	OXAL	FORM
300	75	53	13	19	10	3	2
400	16	15	2	65	15	0	3
500	22	15	3	67	12	0	3

TABLE II. Glycerol oxidation *vs*. the thermal treatment time at 300 °C; GLYA – glyceric acid, TART – tartronic acid, LACT – lactic acid, GLYC – glycolic acid, OXAL – oxalic acid, FORM – formic acid

Treatment ime, min	Glycerol conversion, %	Selectivity, mol %					
		GLYA	TART	LACT	GLYC	OXAL	FORM
5	75	53	13	19	10	3	2
120	84	59	10	20	7	1	3

CONCLUSIONS

The employed extractive-pyrolytic method allowed nano-sized platinum particles on a nano-sized alumina support to be prepared.

The size of platinum crystallites in the catalyst with 4.8 wt. % Pt varied from 20 to 30 nm depending on the thermal treatment conditions.

The produced catalysts could be used for glycerol oxidation by oxygen for the preparation of glyceric or lactic acid with a glycerol conversion of up to 84 %.

Acknowledgement. This work was supported by the European Regional Development Fund – National Project No. 2010/0304/2DP/2.1.1.1.0/10/APIA/VIAA/087.

ИЗВОД

КАТАЛИЗАТОРИ БАЗИРАНИ НА ПЛАЗМА-ОБРАЂЕНОМ НАНОПРАХУ АЛУМИНИЈУМА

ERIKS PALCEVSKIS[1], LIDIJA KULIKOVA[1], VERA SERGA[1], ANTONS CVETKOVS[1], SVETLANA CHORNAJA[2], ELINA SPROGE[2] и KONSTANTINS DUBENCOVS[2]

[1]*Institute of Inorganic Chemistry, Riga Technical University, 34 Miera str., Salaspils, LV-2169, Latvia* и [2]*Faculty of Material Science and Applied Chemistry, Riga Technical University, 14/24 Azenes str., Riga, LV-1048, Latvia*

Платински катализатор за оксидацију глицерола молекуларним кисеоником је развијен применом екстрактивно-пиролитичке методе, и коришћењем носача од финог алуминијумског праха (величине честица 30–60 nm), процесираног плазма технологијом. Екстрактивно-пиролитички метод (EPM) омогућава додавање малих количина каталитичког метала (1–5 %) величине честица од неколико до неколико десетина нанометара, на површину подлоге. Добијени материјал – 4,8 тежинских процената платине на нано честицама алуминијума – може се употребити као катализатор за оксидацију глицерола кисеоником, са конверзијом до 84 %, у циљу добијања неких органских киселина (глицеринска и млечна), са селективношћу од око 60 %.

(Примљено 16. новембара, ревидирано 10 децембра 2012)

2012 Copyright (CC) SCS

REFERENCES

1. J. Gao, D. Liang, P. Chen, Z. Hou, X. Zheng, *Catal. Lett.* **130** (2009**)** 185
2. M. Pagliaro, R. Ciriminna, H. Kimura, M. Rossi, C. D. Pina, *Angew. Chem. Int. Edit.* **46** (2007) 4434
3. C. L. Bianchi, P. Canton, N. Dimitratos, F. Porta, L. Prati, *Catal. Today* **102–103** (2005) 203
4. M. Zhang, D. Liang, R. Nie, X. Lu, P. Chen, Z. Hou, *Chin. J. Catal*. **33** (2012) 1340
5. A. Vazquez, T. Lopez, R. Gomez, X. Bokhimi. *J. Mol. Catal.* **167** (2001) 91
6. M. Royker, J. Case, E. van Steen, *J. S. Afr. Inst. Min. Metall*. **7A** (2012) 577
7. D. Liang, J. Gao, J. Wang, P. Chen, Z. Hou, X. Zheng, *Catal. Comm.* **10** (2009) 1586
8. D. Liang, J. Gao, H. Sun, P. Chen, Z. Hou, X. Zheng, *Appl. Catal., B* **106** (2011**)** 423
9. I. Zalite, J. Grabis, E. Palcevskis, M. Herrmann, *IOP Conf. Ser.: Materials Science and Engineering* **18** (2011) 062024
10. V. Serga, L. Kulikova, A. Cvetkov, A. Krumina, *IOP Conf. Ser.: Materials Science and Engineering* **38** (2012) 012062
11. E. Palcevskis, U. Reichel, M. Lipe, in *Proceedings of X International Baltic Conference "Materials Engineering & BALTTRIB *2001"*, Latvia, 2001, p.87.

2012 Copyright (CC) SCS

Journal of the Serbian Chemical Society
JSCS@tmf.bg.ac.rs • www.shd.org.rs/JSCS
J. Serb. Chem. Soc. *77* (12) 1807–1818 (2012)

Contents of Volume 77

NUMBER 1

Available online at shd.org.rs/JSCS/

2012 Copyright (CC) SCS

NUMBER 2

2012 Copyright (CC) SCS

NUMBER 3

NUMBER 4

2012 Copyright (CC) SCS

2012 Copyright (CC) SCS

NUMBER 6

2012 Copyright (CC) SCS

2012 Copyright (CC) SCS

2012 Copyright (CC) SCS

2012 Copyright (CC) SCS

2012 Copyright (CC) SCS

2012 Copyright (CC) SCS

NUMBER 12

2012 Copyright (CC) SCS

2012 Copyright (CC) SCS

Journal of the Serbian Chemical Society
JSCS-info@shd.org.rs • www.shd.org.rs/JSCS
J. Serb. Chem. Soc. *77* (12) 1819–1825 (2012)

Author Index

Available online at shd.org.rs/JSCS/

2012 Copyright (CC) SCS

2012 Copyright (CC) SCS

2012 Copyright (CC) SCS

2012 Copyright (CC) SCS

2012 Copyright (CC) SCS

2012 Copyright (CC) SCS

Subject Index of Vol. **77** and *List of Referees* in the year *2012* are given in the electronic form at the Internet address of the Journal of the Serbian Chemical Society (http://www.shd.org.rs/JSCS/Vol77/No12.html).

End of Volume 77.

2012 Copyright (CC) SCS

Journal of the Serbian Chemical Society
JSCS-info@shd.org.rs • www.shd.org.rs/JSCS
Volume *77* (2012)

Subject index

2012 Copyright (CC) SCS

2012 Copyright (CC) SCS

2012 Copyright (CC) SCS

2012 Copyright (CC) SCS

2012 Copyright (CC) SCS

2012 Copyright (CC) SCS

2012 Copyright (CC) SCS

2012 Copyright (CC) SCS

Journal of the Serbian Chemical Society
JSCS-info@shd.org.rs • www.shd.org.rs/JSCS
Volume 77 (2012)

2012 List of Referees

Editorial Board of the Journal is grateful to the following referees for reviewing the manuscripts during 2012:

Ornela Abollino, *Dipartimento di Chimica Analitica, Università di Torino, Italy*
Biljana Abramović, *Faculty of Science, University of Novi Sad, Serbia*
Antreas Afantitis, *Department of ChemoInformatics, NovaMechanics Ltd, Nicosia, Cyprus*
Jasmina Agbaba, *Faculty of Sciences, University of Novi Sad, Serbia*
Abdulaziz Ajlouni, *Jordan University of Science and Technology, Irbid, Jordan*
Diego A. Alonso, *Departamento de Química Organica & Instituto de Síntesis Organica, Universidad de AlicanteAlicante, Spain*
Gilberto Lourenço Alves, *University of Beira Interior, Covilhã, Portugal*
Diego Alves, *LASOL, IQG, Universidade Federal de Pelotas, Pelotas, RS, Brazi*
Suresh C. Ameta, *Department of Chemistry, M. L. Sukhadia University, India*
Deana Andrić, *Faculty of Chemistry, University of Belgrade, Serbia*
Ryszard Andruszkiewicz, *The Faculty of Chemistry, Gdańsk University of Technology, Gdańsk, Poland*
Tatjana Anđelković, *Faculty of Sciences and Mathematics, University of Niš, Serbia*
Zoran Anđić, *Innovation center of the Faculty of Chemistry, University of Belgrade, Serbia*
Mališa Antić, *Faculty of Agriculture, University of Belgrade, Serbia*
Nazlı Arda, *Faculty of Science, Istanbul University, Turkey*
Kapil Arya, *Department of Chemistry, University of Delhi, Delhi, India*
Nora Aptula, *Unilever - Safety & Environmental Assurance Centre, UK*
Ilaria Armentano, *Biomaterial Science Group, Engineering Department, University of Perugia, Italy*
Natalia Artemieva, *Planetary Science Institute, Tucson, USA*
Fareeda Athar, *Centre for Interdisciplinary Research in Basic Sciences, Jamia Millia Islamia, Maulana Ali Jauhar Marg, New Delhi, India*
Mihaela Baibarac, *National Institut of Materials Physics, Bucharest, Romania*
Jelena Bajat, *Faculty of Technology and Metallurgy, University of Belgrade, Serbia*
Alexandru T. Balaban, *Texas A&M University, Galveston, USA*
Eva Baldrich, *Institut de Microelectronica de Barcelona (IMB-CNM, CSIC), Barcelona, Spain*
Mara Banović, *Faculty of Food Technology and Biotechnology, Zagreb, Croatia*
Jiri Barek, *Charles University, Prague, Czech Republic*
Zorica Basić, *Military Medical Academy, Institute of Hygiene, Beograd, Serbis*
Ayoob Bazgir, *Department of Chemistry, Shahid Beheshti University, Tehran, Iran*
Haider Behbehani, *Chemistry Department, Faculty of Science, Kuwait University, Safat, Kuwait*

Available online at shd.org.rs/JSCS/
2012 Copyright (CC) SCS

Vladimir Beškoski, *Institute of Chemistry, Technology and Metallurgy, University of Belgrade, Serbia*
Asim Bhaumik, *Indian Association for the Cultivation of Science, Jadavpur, India*
Filip Bihelović, *Faculty of Chemistry, University of Belgrade, Serbia*
Srđan Blagojević, *Faculty of Agriculture, University of Belgrade, Serbia*
Duško Blagojevic, *IBISS, Department of Physiology, Belgrade, Serbia*
Moira L. Bode, *School of Chemistry, University of the Witwatersrand, South Africa*
Bojin Bojinov, *Agricultural University of Plovdiv, Bulgaria*
Srđan Bojović, *Institute "Siniša Stanković", University of Belgrade, Serbia*
Gennadii Borovskii, *Siberian Inst Plant Physiol & Biochem SB RAS, Irkutsk, Russia*
Snežana Bošković, *Vinča Institute of Nuclear Sciences, Belgrade, Serbia*
Karel Bouzek, *Institute of Chemical Technology Prague*, *Czech Republic*
Nataša Božić, *Institute of Chemistry, Technology and Metallurgy, University of Belgrade, Serbia*
Sunčica Borozan, *Faculty of Veterinary Medicine, University of Belgrade, Serbia*
Maria José Calhorda, *CQB, Faculdade de Ciências, Universidade de Lisboa, Portugal*
John F. Carroll, *USDA, ARS, Invasive Insect Biocontrol and Behavior Laboratory, Beltsville, MD, USA*
Eduardo Castro, *Universidad Nacional de La Plata , La Plata, Argentina*
Janos Canadi, *Faculty of Science, University of Novi Sad, Serbia*
Pietro Luigi Cavallotti, *Dip. CMIC "G.Natta", Politecnico, Milano, Italy*
Yong Chen, *Sigma-Aldrich, Supelco, Bellefonte, PA, USA*
Tanja Ćirković Veličković, *Faculty of Physical Chemistry, University of Belgrade, Serbia*
Asit K. Chakraborti, *Department of Pharmacology, L.L.R.M. Medical College, Meerut (U.P.), India*
Shenhao Chen, *State Key laboratory for Corrosion and Protection, Shenyang, P. R. China*
Xueli Cheng, *Taishan University, Taishan, P.R. China*
Patricia Cerrutti, *Facultad de Ingeniería- Universidad de Buenos Aires, Argentina*
Marek Chmielewski, *Institute of Organic Chemistry, Polish Academy of Sciences, Warsaw, Poland*
Cheon-Gyu Cho, *Department of Chemistry and Research Institute for Natural Sciences, Hanyang University, Seoul, Republic of Korea*
Inho Choi, *School of Biotechnology, Yeungnam University, Gyeongshan, South Korea*
Cecilia Coletti *Dipartimento di Scienze del Farmaco, Università "G. d'Annunzio" Chieti-Pescara, Chieti, Italy*
M. Marta Costa, *Department of Chemistry, University of Minho, Braga, Portugal*
Uroš Cvelbar, *Institut Jožef Štefan, Ljubljana, Slovenia*
Vitomir Čupić, *Faculty of Veterinary Medicine, University of Belgrade, Serbia*
Minoo Dabiri, *Department of Chemistry, Faculty of Science, Shahid Beheshti University, Tehran, Iran*
Bhaskar S. Dawane, *Department of Chemistry, Yeshwant Mahavidyalaya, Nanded, India*
Aleksandar Dekanski,, *Institute of Chemistry, Technology and Metallurgy, University of Belgrade, Serbia*
Neslihan Demirbas, *Karadeniz Technical University, Department of Chemistry, Trabzon, Turkey*
Jasmina Dimitrić Marković, *Faculty of Physical Chemistry, University of Belgrade, Serbia*

2012 Copyright (CC) SCS

Luca Di Palma, *Chemical Engineering Materials Environment Department, Sapienza University, Rome, Italy*
Takayuki Doi, *Graduate School of Pharmaceutical Sciences, Tohoku University, Aramaki, Aoba-ku, Sendai, Japan*
Vera Dondur, *Faculty of Physical Chemistry, University of Belgrade, Serbia*
Sergey Dorozhkin, *Kudrinskaja sq. 1-155, Moscow, Russia*
Snežana Dragović, *Institute for the Application of Nuclear Energy, University of Belgrade, Belgrade, Serbia*
Patrick H. Dussault, *Department of Chemistry, University of Nebraska–Lincoln, Lincoln, USA*
Predrag Đurđević, *Department of Chemistry, Faculty of Science, University of Kragujevac, Serbia*
Milos I. Đuran, *Department of Chemistry, Faculty of Science, University of Kragujevac, Serbia*
Rada Đurović, *Institute of Pesticides and Environmental Protection, Belgrade, Serbia*
Enis Džunuzović, *Faculty of Technology and Metallurgy, University of Belgrade, Serbia*
Frank T. Edelmann, *Chemisches Institut der Otto-von-Guericke-Universität Magdeburg, Magdeburg, Germany*
Michail N. Elinson, *N. D. Zelinsky Institute of Organic Chemistry, Moscow, Russia*
Candace Elliott, *School of Botany, University of Melbourne, Victoria, Australia*
Hossein Eshghi, *Department of Chemistry, Ferdowsi University of Mashhad, Iran*
Slavica Erić, *Faculty of Pharmacy, University of Belgrade, Serbia*
Mihailo Etinski, *Faculty of Physical Chemistry, University of Belgrade, Serbia*
Paola Fabbri, *Dipartimento di Ingegneria "Enzo Ferrari", Università degli Studi di Modena e Reggio Emilia, Italy*
Jovanka Filipović, *Institute of Chemistry, Technology and Metallurgy, University of Belgrade, Serbia*
Bin Fu, *College of Chemistry and Molecular Engineering, Peking University, Beijing, P.R. China*
Boris Furtula, *Department of Chemistry, Faculty of Science, University of Kragujevac, Serbia*
Qiang Gao, *Department of Chemistry, University of Houston, Houston, TX, USA*
Agustín Costa García, *University of Oviedo, Spain*
Marija Gavrović-Jankulović, *Faculty of Chemistry, University of Belgrade, Serbia*
Athina Geronikaki, *School of Pharmacy, Aristotle University of Thessaloniki, Thessaloniki, Greece*
Mohamed Ghrab, *Olive Tree Institute, Tunisia*
Dejan Gođevac, *Institute of Chemistry, Technology and Metallurgy, University of Belgrade, Serbia*
Sabina Gojak, *Faculty of Science, Sarajevo, Bosnia and Herzegovina*
Gordana Gojgić-Cvijović, *Institute of Chemistry, Technology and Metallurgy, University of Belgrade, Serbia*
Snežana Gojković, *Faculty of Technology and Metallurgy, University of Belgrade, Serbia*
Anatoly K. Golovko, *Institute of Petroleum Chemistry, Tomsk, Russia*
Kristina Gopčević, *Faculty of Medicine, University of Belgrade, Serbia*
Steffen Graether, *University of Guelph, Canada*
Boško Grbić *Institute of Chemistry, Technology and Metallurgy, University of Belgrade, Serbia*
Branimir Grgur, *Faculty of Technology and Metallurgy, University of Belgrade, Serbia*

2012 Copyright (CC) SCS

Ivan Gutman, *Department of Chemistry, Faculty of Science, University of Kragujevac, Serbia*
Abraha Habtemariam, *Department of Chemistry, University of Warwick, Coventry, UK*
Robert G. Hamilton, *Johns Hopkins University School of Medicine, Baltimore, Maryland USA*
Dong Han, *Fujian Institute of Research on the Structure of Matter, Chinese Academy of Sciences, Fujian, P. R. China*
Radmila Hercigonja, *Faculty of Physical Chemistry, University of Belgrade, Serbia*
Ivanka Holclajtner-Antunović, *Faculty of Physical Chemistry, University of Belgrade, Serbia*
Paul F. Hudrlik, *Department of Chemistry, Howard University, Washington, D. C. USA*
Roger Hunter, *Department of Chemistry, University of Cape Town, South Africa*
Cemil Ibis, *Engineering Faculty, Istanbul University, Turkey*
Amri Ismail, *Department of Biology, Faculty of science Bizerte, Tunisia*
Suryadi Ismadji, *Universitas Katolik Widya Mandala Surabaya, Indonesia*
Đorđe Janaćković, *Faculty of Technology and Metallurgy, University of Belgrade, Serbia*
Svjetlana Janjić, *Faculty of Technology, University of Banja Luka, Republic of Srpska, BiH*
Magdalena Jaworska, *Centre of Molecular and Macromolecular Studies, Polish Academy of Science, Łódź, Poland*
Yeon Tae Jeong, *Pukyong National University, Busan, Republic of Korea*
Marjan Jereb, *Faculty of Chemistry and Chemical Technology, University of Ljubljana, Slovenia*
Stanka Jerosimić, *Faculty of Physical Chemistry, University of Belgrade, Serbia*
Branimir Jovančićević, *Faculty of Chemistry, University of Belgrade, Serbia*
Ljiljana Jovanović, *Faculty of Science, University of Novi Sad, Serbia*
Slobodan Jovanović, *Faculty of Technology and Metallurgy, University of Belgrade, Serbia*
Vladislava Jovanović, *Institute of Chemistry, Technology and Metallurgy, University of Belgrade, Serbia*
Nick Kalogeropoulos, *Department of Dietetics and Nutrition, Harokopio University, Athens, Greece*
Goran N. Kaluđerović, *Institut fur Chemie, Martin-Luther-Universität Halle-Wittenberg, Halle, Germany*
Vera Kapetanović, *Faculty of Pharmacy, University of Belgrade, Serbia*
Ivanka Karadžić, *Department of Chemistry, School of Medicine, University of Belgrade, Serbia*
Miltiades I. Karayannis, *University of Ioannina, Greece*
Hassan Karimi-Maleh, *Department of Chemistry, Islamic Azad University, Iran*
Hiroyuki Kataoka, *Shujitsu University, Japan*
Reza Khodarahmi, *Medical Biology Research Center, Kermanshah University of Medical Sciences, Kermanshah, Iran*
Berthold Kersting, *Institut für Anorganische Chemie, Universität Leipzig, Germany*
Md. Asaduzzaman Khan, *Department of Biochemistry, School of Biological Science & Technology, Central South University, P. R. China*
Mirjana Kijevčanin, *Faculty of Technology and Metallurgy, University of Belgrade, Serbia*
Joong Kyun Kim, *Pukyong National University, South Korea*
Brian John Kinsella, *Curtin University, Perth, Australia*
Željko Knez, *Faculty of Chemistry and Chemical Engineering, University of Maribor, Slovenia*
Lívia Kocúrová, *Department of Analytical Chemistry, Pavol Jozef Šafárik University in Košice, Czech Republic*

2012 Copyright (CC) SCS

Kianoush Khosravi-Darani, *National Nutrition and Food Technology Research Institute, Teheran, Iran*
Klára Kosová, *Crop Research institute, Prague, Czech Republic*
Vipan Kumar, *Department of Chemistry, Guru Nanak Dev University, Amritsar, India*
Kijnga Kutasi, *Institute for Solid State Physics Hungarian Academy of Sciences, Budapest, Hungary*
Pascal G. Lacroix, *Laboratoire de Chimie de Coordination du CNRS, Toulouse, France*
Peter Langer, *Institut für Chemie, Universität Rostock, Rostock, Germany*
Nada Lazić, *Institute of General and Physical Chemistry, University of Belgrade, Serbia*
Hvi Lee, *Department of Chemical Engineering, Korea Advanced Institute of Science and Technology, Daejeon, Republic of Korea*
Vukadin Leovac, *Faculty of Sciences, University of Novi Sad, Serbia*
Jürgen Liebscher, *Institut für Chemie, Humboldt-Universität zu Berlin, Berlin, Germany*
Wolfgang Lindner, *University of Vienna, Institute of Analytical Chemistry, Austria*
Wolfgang Linert, *Technical University of Vienna, Vienna, Austria*
Qingzhong Li, *Yantai University, Yantai, P.R. China*
Long-Liu Lin, *Department of Applied Chemistry, National Chiayi University, Chiayi, Taiwan*
Xinyong Liu. *School of Pharmaceutical Sciences, Shandong University, Jinan, P.R. China*
Chunlin Long, *Minzu University of China, Beijing, P.R. China*
Rafael López-Garzón, *Departamento de Química Inorgánica y Orgánica, Facultad de Ciencias Experimentales, Universidad de Jaén, Spain*
Jaap N. Louwen, *Albemarle Catalysts Company BV, Amsterdam, The Netherlands*
Milivoj Lovrić, *Ruđer Bošković Institute, Zagreb, Croatia*
Ester Lovsin Barle, *Novartis Pharma AG, Bazel, Switzerland*
Gui Lu, *School of Pharmaceutical Sciences, Sun Yat-sen University, Guangzhou, P R China*
Feng Luan, *Department of Applied Chemistry, Yantai University, Yantai, China*
Miodrag Maksimović, *Faculty of Technology and Metallurgy, University of Belgrade, Serbia*
Palash Mandal, *North Bengal University, West Bengal, India.*
Dragan Manojlović, *Faculty of Chemistry, University of Belgrade, Serbia*
Leonid Margolis, *National Institute of Child Health and Human Development, Bethesda, MD, USA*
Dragan Markušev, *Insitute of Physics, University of Belgrade, Serbia*
Smilja Marković, *Institute of Technical Sciences of the Serbian Academy of Sciences and Arts; Belgrade, Serbia*
Svetlana Marković, *Department of Chemistry, Faculty of Science, University of Kragujevac, Serbia*
Lucia Helena Mascaro, *Departamento de Quımica, Universidade Federal de Sao Carlos, Sao Carlos, SP, Brazil*
Romana Masnikosa, *Institute for the Application of Nuclear Energy, University of Belgrade, Serbia*
Anelia Ts. Mavrova, *University of Chemical Technology and Metallurgy, Sofia, Bulgaria*
Adam McCluskey, *Australian Cancer Research Foundation Centre for Kinomics, The University of Newcastle, Australia*
Brian F. McGuinness, *Ligand Pharmaceuticals, NJ, USA*
Slavko Mentus, *Faculty of Physical Chemistry, University of Belgrade, Serbia*
Harshadas Mitaram Meshrama, *Indian Institute of Chemical Technology, Hyderabad, India*

2012 Copyright (CC) SCS

Ion N. Mihailescu, *National Institute for Lasers, Plasma and Radiation Physics, Bucharest, Romania*
Nevena Mihailović, *Institute for the Application of Nuclear Energy, University of Belgrade, Serbia*
Dušan Mijin, *Faculty of Technology and Metallurgy, University of Belgrade, Serbia*
Jelena Miladinović, *Faculty of Technology and Metallurgy, University of Belgrade, Serbia*
Dušanka Milojković-Opsenica, *Faculty of Chemistry, University of Belgrade, Serbia*
Slobodan Milonjić, *The Vinca Institute of Nuclear Sciences, Belgrade University, Belgrade*
Nenad Milosavić, *Faculty of Chemistry, University of Belgrade, Serbia*
Makoto Minato, *Graduate School of Engineering, Yokohama National University, Yokohama, Japan*
Dragica Minić, *Faculty of Physical Chemistry, University of Belgrade, Serbia*
Valentine Mirceski, *Institute of Chemistry, UKIM Skopje R. Macedonia*
Bi Bi Fatemeh Mirjalili, *College of Science, Yazd University, Yazd, Iran*
Mosaad S. Mohamed, *University College of Pharmaceutical Sciences, Kakatiya University Warangal Andhra Pradesh, India*
Mostafa Mohammadpour Amini, *Department of Chemistry, Shahid Beheshti University, Tehran, Iran*
Virtudes Moreno Martínez, *Departament de Química Inorgànica, Universidad de Barcelona, Spain*
Rodrigo Moreno, *Institute of Ceramics and Glass, CSIC, Madrid, Spain*
Hassan Zavvar Mousavi, *College of Sciences, Semnan University, Semnan, Iran*
Jerzy Mroziński, *Faculty of Chemistry, University of Wroclaw, Wroclaw, Poland*
Ibrahim Mujić, *Collegium Fluminense Polytechnic of Rijeka, 51000 Rijeka, Croatia*
Liana Maria Muresan, *Babes-Bolyai University, Faculty of Chemistry and Chemical Engineering, Cluj-Napoca, Romania*
Dragana Mutavdžić Pavlović, *Faculty of Chemical Engineering and Technology, University of Zagreb, Croatia*
Jelena Mutić, *Faculty of Chemistry, University of Belgrade, Serbia*
Bekington Myrboh, *Department of Chemistry, North-Eastern Hill University, Umshing, Mawlai, Shillong, India*
Vesna Najdanović-Višak, *Faculty of Science and Technology, New University of Lisbon, Portugal*
Carmen Nájera, *Departamento de Química Organica & Instituto de Síntesis Organica, Universidad de Alicante, Alicante, Spain*
Olgica Nedić, *Institute for the Application of Nuclear Energy, University of Belgrade, Serbia*
Stevan Nemoda, *Institute for Nuclear Sciences Vinca, Belgrade, Serbia*
Biljana Nigović, *Faculty of Pharmacy and Biochemistry, University of Zagreb, Croatia*
Branislav Ž. Nikolić, *Serbian Chemical Society, Belgrade, Serbia*
Milan Nikolić, *Faculty of Chemistry, University of Belgrade, Serbia*
Snežana Nikolić-Mandić *Faculty of Chemistry, University of Belgrade, Serbia*
Jasmina Novaković, *Apotex Inc, Toronto, Ontario, Canada*
Reiko Oda, *Institut Européen de Chimie et Biologie, University of Bordeaux, Pessac, France*
Antonije Onjia, *Vinča Institute of Nuclear Sciences, Belgrade, Serbia*
Feyyaz Onur, *Faculty of Pharmacy, University of Ankara, Turkey*
Dejan Opsenica, *Faculty of Chemistry, University of Belgrade, Serbia*
Igor M. Opsenica, *Faculty of Chemistry, University of Belgrade, Serbia*

2012 Copyright (CC) SCS

Ilkay E. Orhan, *Gazi University, Faculty of Pharmacy, Ankara, Turkey*
Ryszard Ostaszewski, *Institute of Organic Chemistry, Polish Academy of Sciences, Warsaw, Poland*
Manojit Pal, *Institute of Life Sciences, Gachibowli, Hyderabad, India*
Vladimir Panić, *Institute of Chemistry, Technology and Metallurgy, University of Belgrade, Serbia*
Svetlana Paskaš, *Institute for the Application of Nuclear Energy-INEP, Belgrade-Zemun, Serbia*
Natalija Pejić, *Faculty of Pharmacy, University of Belgrade, Serbia*
Miljenko Perić, *Faculty of Physical Chemistry, University of Belgrade, Serbia*
P. T. Perumal, *Organic Chemistry Division, Central Leather Research Institute, Adyar, Chennai, Tamilnadu, India*
Milena Petković, *Faculty of Physical Chemistry, University of Belgrade, Serbia*
Rada Petrović, *Faculty of Technology and Metallurgy, University of Belgrade, Serbia*
Slobodan Petrović, *Faculty of Technology and Metallurgy, University of Belgrade, Serbia*
Zorica Petrović, *Faculty of Sciences, University of Kragujevac, Serbia*
Allan R. Pinhas, *Department of Chemistry, University of Cincinnati, Cincinnati, OH, USA*
Athanassios I. Philippopoulos, *Department of Chemistry, National and Kapodistrian University of Athens, Greece*
Winfried Plass, *Institut für Anorganische und Analytische Chemie, Friedrich-Schiller-Universität Jena, Germany*
Lionello Pogliani, *University of Calabria, Arcavacata di Rende, Italy*
Georgeta Postole, *Université Claude Bernard; Institut de recherches sur la catalyse et l'environnement de Lyon, France*
Milan Pour, *Faculty of Pharmacy, Charles University, Hradec Králové, Czech Republic*
Aurel Pui, *Faculty of Chemistry, "Al. I. Cuza" Iasi University, Iaşi, Romania*
Bojan Radak, *Vinča Institute of Nuclear Sciences, Belgrade, Serbia*
Dušanka Radanović, *Institute of Chemistry, Technology and Metallurgy, University of Belgrade, Serbia*
Tatjana Radosavljević, *Faculty of Pharmacy University of Belgrade, Serbia*
Maja Radetić, *Faculty of Technology and Metallurgy, University of Belgrade, Serbia*
Jelena Radosavljević, *Faculty of Chemistry, University of Belgrade, Serbia*
Ivona Radović, *Faculty of Technology and Metallurgy, University of Belgrade, Serbia*
Ljubinka Rajaković, *Faculty of Technology and Metallurgy, University of Belgrade, Serbia*
Nevenka Rajić, *Faculty of Technology and Metallurgy, University of Belgrade, Serbia*
M. Manuela M. Raposo, *Center of Chemistry, University of Minho, Campus of Gualtar, Braga, Portugal*
Bernab Rivas Quiroz, *Universidad de Concepcin, Facultad de Ciencias Qumicas, Chile*
Anna Roglans, *Department of Chemistry, Universitat de Girona, Girona, Spain*
Hassan Sabzyan, *Department of Chemistry, University of Isfahan, Iran*
Marco Sangermano, *DISMIC - Department of Materials Science and Chemical Engineering, Politecnico di Torino, Italy*
Victoria Samanidou, *Analytical Chemistry, University of Thessaloniki, Greece*
Claudio Santi, *Dipartimento di Chimica e Tecnologia del Farmaco, Università di Perugia,, Italy*
Shailendra K. Saraf, *Faculty of Pharmacy, Northern India Engineering College, Uttar Pradesh, India*

2012 Copyright (CC) SCS

Vladimir Savić, *Faculty of Pharmacy, University of Belgrade, Serbia*
Beat Schilling, *BGB Analytik AG, Adliswil, Switzerland*
Brian Singer, *School of Life Sciences, Northumbria University, Newcastle, UK*
Abbas Shafiee, *Department of Medicinal Chemistry, Tehran University of Medical Sciences, Tehran, Iran*
Hamid Reza Shaterian, *Faculty of Sciences, University of Sistan and Baluchestan, Zahedan, Iran*
Mohsen Shekouhy, *College of Chemistry, Islamic Azad University, Bandar Abbas Branch, Hormozgan, Iran*
Maya Shankar Singh, *Faculty of Science, Banaras Hindu University, Varanasi, U.P., India*
Andrey E. Shchekotikhin, *Gause Institute of New Antibiotics, Moscow, Russia*
Dejan Skala, *Institute of Chemistry, Technology and Metallurgy, University of Belgrade, Serbia*
Jacek Skarżewski, *Faculty of Chemistry, Wrocław University of Technology, Wrocław, Poland*
Rita Skoda-Földes *University of Pannonia, Institute of Chemistry, Veszprém, Hungary*,
Dušan Sladić, *Faculty of Chemistry, University of Belgrade, Serbia*
Björn C. G. Söderberg, *West Virginia University, Morgantown, USA*
Rafael Mateo Soria, *Instituto de Investigación en Recursos Cinegéticos, IREC (CSIC, UCLM, JCCM), Ciudad Real, Spain*
Sofija Sovilj, *Faculty of Chemistry, University of Belgrade, Serbia*
Ivan Spasojević, *Institute for Multidisciplinary Research, University of Belgrade, Serbia*
Biljana Jančić Stojanović, *Faculty of Pharmacy, University of Belgrade, Serbia*
Vojislav Stanič, *Vinča Institute of Nuclear Sciences, Belgrade, Serbia*
Slavka Stanković, *Faculty of Technology and Metallurgy, University of Belgrade, Serbia*
Srđan Stojanović, *Institute of Chemistry, Technology and Metallurgy, University of Belgrade, Serbia*
Ivana Stojković Simatović, *Faculty of Physical Chemistry, University of Belgrade, Serbia*
Ksenija Stojanović, *Faculty of Chemistry, University of Belgrade, Serbia*
Gordana Subakov Simić, *Faculty of Biology, University of Belgrade, Serbia*
Colin J. Suckling, *Department of Pure and Applied Chemistry, University of Strathclyde, Glasgow, Scotland, UK*
Diana Svetleva, *Department of Genetics and Plant Breeding, Agricultural University, Plovdiv Bulgaria*
Ivanka Stankova, *South-West University, Departmen of Chemistry, Blagoevgrad, Bulgaria*
Zoran Šaponjić, *Vinča Institute of Nuclear Sciences, Belgrade, Serbia*
Radovan Šebesta, *Faculty of Organic Chemistry, Comenius University, Bratislava, Slovakia*
Slobodan Šerbanović, *Faculty of Technology and Metallurgy, University of Belgrade, Serbia*
Ugur Tamer, *Gazi University, Faculty of Pharmacy, Ankara, Turkey*
Chak-Yin Tang, *The Hong Kong Polytechnic University, P.R. China*
Leman Tarhan, *Faculty of Science, Dokuz Eylul University, Buca, Izmir, Turkey*
Reza Tayebee, *Department of Chemistry, School of Sciences, Sabzevar Tarbiat Moallem University, Iran*
Ángel Terrón, *Departament de Quımica, Universitat de les Illes Balears, alma de Mallorca, Spain*
Tamara Todorović, *Faculty of Chemistry*, *University of Belgrade, Serbia*
Eric J. Thomas, *The University of Manchester, Manchester, UK*

2012 Copyright (CC) SCS

Anđelka Tomašević, *Institute of Pesticides and Environmental Protection, Belgrade-Zemun, Serbia*
Fotios Tsopelas, *School of Chemical Engineering, National Technical University of Athens, Greece*
Madalina Tudorache, *University of Bucharest, Romania*
Lemi Turker, *Middle East Technical University, Ankara, Turkey*
Paraskevas Tzanavaras, *Department of Chemistry, Aristotle University of Thessaloniki, Greece*
Petar Uskoković, *Faculty of Technology and Metallurgy, University of Belgrade, Serbia*
Gregorio Valencia, *Institut de Química Avançada de Catalunya, Consejo Superior de Investigaciones Científicas (IQAC-CSIC), Barcelona, Spain*
Laura Valencia, *Universidade de Vigo, Vigo, Spain*
Miloš Vasić, *Institute for the Testing of Materials, Belgrade, Serbia*
Tatjana Vasiljević, *Faculty of Technology and Metallurgy, University of Belgrade, Serbia*
Marjan Veber, *Faculty of Chemistry and Chemical Technology, University of Ljubljana, Slovenia*
Daniel Végh, *Faculty of Chemical and Food Technology, Slovak University of Technology, Bratislava, Slovakia*
Hojat Veisi, *Department of Chemistry, Payame Noor University, Iran*
Sonja Veljović - Jovanović, *Institute for Multidisciplinary Research, Belgrade, Serbia*
Vlada Veljković, *Faculty of Technology, University of Niš, Serbia*
Bruno Viana, *Chimie Paris Tech, France*
Zoran P. Višak, *Instituto Superior Técnico, Universidade Técnica de Lisboa, Lisbon, Portugal*
Miroslav Vrvić, *Faculty of Chemistry, University of Belgrade, Serbia*
Zerong Daniel Wang, *Department of Chemistry, University of Houston-Clear Lahe, Houston, TX, USA*
Shuya Wei, *Academy of Fine Arts in Vienna, Austria*
Xinliang Yu, *Department of Chemistry and Chemical Engineering, Hunan Institute of Engineering, Xiangtan, Hunan, China,*
Mohamad-Reza Yazdanbakhsh, *Chemistry Department, Faculty of Science, Guilan University, Rasht, Iran*
Constantinos K. Zacharis, *Department of Chemistry, Aristotle University of Thessaloniki, , Greece*
George Zachariadis, *Aristotle University of Thessaloniki, Greece*
Maaroof Zarei, *College of Sciences, Hormozgan University, Bandar Abbas, Iran*
Ljubisa Zeković, *Faculty of Physics, University of Belgrade, Serbia*
Wei Zhang, *State Key Laboratory of Applied Organic Chemistry, Lanzhou University,, Lanzhou, P.R. China*
Gang Zhao, *Shanghai Institute of Organic Chemistry, Chinese Academy of Sciences, Shanghai, P.R. China*
Branka Žarković, *Faculty of Agriculture, University of Belgrade, Serbia*
Emila Živković, *Faculty of Technology and Metallurgy, University of Belgrade, Serbia*
Ljiljana Živković, *Vinča Institute of Nuclear Sciences, Belgrade, Serbia*
Dragana Životić, *Faculty of Mining and Geology, University of Belgrade, Serbia*

2012 Copyright (CC) SCS